Title
Mitochondrial Fission in Neuronal Function and Models of Alzheimer's Disease

Permalink
https://escholarship.org/uc/item/193221jh

Author
Shields, Lauren Yoshimura

Publication Date
2016

Peer reviewed|Thesis/dissertation

Mitochondrial Fission in Neuronal Function
and Models of Alzheimer's Disease

by

Lauren Yoshimura Shields

DISSERTATION

Submitted in partial satisfaction of the requirements for the degree of

DOCTOR OF PHILOSOPHY

in

Biomedical Sciences

in the

For Mom and Dad-

the doctors who inspired me to become one myself.

Acknowledgements

Many individuals have been instrumental in my completion of this dissertation work – from my initial experiments as a rotation student that eventually contributed to the manuscript of Divya Pathak to my final first-author manuscript. First and foremost, I would like to thank my thesis advisor, Ken Nakamura. I am grateful for your support and guidance throughout these past five years as I moved forward in my progression to become an independent scientist. Secondly, I would like to thank my thesis chair, Yadong Huang. Thank you for your mentorship and support throughout my graduate studies. I would also like to thank my thesis committee members, Lennart Mucke and Eric Verdin, for their insight and scientific guidance. Additionally, I would like to thank the many members of the Nakamura lab, both past and present - in particular, Divya Pathak and Amandine Berthet for their training, guidance and company, and Bryce Mendelsohn and Dominik Haddad for being scientific sounding boards. Finally, none of this would have been possible without the support system in my life – Tom Bottiglieri, Avantika Chitre, Judy Ho, Kristen Watkins, Alice Yu, Jordan 'JoJo' Limor, and Jeff 'the Wong' Wong. And of course my wonderful family of doctors - Mom, Dad and Ryan.

Contributions

Chapter I contains excerpts of figures and text reprinted from Pathak et al. published in *The Journal of Biological Chemistry* on September 11th, 2015 (http://www.jbc.org/content/290/37/22325). These were conceived of and performed by Divya Pathak, Ken Nakamura, Bryce Mendelsohn, Dominik Haddad, Wei Lin and myself, with contributions from collaborators in Martin Brand's laboratory at the Buck Institute and guidance from Rob Edwards.

Chapter II contains figures and text reprinted from Shields, Kim et al., published in *Cell Death and Disease* on April 16th, 2015 (cddis201594a.html). The experiments published in this chapter were conceived of and performed by Hwajin Kim, Ken Nakamura, Dominik Haddad, Amandine Berthet, Divya Pathak, and Mable Lam, with contributions from our collaborators Lei Zhu and Lennart Mucke. The Drp1$^{lox/lox}$ mice were generated by our collaborator Hiromi Sesaki. The electron microscopy experiments were performed by our collaborators in Eric Huang's laboratory. Behavior experiments were performed with the guidance of Ravikumar Ponnusamy and T. Michael Gill from the Behavioral Core. Statistical analyses of the behavior experiments were performed by Grisell Diaz-Ramirez in the Bioinformatics cores at Gladstone.

Chapter III contains figures and text from a manuscript under preparation for submission. The project was first conceived of by Ken Nakamura and Hwajin Kim. Experiments were designed by Ken Nakamura and myself, and performed by myself, Hui Hui Li and Witney Chen. Behavior experiments were performed with the guidance of Ravikumar Ponnusamy and T. Michael Gill from the Behavioral Core. Statistical analysis of the behavior experiments were performed by Grisell Diaz-Ramirez and Clifford Anderson-Bergman in the Bioinformatics cores at Gladstone. Many of the microscopy experiments and analyses were guided by the expertise of Meredith Calvert, head of the Gladstone microscopy core.

Abstract

Mitochondria play critical roles in neurons, supporting energy levels and processes, such as neural transmission. Indeed, a breakdown of mitochondrial function may underlie neurodegenerative disease and synaptic degeneration. The process of mitochondrial fission is thought to be particularly important for maintaining mitochondrial health and function. However, the requirement and roles of fission in neuronal populations is unknown. In this thesis, we investigate synaptic energy and the role of mitochondrial fission in neurons. Using newly developed assays, we employ fluorescent probes to simultaneously measure synaptic ATP levels and synaptic vesicle cycling, showing that the endocytotic step is the most energy-demanding. Additionally, we demonstrate a requirement for the key fission protein dynamin-related protein 1 (Drp1) in the hippocampus, a critical learning and memory center of the brain, using a knockout model. We further show that neurons lacking Drp1 have an intrinsic deficit in mitochondrial respiration, specifically at the axon. Finally, we identify novel functions of Drp1 in maintaining ER-mitochondrial contacts and calcium dynamics, a necessity enhanced in the presence of the Alzheimer's protein amyloid precursor protein. Together, these studies further characterize the energetic requirements at the synapse and the neuronal requirements for Drp1 physiologically and in the context of models of AD.

Table of Contents

List of Figures

Chapter I:

Chapter II:

Chapter III:

Introduction

<u>Energy in neurons</u>

The brain uses 20% of the body's resting energy in spite of making up only 1/50th of the body's mass. The majority of this energy is thought to maintain excitatory synaptic transmission, supporting action potentials and postsynaptic receptors *(1)*. In light of these theoretical estimates, the synapse may have a particularly high requirement for energy compared to neuronal cell body. A breakdown of this energetic support could lead to insufficient energy for neuronal processes, termed energy failure. Indeed, energy failure may contribute to neurodegenerative diseases, including Parkinson's, and Alzheimer's disease (AD), and explain the early loss of synapses *(2)*. However, to understand whether energy failure occurs we first need to fully understand how neurons normally use energy.

Canonically, glucose is believed to be the main source of energy for neurons, metabolized via glycolysis to provide mitochondria with pyruvate for respiration. In contrast, a more recently proposed model – termed the astrocyte-neuron lactate shuttle - suggests that astrocytes primarily metabolize glucose, producing lactate via glycolysis, which is then imported into neurons via monocarboxylate transporters (MCT) to be used in respiration (after conversion into pyruvate) *(3)*. In support of this hypothesis, previous work has shown that knock-down of neuronal MCTs impairs learning and memory in a mouse model *(4)*. Contradictorily, other recent work has shown that glucose is primarily taken up by neurons using in vivo imaging in awake, behaving mice *(5)*. Similarly, another study showed direct glucose utilization in isolated synapses *(6)*. Therefore, additional work is necessary to understand the substrate preference of neurons.

Furthermore, the synapse may have specific energetic requirements in order to support aspects of synaptic transmission. Mitochondria move to and from the axon by previously identified cellular machinery *(7)* and studies have shown that this movement is arrested when

synaptic transmission occurs, likely to support local energy requirements *(8)*. Many processes at the synapse require energetic support - including maintenance of ionic gradients, neurotransmitter recycling and synaptic vesicle cycling *(9)*. A better understanding of the exact energy needs for each of these processes will help the field better understand which steps are most affected by energy failure.

Many tools currently exist to measure cellular metabolism, however they lack the resolution to answer these remaining questions. Current techniques measure global energetic usage in vivo, including nuclear magnetic resonance spectroscopy, and can examine the metabolism of specific substrates *(10)*. Assays in cultured neurons examine population metabolism (i.e. of both neurons and glia) – for example using radiolabeled substrates *(11,12)*. However, neither of these types of assays have the resolution to distinguish cell-type or synapse-specific contributions. Additional new assays in individual cells will help clarify the contribution of neuronal vs. astrocytic metabolism and the subcellular requirement at the cell body vs. synapse.

Mitochondrial dynamics in neurons

In order to maintain mitochondrial functions and energetic capacity necessary to support neurons and other cell types, these organelles undergo processes known as mitochondrial dynamics. Mitochondrial fission and fusion are two balanced processes which split mitochondria apart and fuse them together *(13)*. This balance is thought to be important for protein mixing, in particular to dilute dysfunctional mitochondrial proteins, mitophagy, and mitochondrial movement *(13)*. Fission is mediated via the critical protein dynamin-related protein 1 (Drp1), a GTPase that forms filaments around mitochondria, causing scission upon GTP hydrolysis *(13)*. Multiple de novo mutations in Drp1 have been found in patients, leading to a range of phenotypes - from neonatal lethality accompanied with abnormal brain development to epilepsy accompanied with encephalopathy *(14-17)*. All cases exhibited neuronal abnormalities, whether

pathologically or functionally. Similarly, global Drp1 knockout (Drp1KO) in mice causes embryonic lethality at E11.5 and neuron specific Drp1KO leads to neuronal and synaptic defects *(18,19)*.

Neurons may have a particular requirement for mitochondrial dynamics due to their morphology. In a knockout model, mitochondrial fission was shown to be necessary for targeting mitochondria down distal axons *(20)*. This targeting may be necessary to move mitochondria to sites of energetic need, but may also be related to other functions of these organelles. Mitochondria also produce reactive oxygen species, buffer calcium, mediate apoptosis, are involved in lipid biosynthesis, and neurotransmitter metabolism *(21,22)*. Indeed, different neuronal populations have varying susceptibility to mitochondrial insults *(23)*. Likewise, different neuronal populations may have different requirements for Drp1. Previous studies in a post-development Purkinje cell Drp1KO show that loss of fission leads to an accumulation of impaired mitochondria, oxidative damage and cell death *(24,25)*. Oxidative stress may be the causative mechanism given that treatment with anti-oxidants decreased the phenotype in cultured Purkinje neurons. Additional studies from our lab show that, in the midbrain, Drp1 is required for neuronal survival, mouse motor function and targeting down distal axons in dopaminergic neurons *(26)*. This requirement may reflect particular characteristics of dopamine neurons – their long, unmyelinated processes and large axonal arbors *(27-29)*.

Mitochondrial fission may also impact other mitochondrial processes in neurons, such as respiration. Indeed, given the drastic changes in mitochondrial morphology in Drp1KO models (elongation and swelling of mitochondria), one might expect that mitochondrial respiratory function would be compromised. Surprisingly, Drp1KO mouse embryonic fibroblasts had normal respiration *(18,30)*. However, this phenotype may be cell-type specific and not hold true in neurons, which have far greater energy needs. Furthermore, Drp1 also interacts at the interface of mitochondria and the endoplasmic reticulum (ER). Mitochondria and the ER interact at sites known as mitochondrial-associated membranes (MAMs) that are important in processes

overlapping with mitochondrial functions: calcium buffering, lipid homeostasis and apoptosis. ER tubule interaction has been shown to mark the sites of Drp1-mediated fission, prior to Drp1 recruitment, suggesting it is upstream an event and Drp1-independent *(31)*. However, whether Drp1 also plays a role in MAM function and impacts MAM formation remains unknown.

Mitochondrial fission in Alzheimer's disease

Changes in mitochondrial fission may also contribute to the pathophysiology of several neurodegenerative diseases *(32-35)* including Alzheimer's disease (AD) *(13,36,37)*. AD is the most common neurodegenerative disease, affecting 5.4 million Americans and projected to impact 13.8 million Americans by 2050 *(38)*. Pathologically, it is characterized by extracellular deposition of the protein amyloid-beta (Aβ) and intracellular deposits of the protein tau. Disease pathogenesis leads to progressive neuronal loss, particularly in the hippocampus, which plays a key role in memory formation. This cell death in turn leads to cognitive changes, memory loss and functional impairment. Although Alois Alzheimer initially identified the disease over 100 years ago, there is still no cure nor a complete understanding of the processes that underlie disease progression.

One contributor to AD may be changes in mitochondria. In particular, mitochondrial energy failure may contribute to AD pathogenesis. Positron emission tomography (PET) imaging in patients shows a decrease in glucose uptake that far precedes cognitive changes, appearing even in college-age carriers of the primary AD risk factor apolipoprotein E4 (apoE4) *(39)*. While decreases in glucose uptake have been well-characterized, these measurements only account for the initial step in glucose metabolism. Further measurements of downstream metabolism have shown that patients have an upregulation of glycolysis, as opposed to respiration, that spatially correlates with Aβ plaque deposition *(40)*. This upregulation could reflect either more anaerobic respiration and/or more flux through the pentose phosphate pathway, a metabolic pathway which helps regulate the oxidative state of the cell and is

particularly necessary in neurons *(11)*. If anaerobic respiration is upregulated, these changes may develop in response to respiratory dysfunction, requiring a shift in metabolic support. Indeed, post-mortem tissue from patients shows functional and expression changes in mitochondrial respiratory proteins *(41,42)*. These changes have been replicated in AD mouse models, which indicate that tau may cause complex I dysfunction in the electron transport chain while Aβ causes complex IV dysfunction *(43)*. Alternatively, if the pentose phosphate pathway (PPP) is upregulated, the shift could be in response to mitochondrial or non-mitochondrial oxidative stress. Thus, the cell may divert glucose to the PPP to combat ROS, leaving insufficient substrate for respiration. Finally, increased energy consumption may also contribute. In AD, energy requirements may also be required to support increased network activity seen in animal models and patients*(44,45)*, which could also lead to insufficient energy.

In particular, mitochondrial fission may contribute to AD progression. Drp1 levels are frequently elevated in post-mortem tissue from AD patients while fusion proteins are downregulated *(46,47)*, suggesting that mitochondria may be more fragmented in AD (although this remains to be proven). Moreover, Aβ is proposed to produce toxicity by increasing the relative rate of fission to fusion through a Drp1-dependent mechanism *(48)*, via increased Drp1 activity. However, downregulation of Drp1 has also been hypothesized to mediate tau toxicity *(49)*. Therefore, the roles of mitochondrial fission and bioenergetics in AD pathogenesis remain unclear.

In this thesis, I describe key findings furthering our understanding of the normal requirements for energy and mitochondrial fission in neurons, including at the synapse, and the requirement of fission in AD. First, I describe two newly developed assays that allow measurement of mitochondrial-derived ATP at the synapse and synaptic vesicle cycling. These assays show that either glycolysis or respiration can support synaptic vesicle cycling, depending on substrate availability, and that endocytosis has high energy requirements compared to vesicle

reacidification or exocytosis. Second, using a knockout model, I demonstrate a requirement for Drp1 in hippocampal neurons. With Drp1 loss, learning and memory is impaired, likely due to an intrinsic deficit in synaptic respiration. Further, this work shows that mitochondrial fission is necessary to maintain energy levels at the synapse, reflecting an intrinsic impairment in the mitochondria, rather than a change in distribution. Finally, this thesis describes a new role for Drp1 in neurons – of being required for MAM stability both in number and size - and calcium dynamics. This requirement is enhanced in the presence of the amyloid precursor protein, the protein cleaved to produce Aβ, in a model of AD.

References:

1. Attwell D, Laughlin SB (2001) An energy budget for signaling in the grey matter of the brain. J Cereb Blood Flow Metab 21, 1133-1145

2. Pathak D et al. (2013) Energy failure: does it contribute to neurodegeneration? Ann Neurol 74, 506-516

3. Bélanger M et al. (2011) Brain energy metabolism: focus on astrocyte-neuron metabolic cooperation. Cell metabolism 14, 724-738

4. Suzuki A et al. (2011) Astrocyte-neuron lactate transport is required for long-term memory formation. Cell 144, 810-823

5. Lundgaard I et al. (2015) Direct neuronal glucose uptake heralds activity-dependent increases in cerebral metabolism. Nat Commun 6, 6807

6. Patel AB et al. (2014) Direct evidence for activity-dependent glucose phosphorylation in neurons with implications for the astrocyte-to-neuron lactate shuttle. Proc Natl Acad Sci U S A 111, 5385-5390

7. Schwarz TL (2013) Mitochondrial trafficking in neurons. Cold Spring Harb Perspect Biol 5,

8. Sheng ZH (2014) Mitochondrial trafficking and anchoring in neurons: New insight and implications. J Cell Biol 204, 1087-1098

9. Harris JJ et al. (2012) Synaptic Energy Use and Supply. Neuron 75, 762-777

10. Soares DP, Law M (2009) Magnetic resonance spectroscopy of the brain: review of metabolites and clinical applications. Clin Radiol 64, 12-21

11. Herrero-Mendez A et al. (2009) The bioenergetic and antioxidant status of neurons is controlled by continuous degradation of a key glycolytic enzyme by APC/C–Cdh1. Nature Cell Biology 11, 747-752

12. Bak LK et al. (2012) Novel model of neuronal bioenergetics: postsynaptic utilization of glucose but not lactate correlates positively with Ca2+ signalling in cultured mouse glutamatergic neurons. ASN Neuro 4,

13. Itoh K et al. (2013) Mitochondrial dynamics in neurodegeneration. Trends in Cell Biology 23, 64-71

14. Waterham HR et al. (2007) A lethal defect of mitochondrial and peroxisomal fission. N Engl J Med 356, 1736-1741

15. Fahrner JA et al. (2016) A novel de novo dominant negative mutation in DNM1L impairs mitochondrial fission and presents as childhood epileptic encephalopathy. Am J Med Genet A,

16. Vanstone JR et al. (2016) DNM1L-related mitochondrial fission defect presenting as refractory epilepsy. Eur J Hum Genet 24, 1084-1088

17. Yoon G et al. (2016) Lethal Disorder of Mitochondrial Fission Caused by Mutations in DNM1L. J Pediatr 171, 313-316 e312

18. Wakabayashi J et al. (2009) The dynamin-related GTPase Drp1 is required for embryonic and brain development in mice. The Journal of Cell Biology 186, 805-816

19. Ishihara N et al. (2009) Mitochondrial fission factor Drp1 is essential for embryonic development and synapse formation in mice. Nature Cell Biology 11, 958-966

20. Verstreken P et al. (2005) Synaptic mitochondria are critical for mobilization of reserve pool vesicles at Drosophila neuromuscular junctions. Neuron 47, 365-378

21. Nunnari J, Suomalainen A (2012) Mitochondria: in sickness and in health. Cell 148, 1145-1159

22. Waagepetersen HS et al. (2003) Compartmentation of glutamine, glutamate, and GABA metabolism in neurons and astrocytes: functional implications. Neuroscientist 9, 398-403

23. Wimalasena K (2016) The inherent high vulnerability of dopaminergic neurons toward mitochondrial toxins may contribute to the etiology of Parkinson's disease. Neural Regen Res 11, 246-247

24. Kageyama Y et al. (2012) Mitochondrial division ensures the survival of postmitotic neurons by suppressing oxidative damage. The Journal of cell biology 197, 535-551

25. Zhang Z et al. (2012) Mitochondrial division prevents neurodegeneration. Autophagy 8, 1531-1533

26. Berthet A et al. (2014) Loss of mitochondrial fission depletes axonal mitochondria in midbrain dopamine neurons. J Neurosci 34, 14304-14317

27. Matsuda W et al. (2009) Single nigrostriatal dopaminergic neurons form widely spread and highly dense axonal arborizations in the neostriatum. J Neurosci 29, 444-453

28. Pickel VM et al. (1992) Ultrastructure of spared dopamine terminals in caudate-putamen nuclei of adult rats neonatally treated with intranigral 6-hydroxydopamine. Brain Res Dev Brain Res 70, 75-86

29. Braak H, Del Tredici K (2004) Poor and protracted myelination as a contributory factor to neurodegenerative disorders. Neurobiol Aging 25, 19-23

30. Ishihara N et al. (2009) Mitochondrial fission factor Drp1 is essential for embryonic development and synapse formation in mice. Nat Cell Biol 11, 958-966

31. Friedman JR et al. (2011) ER tubules mark sites of mitochondrial division. Science 334, 358-362

32. Kamp F et al. (2010) Inhibition of mitochondrial fusion by alpha-synuclein is rescued by PINK1, Parkin and DJ-1. EMBO J 29, 3571-3589

33. Nakamura K et al. (2011) Direct membrane association drives mitochondrial fission by the Parkinson disease-associated protein alpha-synuclein. J Biol Chem 286, 20710-20726

34. Wang X et al. (2012) LRRK2 regulates mitochondrial dynamics and function through direct interaction with DLP1. Hum Mol Genet 21, 1931-1944

35. Wang W et al. (2015) Parkinson's disease-associated mutant VPS35 causes mitochondrial dysfunction by recycling DLP1 complexes. Nat Med,

36. Wang X et al. (2008) Amyloid-beta overproduction causes abnormal mitochondrial dynamics via differential modulation of mitochondrial fission/fusion proteins. Proc Natl Acad Sci U S A 105, 19318-19323

37. Cho DH et al. (2009) S-nitrosylation of Drp1 mediates beta-amyloid-related mitochondrial fission and neuronal injury. Science 324, 102-105

38. Alzheimer's A (2016) Alzheimer's Association Facts and Figures Report.

39. Saunders AM et al. (1993) Association of apolipoprotein E allele ϵ4 with late‐onset familial and sporadic Alzheimer's disease. Neurology 43, 1467-1467

40. Vlassenko AG et al. (2010) Spatial correlation between brain aerobic glycolysis and amyloid-β (Aβ) deposition. Proceedings of the National Academy of Sciences of the United States of America 107, 17763-17767

41. Valla J et al. (2001) Energy hypometabolism in posterior cingulate cortex of Alzheimer's patients: superficial laminar cytochrome oxidase associated with disease duration. The Journal of Neuroscience: The Official Journal of the Society for Neuroscience 21, 4923-4930

42. Liang WS et al. (2008) Alzheimer's disease is associated with reduced expression of energy metabolism genes in posterior cingulate neurons. Proceedings of the National Academy of Sciences of the United States of America 105, 4441-4446

43. Rhein V et al. (2009) Amyloid-beta and tau synergistically impair the oxidative phosphorylation system in triple transgenic Alzheimer's disease mice. Proceedings of the National Academy of Sciences of the United States of America 106, 20057-20062

44. Palop JJ et al. (2007) Aberrant Excitatory Neuronal Activity and Compensatory Remodeling of Inhibitory Hippocampal Circuits in Mouse Models of Alzheimer's Disease. Neuron 55, 697-711

45. Vossel KA et al. (2013) Seizures and epileptiform activity in the early stages of Alzheimer disease. JAMA Neurol 70, 1158-1166

46. Kandimalla R, Reddy PH (2016) Multiple faces of dynamin-related protein 1 and its role in Alzheimer's disease pathogenesis. Biochim Biophys Acta 1862, 814-828

47. Manczak M et al. (2011) Impaired mitochondrial dynamics and abnormal interaction of amyloid beta with mitochondrial protein Drp1 in neurons from patients with Alzheimer's disease: implications for neuronal damage. Human molecular genetics 20, 2495-2509

48. Cho D-H et al. (2009) S-nitrosylation of Drp1 mediates beta-amyloid-related mitochondrial fission and neuronal injury. Science (New York, NY) 324, 102-105

49. DuBoff B et al. (2012) Tau Promotes Neurodegeneration via DRP1 Mislocalization In Vivo. Neuron 75, 618-632

Chapter I: The bioenergetic requirements of neurons

Abstract

Synaptic mitochondria are thought to be critical in supporting neuronal energy requirements at the synapse, and bioenergetic failure at the synapse may impair neural transmission and contribute to neurodegeneration. However, little is known about the energy requirements of synaptic vesicle release, or if these energy requirements go unmet in disease, primarily due to a lack of appropriate tools and sensitive assays. To determine the dependence of synaptic vesicle cycling on mitochondria-derived ATP levels, we developed two complementary assays sensitive to mitochondria-derived ATP in individual, living hippocampal boutons. The first is a functional assay for mitochondria-derived ATP that uses the extent of synaptic vesicle cycling as a surrogate for ATP level. The second uses ATP FRET sensors to directly measure ATP at the synapse. Using these assays, we show that endocytosis has high ATP requirements and that vesicle reacidification and exocytosis require comparatively little energy.

Introduction

Mitochondria likely provide the main source of ATP that supports synaptic transmission, whereas anaerobic respiration from glycolysis contributes much less ATP *(1)*. Yet, surprisingly, less than half of all synaptic boutons in adult rodent hippocampus or in cultured hippocampal neurons contain mitochondria *(2,3)*. This raises questions about where synaptic ATP originates, how it is distributed among boutons, and how much energy is needed to support synaptic transmission. Dysfunction of axonal mitochondria may also have a critical role in the pathogenesis of neurodegenerative diseases, including Parkinson's disease and Alzheimer's disease. Indeed, multiple neurodegenerative pathways are thought to converge on energy failure, and synaptic terminals degenerate early in many neurodegenerative diseases associated with impaired energy metabolism *(4-6)*. These findings indicate that significant changes in bioenergetic function may occur that are restricted to—or occur first in—neuronal processes. In addition, axonal mitochondria have unique properties and exist in distinct microenvironments, and thus, it is critical that we first understand the bioenergetics of intact axons. But surprisingly, energy failure has never been proved to occur in dysfunctional or dying disease-affected neurons or in the intact neurons used in genetic disease models *(6)*. Therefore, without knowing the normal energy requirements of neurons or how much energy depletion occurs in disease, we cannot know if energy failure plays a causative role in degeneration.

Our understanding of neuronal bioenergetics has been limited because the established assays have insufficient resolution *(6)*. Although respiration, glycolysis, and ATP can be measured in whole neuronal cultures, these approaches cannot accurately factor out ATP contributions from glia or provide subcellular spatial resolution. Synaptosome analyses continue to elucidate synaptic bioenergetic functions, but are challenging in specific neuronal types *(7)* and are also subject to artifacts related to the isolation process. Mitochondrial membrane potential can be studied in intact neurons *(8)*, but this is difficult in small axonal mitochondria

12

and provides only indirect bioenergetic information. In addition, the mass and distribution of axonal mitochondria are just as important as their function *(6)*.

To measure mitochondria-derived energy at the synapse, we designed sensitive ATP assays that suppress glycolysis so neurons must rely on mitochondria for energy. Using these assays, we identified the energy threshold needed to support synaptic vesicle cycling and showed that, when ATP drops below this threshold, endocytosis is blocked at or before the vesicle scission step. In contrast to the high energy requirement of endocytosis, we also show that vesicle reacidification and exocytosis require comparatively little energy. These new assays provide novel insights into the physiologic energy requirements at the synapse.

Results

Substrate Availability Determines Extent of Reliance on Mitochondria for ATP

Physiologic brain glucose levels (≈1–1.5 mM *(9,10)*) are far lower than those typically used to culture neurons and perform mitochondrial function assays (≈25–30 mM). Under these high-glucose conditions, glycolysis likely compensates for any respiratory deficits and obscures our ability to detect if and how any respiratory deficits affect neuronal function/survival. Therefore, to develop sensitive assays to measure mitochondria-derived ATP in neurons, we first delineated how the relative ATP contributions of aerobic and anaerobic respiration are influenced by substrate availability. Using a Seahorse instrument, we measured the rates of respiration and glycolysis in E18 hippocampal cultures grown for 11 days. In 30 mM glucose—a supra-physiological concentration often used in cell culture and imaging buffers—basal and maximal OCRs were low, indicating little aerobic respiration (Figure 1). But when pyruvate (10 mM) was substituted for glucose for 30 min, respiration increased, as did the ratio of OCR to ECAR (Figure 1d), indicating a greater reliance on aerobic respiration. Importantly, these data reflect bioenergetic changes in neurons specifically, as we both minimized glial content (using embryonic cultures grown in serum-free medium) and used parallel glia-only cultures to correct for the ATP contribution of remaining glia. As such, our normalized glial OCR calculations show that glia only minimally contribute to the total OCR regardless of substrate (Figure 1). Therefore, neurons derive more energy from mitochondrial respiration when exposed to pyruvate, but they rely more on glycolysis when exposed only to high glucose levels. So, we hypothesized that, to detect the consequences of lower mitochondrial ATP levels, we should use substrates that promote aerobic respiration and minimize glycolysis.

To test this at the synapse, which is the first area to degenerate in several neurodegenerative diseases involving mitochondria *(4,5)*, we first examined how the substrate affects the ATP-dependent capacity of synaptosomes to maintain low calcium levels *(7)*. We

used fluorescence microscopy of the low-affinity Ca^{2+}-probe fura-4F AM to measure the loss of

Ca^{2+} homeostasis in single synaptosomes. Most synaptosomes maintained low resting calcium

levels (below the sensitive range of fura-4F; <100 nM $[Ca^{2+}]$) even without substrates in the

medium, suggesting that endogenous substrates suffice (Figure 1e). Glycolysis alone also

maintained calcium homeostasis, but inhibiting all glycolysis (by iodoacetate; 250 µM), oxidative

phosphorylation (oligomycin; 1 µg/mL) and creatine kinase (iodoacetamide; 250 µM) disrupted

synaptosome calcium regulation, manifesting in a precipitous increase in $[Ca^{2+}]$ (>6 µM). This

suggests that ATP fell below the threshold required to maintain normal low calcium levels. So,

because calcium regulation can be supported by either glycolysis or respiration, we must

suppress glycolysis to determine how impaired mitochondrial ATP production affects calcium
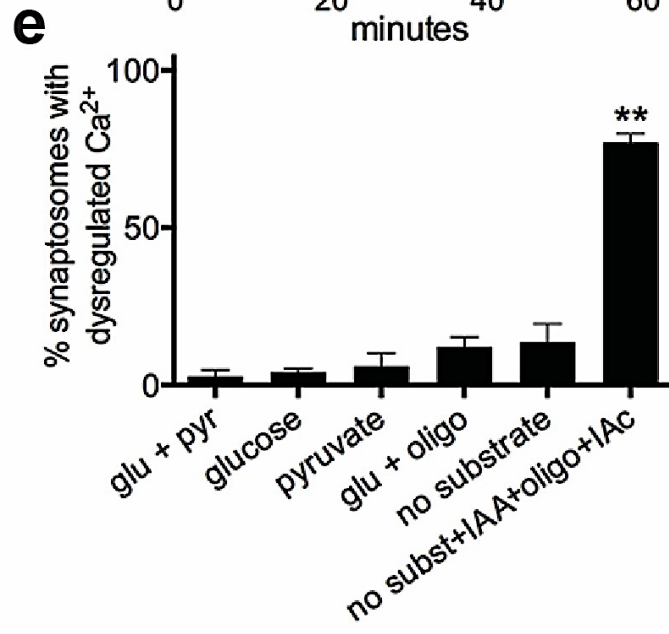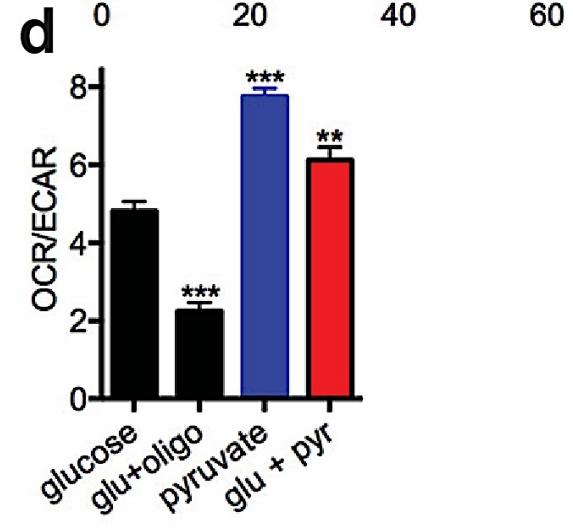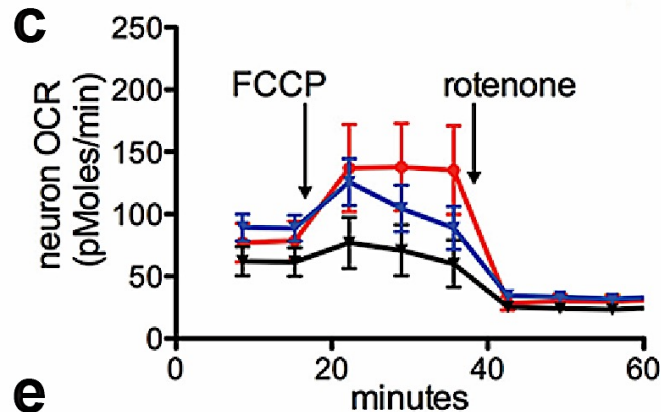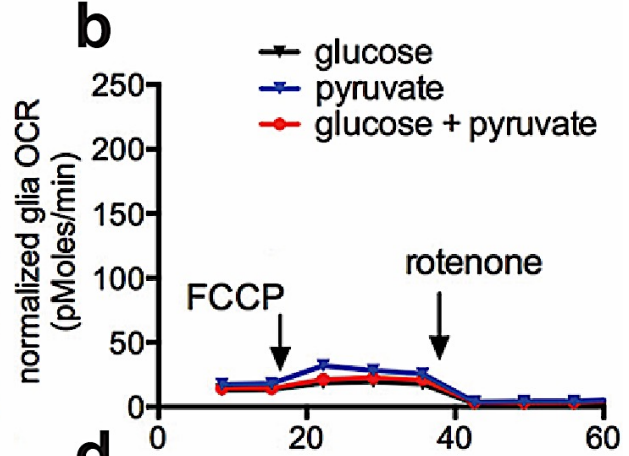
levels.
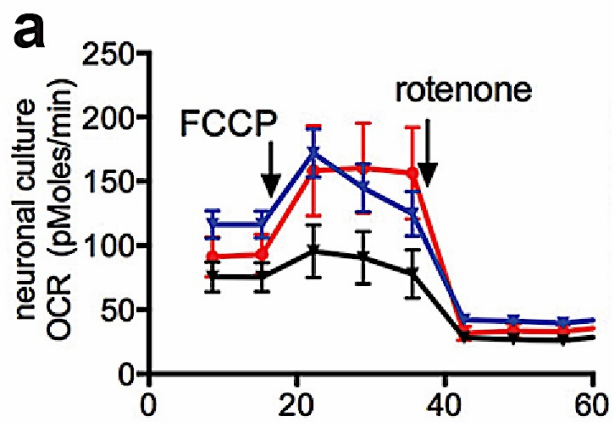
Figure 1. Pyruvate and glucose availability regulates the level of neuronal aerobic and anaerobic energy metabolism. Aerobic respiration rates (oxygen consumption rate, OCR) were measured in 11-day-old primary E18 rat hippocampal neuronal and parallel glia-only cultures with a 96-well Seahorse Extracellular Flux Analyzer. **(a)** In neuronal cultures, basal OCR is greater in medium containing 10 mM pyruvate ($p < 0.001$ vs 30 mM glucose alone by two-way ANOVA with repeated measures). After FCCP addition at the arrow (a mitochondrial uncoupler, 1 µM), maximal respiration is greater in medium containing pyruvate ($p < 0.001$) or pyruvate + glucose ($p < 0.01$). Subsequent addition of the mitochondrial complex I inhibitor rotenone (2 µM) blocks respiration and decreases OCR to the same level in all groups. **(b)** In comparison, normalized glial respiration rates in parallel glia-only cultures were far lower than neuronal rates. **(c)** Subtraction of estimated glial contribution to total OCR in neuronal cultures revealed the "neuron OCR," which showed similar results to the total OCR of the neuronal culture. Therefore, although glia constitute a significant proportion of cells even in "pure" neuronal cultures, they respire at much lower levels than neurons, and hence, the overall pattern of neuron-corrected OCR is similar to the total-well OCR. Data are mean ± SEM from a representative experiment with 5–12 wells/group. **(d)** The ratio of OCR/ECAR (extracellular acidification rate) represents neurons' reliance on aerobic respiration versus glycolysis for ATP. When pyruvate is present, neurons rely more on aerobic respiration, but this decreased when we added the ATP synthase inhibitor oligomycin (oligo; 4 µM). Data are mean ± SEM from a representative experiment with 5–12 wells/group. **$p < 0.01$, ***$p < 0.001$, versus the glucose-only group by one-way ANOVA and Dunnett's post hoc test. **(e)** Percentage of synaptosomes that failed to maintain Ca2+ homeostasis (fura-4F ratio was above 2, equivalent to 6 µM) 15 min after changing to medium containing glucose (glu; 15 mM), pyruvate (pyr; 10 mM), or neither. Combined inhibition of glycolysis (by iodoacetate, IAA; 250 µM), oxidative phosphorylation (by oligomycin; 1 µg/mL), and creatine kinase (by iodoacetamide, IAc; 250 µM) caused Ca2+ dysregulation in most synaptosomes. Therefore, glycolysis must be suppressed to detect how deficits in mitochondrial ATP production affect Ca2+ levels. N=4, data are mean ± SE. **$p < 0.01$, by t test versus glucose + pyruvate.

Aerobic and Glycolytic ATP Requirements of the Synaptic Vesicle Cycle

Synaptic vesicle release may be impaired early in diseases that deplete energy *(11)*, but the ATP requirements of the synaptic vesicle cycle are poorly understood. To investigate how much mitochondria-derived ATP is needed for different phases of the synaptic vesicle cycle, we assessed synaptic vesicle release when neurons were exposed to different substrates. For this and all subsequent live imaging experiments we studied postnatal hippocampal neurons grown in serum-containing media *(12-14)*. These cultures also include glia, and thus better incorporate glia-neuron interactions that likely influence energy metabolism in neurons *(15)*. To monitor the synaptic vesicle cycle in individual boutons, we used the VGLUT1-pHluorin reporter, which targets a pH-sensitive GFP (pHluorin) to the lumen of synaptic vesicles. pHluorin does not fluoresce in an acidified vesicle, but it does fluoresce when a vesicle fuses and its contents are exposed to the alkaline extracellular environment *(16)*. pHluorin fluorescence is then quenched after endocytosis of the vesicle and subsequent reacidification (Figure 2).

Postnatal hippocampal neurons were incubated either in buffer containing 30 mM glucose to facilitate aerobic respiration and glycolysis, or in buffer lacking glucose but containing 10 mM pyruvate to favor reliance on mitochondria. To determine if the synaptic vesicle cycle could function in the different buffers for a range of activity levels, we exposed neurons to two commonly used electrical field–stimulation paradigms: a longer but lower frequency stimulation (60 s at 10 Hz) that facilitates the preferential release of vesicles in the recycling pool   (total pool of vesicles that can undergo activity-dependent synaptic vesicle cycling *(17)*) (Figures 2a-c), or a shorter but higher frequency stimulation (3 s at 30 Hz) that promotes the release of vesicles in the readily releasable pool (vesicles docked and "primed" at the active zone for immediate fusion upon stimulation *(18)*) *(12,19)* (Figures 2d and e).

Synaptic vesicle cycling remained intact with either substrate (glucose or pyruvate) with either stimulation paradigm. But without glucose, the rate that the pHluorin signal returned to baseline was slightly impaired with repetitive 60 s*10 Hz stimulation (Figure 2a), indicating a

small drop-off in endocytosis when glucose was absent. Therefore, since respiration could not fully compensate in this paradigm, some amount of glycolysis is required. These experiments were performed in the presence of glutamate receptor antagonists—10 µM 6-cyano-7-nitroquinoxaline-2,3-dione (CNQX) and 50 µM D,L-2-amino-5-phosphonovaleric acid (APV)—to eliminate endogenous network activity, but these antagonists had no detectable impact on our assays (not shown) and were excluded from subsequent experiments.

Neurons do not store glucose in the form of glycogen *(20)* and cannot replenish their own glucose supply, so synaptic vesicle cycling that occurs in the absence of glucose but with pyruvate is likely supported by mitochondria-derived ATP. To test this, we applied rotenone (500 nM), which inhibits mitochondrial complex I. With rotenone, endocytosis was completely blocked for cells in pyruvate but not for cells in glucose (Figures 2b and e). Similarly, the ATP synthase inhibitor oligomycin (2.5 µg/mL) also blocked endocytosis, but only in the absence of glucose (Figure 2c). This confirms that endocytosis depends on mitochondria-derived ATP when glycolysis is impaired. In contrast, the rate of exocytosis was largely preserved throughout these trials. In particular, exocytosis was fully preserved with 30Hz*3 stimulation targeting the readily releasable pool (Figure 2e), indicating that little energy is required to release vesicles, especially once primed.
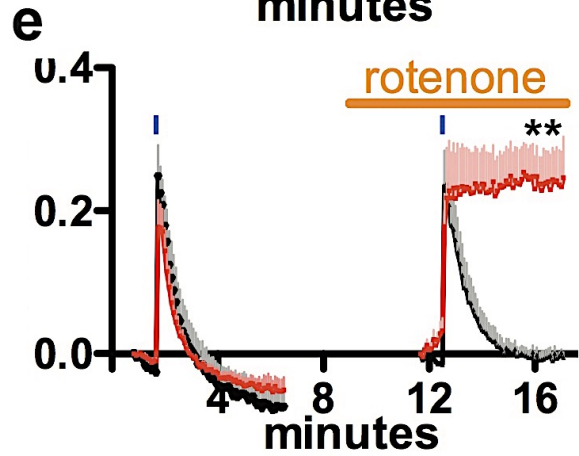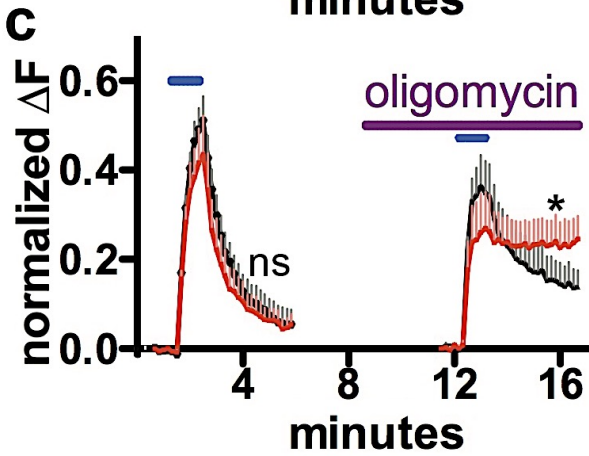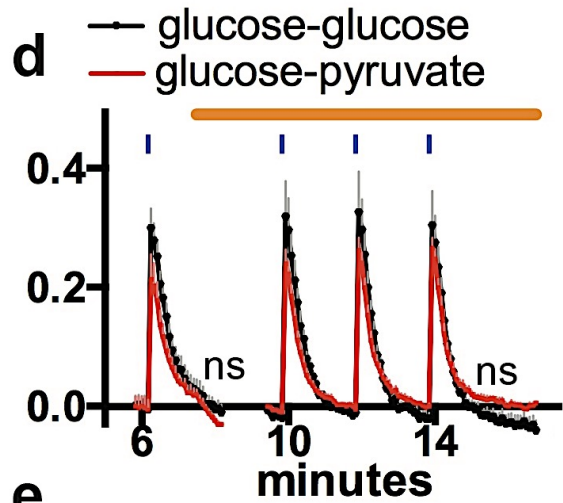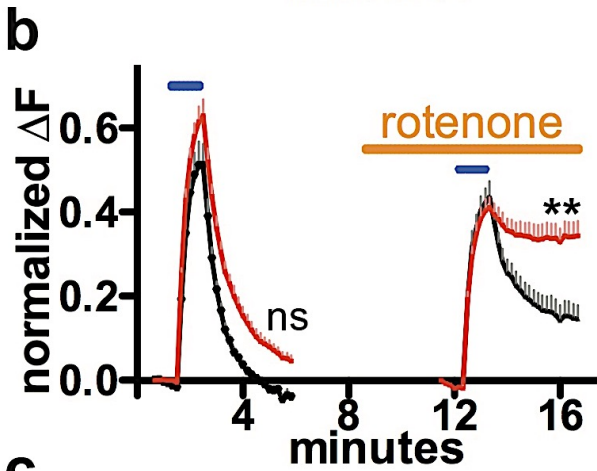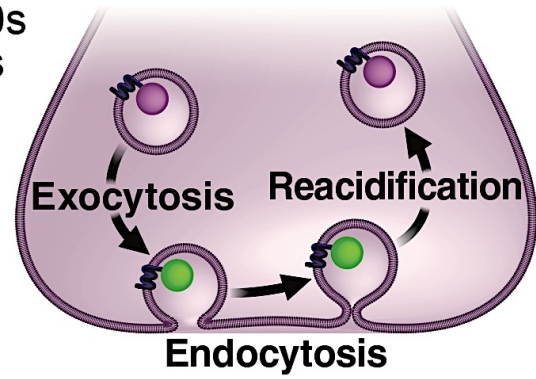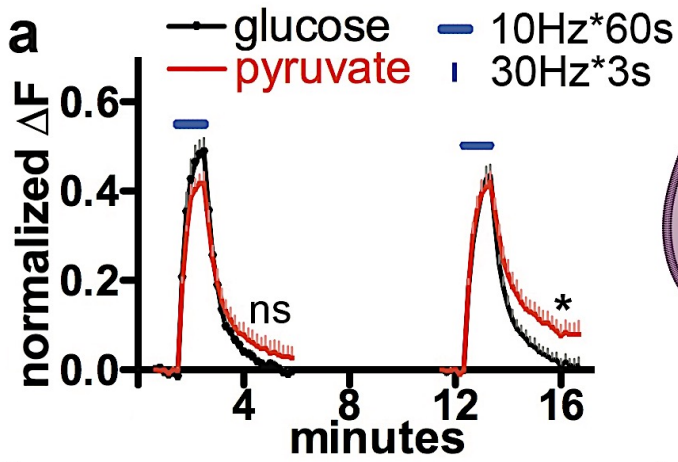
Figure 2. Functional assay for mitochondria-derived ATP reveals differential ATP requirements of the synaptic vesicle cycle. Synaptic transmission at individual boutons was assessed in hippocampal neurons expressing a pH-sensitive GFP targeted to synaptic vesicles (VGLUT1-pHluorin*(16)*, diagram). The rise in the curve during electrical stimulation reflects primarily exocytosis, while the downstroke reflects endocytosis and synaptic vesicle reacidification. **(a-c)** Electrical field stimulation of the recycling pool (10 Hz*60 s, blue lines). Each curve shows the mean change in pHluorin fluorescence (ΔF) normalized to the size of the total pool of VGLUT-pHluorin in each bouton (determined by measuring the fluorescence after application of 50 mM NH4Cl after each run *(12,21)*). **(a)** Without glucose, synaptic vesicle cycling was maintained with pyruvate (red line), but repeat stimulation slightly compromised the extent of endocytosis. **(b and c)** Endocytosis without glucose (red line) versus with glucose (black line) depended on mitochondria-derived ATP and was completely blocked by either rotenone (500 nM) or oligomycin (2.5 µg/mL). **(d)** Electrical stimulation (30 Hz*3 s, blue lines) to release the readily releasable pool. Even without glucose (orange line), synaptic vesicle cycling was maintained with pyruvate (glucose-pyruvate, red line). **(e)** Without glucose (red line) endocytosis depended on mitochondria-derived ATP and was completely blocked by rotenone. This change in endocytosis provides a functional measure of mitochondria-derived energy. N=4–6 coverslips (110–151 boutons)/group. Data show mean ± SE. *$p<0.05$, **$p<0.01$, ns=not significant, for extent of endocytosis [(amplitude endocytosis) / (amplitude exocytosis)] with versus without glucose by two-way ANOVA with repeated measures and Bonferroni post hoc test.

(Of note, the experiments in this figure were performed by others in the Nakamura lab and included in this thesis to introduce the technique and illustrate findings on the energy requirements at the synapse).

Measuring ATP at the Nerve Terminal

To directly assess the ATP requirements of the synaptic vesicle cycle, we developed an approach to measure ATP in individual synapses. To do this, we obtained ATP FRET sensors (ATeams) *(22)*, that are specifically sensitive to ATP (with no response to ADP, other nucleotide triphosphates, NADH or dATP) *(23,24)* and are resistant to physiologic changes in pH. We used the FRET sensor to monitor ATP in neurons given different substrates. At baseline, basal FRET values were stable in boutons over 25 min of imaging even when both glucose and pyruvate were absent (Figures 3a and b); neurons thus had enough substrates to maintain their basal ATP. But when glycolysis was fully blocked, ATP levels quickly dropped, and this was prevented by adding 10 mM pyruvate—a standard dose that enters cells and then mitochondria via monocarboxylate transporters (MCTs) *(25)*—to fuel respiration, indicating that respiration is required to support basal ATP when glycolysis is absent (Figure 3c).
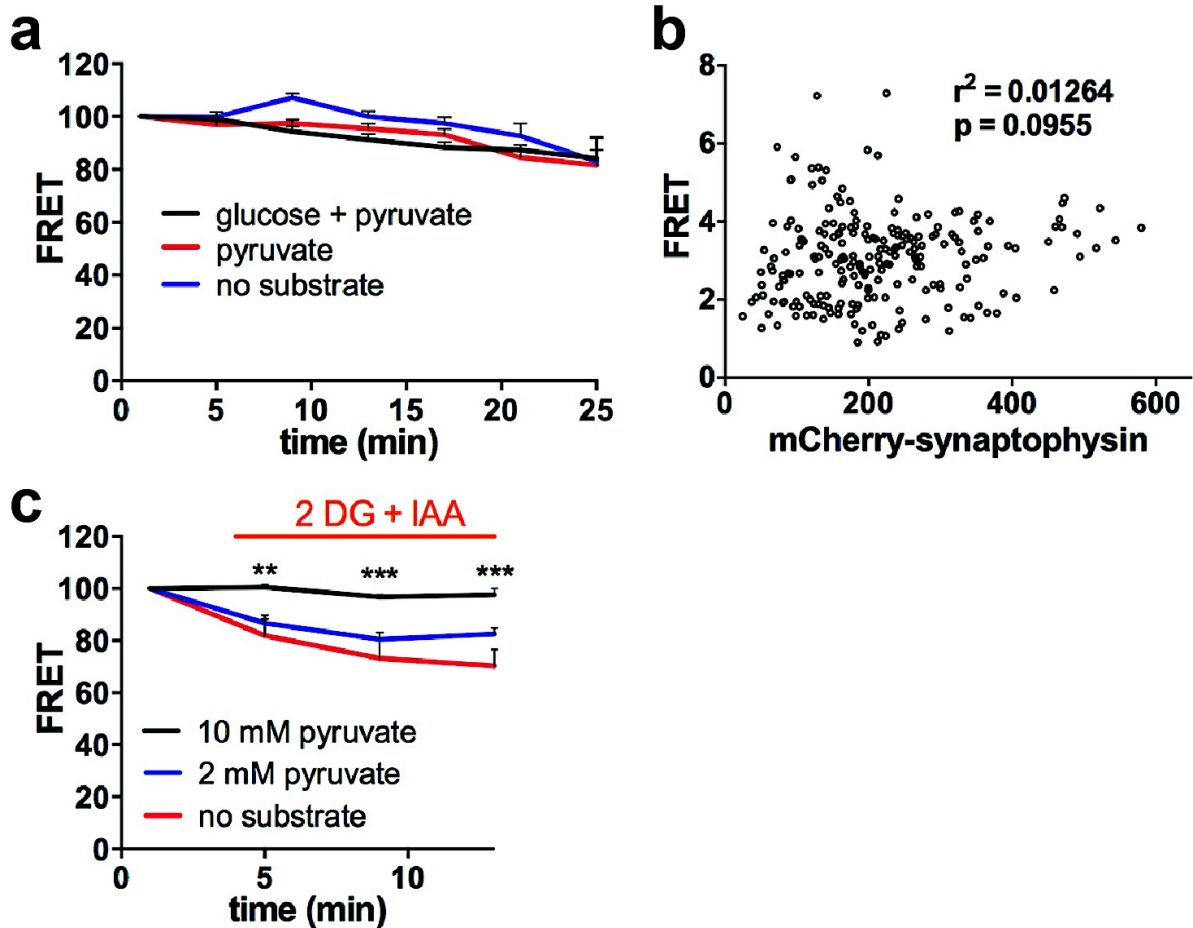
Figure 3. Basal ATP levels at the nerve terminal can be supported by either glycolysis or aerobic respiration. (a) Basal ATP was not affected by acute changes in substrate. ATP levels of hippocampal neuron boutons were assessed using ATP YEMK. At t= 4 min, media was changed from glucose (30 mM) and pyruvate (10 mM) to either pyruvate only (10 mM) or no substrate. Basal ATP levels remained similar in all groups, indicating that the remaining substrates are sufficient to maintain ATP at baseline in both compartments. N=6–8 coverslips/group, with 15–20 boutons/coverslip. Data show mean ± SEM. **(b)** ATP FRET measurements are independent of expression level. In synaptic boutons co-expressing ATP YEMK and mCherry-synaptophysin, linear regression was performed to assess the intensity of mCherry-synaptophysin (as a surrogate for extent of expression) and FRET. There was no significant correlation between the two variables. The square of the correlation coefficient (r2) represents the proportion of variability in FRET that is accounted for by the initial YFP value. **(c)** Neurons require mitochondria-derived ATP when glycolysis is blocked. Basal ATP levels of synaptic boutons drop when glycolysis is blocked (using 2DG at 5 mM and IAA at 1 mM) and if pyruvate is absent. The decrease in ATP is prevented by 10 mM pyruvate, but not 2 mM pyruvate. N= 3–4 coverslips/group, with 15–20 boutons/coverslip. Data are mean ± SEM. **p<0.01, ***p<0.001, versus no substrate group by two-way ANOVA and Tukey's post hoc test.

(Of note, the experiments in this figure were performed by others in the Nakamura lab and included in this thesis to introduce the technique and illustrate findings on the energy requirements at the synapse).

Threshold ATP Requirement for Endocytosis

Having developed an approach to monitor ATP levels in synaptic vesicles, we next examined the ATP requirements of the steps in synaptic vesicle cycling. The pHluorin experiments (Figure 2) show that, unlike the final stages of exocytosis, endocytosis has a high ATP dependence. Because blocking mitochondrial ATP production caused pHluorin fluorescence to remain high after exocytosis (Figure 2), energy depletion may have blocked endocytosis at or before vesicle scission or, in a subsequent step, preventing vesicles from becoming re-acidified. To distinguish between these possibilities, we first examined the ATP requirements of synaptic vesicle reacidification, a known energy requiring process *(26)*. However, bafilomycin (which blocks the reacidification of vesicles, Figure 4a) did not affect the rate or extent of decrease in mitochondria-derived ATP produced by prolonged stimulation (10Hz*150s) (Figure 4b), indicating that vesicle reacidification is not the primary ATP consuming process.

To determine if the block may instead occur proximal to reacidification at the vesicle reinternalization step, we next acutely added MES (pH 5.5) to see if it quenched pHluorin fluorescence when endocytosis was blocked (Figure 4c). We hypothesized that MES would not quench fluorescence if vesicles were blocked at the re-acidification stage because the vesicles would have already been internalized and therefore not accessible to MES. In contrast, MES would rapidly quench fluorescence if the block prevented vesicle scission. When we used rotenone to block endocytosis, MES rapidly quenched the increased pHluorin fluorescence, indicating that endocytosis requires high ATP at or before vesicle scission.

After establishing the stage at which synaptic vesicle cycling is blocked during energy failure, we used our ATP assay to define how much ATP is required for endocytosis (the ATP threshold). Defining this threshold would allow us to determine if it is breached in models of neuronal dysfunction, which is critical for understanding if energy failure truly impairs function and contributes to pathogenesis. We began defining this energy threshold by subjecting

neurons to the same electrical stimulation patterns and non-glucose conditions that forced

reliance on mitochondria-derived ATP in Figures 2b and e. Consistent with these results, the

acute addition of rotenone decreased ATP levels faster in groups lacking glucose, especially

with stimulation (Figures 4d and e), presumably because neurons could not adequately

compensate with glycolysis. Therefore, after acutely blocking energy production, we found that

the ATP threshold required to sustain endocytosis resides between the ATP level with and

without glucose (Figures 4d and e). These results clarify the energy requirements of synaptic

vesicle cycling, furthering our understanding of the physiologic energy demands at the synapse.
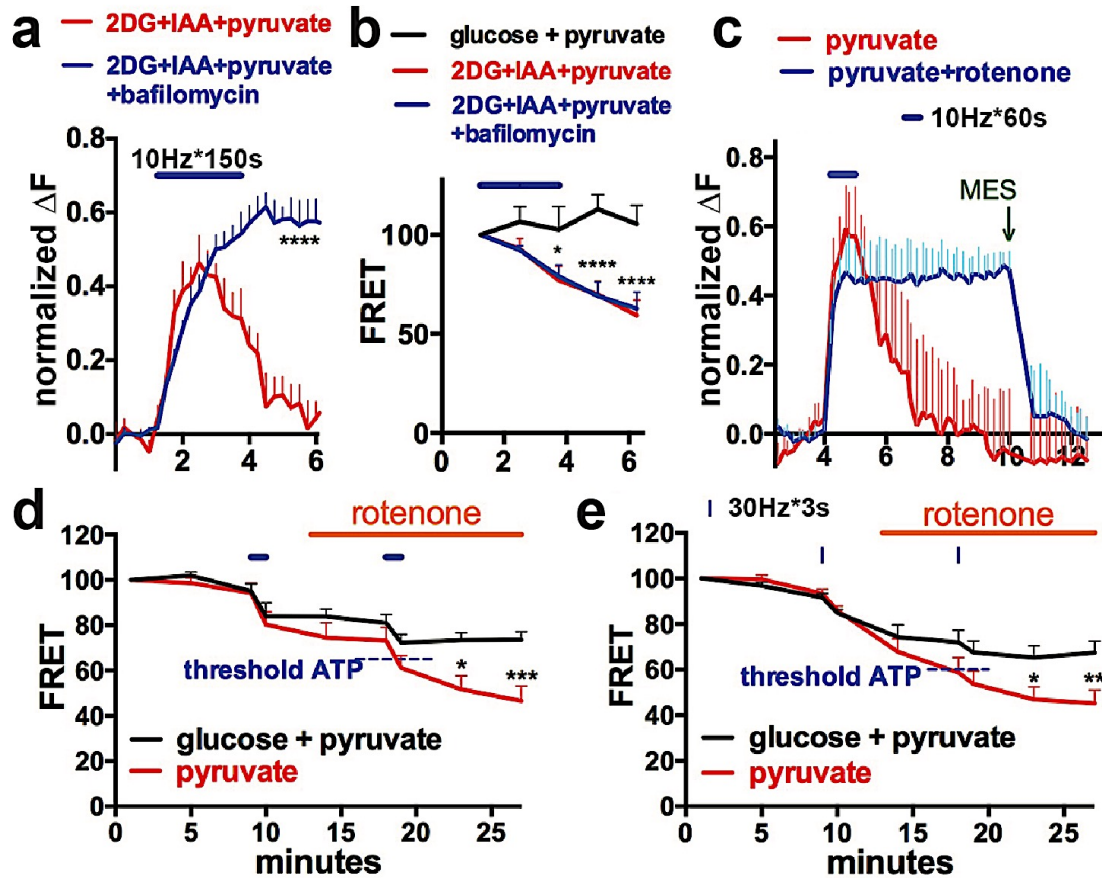
Figure 4. Acute block of respiratory function decreases mitochondrially-derived ATP below the threshold level for endocytosis. (a) Acute treatment with bafilomycin (1µM) inhibits the reacidification of synaptic vesicles after extended stimulation (10 Hz*150 s, blue bar in A and B), assessed with VGLUT1-pHluorin, and performed in pyruvate without glycolysis (2DG and IAA) to force reliance on mitochondria-derived ATP. N=6 coverslips/group, with 10–16 boutons/coverslip. Data show mean ± SEM; ****$p<0.0001$ versus no bafilomycin control group by unpaired two-tailed t test for extent of endocytosis [(amplitude endocytosis)/(amplitude exocytosis)]. **(b)** Inhibition of reacidification by bafilomycin does not prevent the decrease in ATP levels as compared to the no-bafilomycin control group, indicating that this step of vesicle cycling requires comparatively little energy. N=5–9 coverslips/group, with 10–15 boutons/coverslip. Data show mean ± SEM, **$p<0.01$, ****$p<0.0001$ versus glucose + pyruvate by two-way ANOVA with repeated measures and Bonferroni post hoc test. **(c)** Pre-exposing neurons to rotenone before stimulation in pyruvate buffer (10 mM) blocked endocytosis, but MES (25 mM, pH 5.5), which acidifies the extracellular compartment, rapidly quenched fluorescence, indicating that endocytosis was blocked at or before the vesicle scission step. Electrical field stimulation alone (**d**, 10 Hz*60 s; **e**, 30 Hz*3 s) acutely decreased ATP similarly in the presence or absence of glucose (buffer switched to pyruvate without glucose at t=4 min). When rotenone (orange line, beginning after the initial stimulation) was added to impair mitochondrial function, ATP decreased more in cultures without glucose, presumably because these cells could not compensate with glycolysis. N=9–11 coverslips/group, with 15–20 boutons/coverslip. Data show mean ± SEM, *$p<0.05$, **$p<0.01$, ***$p<0.001$ versus glucose by two-way ANOVA with repeated measures and Bonferroni post hoc test.

Discussion

To determine if changes in mitochondrial bioenergetics contribute to neurodegeneration *(6)*, we must first understand the normal energy requirements for neuronal function and survival and determine if and how energy levels change when mitochondria are compromised. Using new assays that provide complementary measures of mitochondria-derived ATP at the nerve terminal—a region that is compromised early in neurodegeneration *(4,5)*—we define the energy thresholds needed to sustain different phases of the synaptic vesicle cycle. We also show that acutely or chronically inhibiting the respiratory chain drops mitochondria-derived ATP levels below the threshold needed to sustain endocytosis, especially when energy consumption is increased by greater neural activity.

Normal Requirement of ATP at the Nerve Terminal

In neurons, most ATP is likely dedicated to supporting synaptic transmission. However, the energy requirements of the synaptic vesicle cycle are poorly understood. Our studies show that endocytosis is far more sensitive to mitochondrial ATP levels than exocytosis. Further, we found that re-acidification is not the key energy requiring step, consistent with recent theoretical estimates of the ATP requirements of synaptic vesicle reacidification *(27)*. Instead, the vesicle scission phase of endocytosis has high energy requirements, consistent with studies that showed ATP is required for the scission of coated pits into sealed vesicles in mammalian cell lines *(28)* and for membrane fission and/or retrieval in goldfish bipolar neurons *(29)*. Indeed, attenuating endocytosis may help neurons preserve ATP when needed, as synaptic vesicle cycling likely uses most of the ATP at the synapse *(30)*. Further studies will be required to determine specifically how low ATP limits vesicle scission. In contrast to endocytosis, we show that vesicle release from the readily releasable pool requires little ATP, which is consistent with studies in permeabilized endocrine cells and goldfish retinal bipolar neurons, showing that once "primed," vesicle release is independent of ATP but depends on Ca^{2+} *(31)*. Although

endocytosis is far more sensitive to decreased energy than exocytosis, some ATP is still needed to facilitate exocytosis, presumably due to the ATPase activity of NSF, which is required before vesicle fusion *(32)*.

Energy Failure at the Synapse in Neurodegeneration

Defects in mitochondrial bioenergetics likely influence the pathogenesis of many neurodegenerative diseases, including Parkinson's disease, Huntington's disease, and Alzheimer's disease *(6)*. Energy status at the synapse may be particularly important because in most neurons, most mitochondria likely reside in axons *(33)*, and degeneration begins in this compartment *(4,5)*. Even before synapses are lost, insufficient ATP may contribute to early disease-related changes in synaptic transmission *(11,34)*. But, energy failure has never been directly proven in affected neurons in these diseases, or even in intact neurons in genetic models of these diseases, leaving the central tenet of the bioenergetic hypothesis unproven *(6,35)*.

The recent emergence of fluorescent sensors for energy metabolites allows us to interrogate energy status on a single-cell basis *(22,36)*; here, we show that this technology can be applied to individual living neurons and their synapses. In the brain, glucose levels are far lower than in standard neuronal culture *(9,10)*, and neurons *in vivo* likely derive a greater proportion of their energy from aerobic respiration. Much of this ATP may be generated from lactate produced by adjacent glial cells and then imported into neurons via the astrocyte-neuron lactate shuttle, where it is converted into pyruvate *(15,37)*. On the other hand, recent evidence suggests that neurons (not astrocytes) directly metabolize much of the glucose entering the brain *(38,39)*, suggesting that glycolysis may actually contribute more to supporting neuronal energy needs than previously suspected. Importantly, we must better understand the role of energy failure in neurodegeneration because mitochondria have other functions: they buffer calcium, produce reactive oxygen species, synthesize lipids, and regulate apoptosis *(40)*. How these other

functions affect synapses is even less well understood than bioenergetics. If a given disease

mutation does not violate a neuron's energy threshold, then energy failure is probably not the

main way the mutation produces degeneration. Conversely, if energy levels dip below the

threshold, insufficient energy may help cause degeneration *(6)*. As such, our assays may

eventually be used to better understand energy failure in neurodegeneration and test

therapeutic interventions that restore energy levels.

Materials and Methods

Molecular Biology—All constructs were subcloned or cloned into the pCAGGS vector downstream of the chicken actin promoter *(16)*. AT1.03^{YEMK} FRET (fluorescence resonance energy transfer) sensor (which uses a variant of CFP (mseCFP) as the donor fluorophore, and YFP (circularly permuted monomeric Venus) as the acceptor fluorophore, surrounding an ATP binding protein) was a kind gift from Hiromi Imamura (Kyoto University) and Hiroyuki Noji (Osaka University) *(22)*. VGLUT1-pHluorin and mCherry-synaptophysin have been described *(16,41)*.

Cell Culture—Postnatal hippocampal neurons used in live-imaging experiments were prepared from P0 rat or mouse pups as described *(12-14)* and were plated in medium containing 5% fetal bovine serum at a density of 650 cells/mm^2. 10 µM FUDR and 10 µM uridine were added on day 4 *in vitro* to prevent glial overgrowth. Floxed tdTomato mice were from the Jackson Laboratory *(42)*. Cells for imaging were transiently transfected by electroporation (Amaxa). Hippocampal neurons for Seahorse experiments were prepared from embryonic day (E)18 embryos *(43)*, plated in serum-free medium at a density of 5 x 10^4 cells per well in a 96-well polystyrene microplate and cultured for 11 days before analysis. Rat glial cultures were prepared from P0 rats and plated 3 days prior at 6 x 10^4 cells per well on the same 96-well microplate *(12)*.

Respiration and Glycolysis—The extracellular acidification rate (ECAR, a surrogate for glycolysis) and oxygen consumption rate (OCR, to assess mitochondrial respiration) were measured using a Seahorse XF96 Extracellular Flux Analyzer (Seahorse Bioscience). Cells were washed and preincubated for 30 min in Seahorse assay medium (pH 7.4) containing substrates of interest (30 mM glucose, 10 mM pyruvate, or both). OCR and ECAR were measured at baseline and again after sequential addition of respiratory inhibitors at final concentrations of 1 µM FCCP (carbonyl cyanide-4-(trifluoromethoxy)phenylhydrazone, a

protonophore that uncouples oxidative phosphorylation in mitochondria), 2 μM rotenone (an inhibitor of mitochondrial complex I), or 4 μM oligomycin ((inhibitor of ATP synthase). After each run, cells were fixed with 4% paraformaldehyde and stained with microtubule-associated protein 2 (MAP2) and glial fibrillary acidic protein (GFAP) to distinguish glia from neurons. To correct for the glial contribution, we estimated the glial content in each well by creating a ratiometric image of GFAP staining/MAP2 staining, which allowed us to clearly resolve glia from neurons (this was done because both antibodies had some non-specific staining). In parallel, we used pure astrocyte cultures to estimate the contribution of an equivalent number of astrocytes. Neuronal respiration corrected for glial contamination was calculated based on the following formula: neuron OCR = neuronal culture OCR – (glia OCR, the respiration of pure glia cultures) * (glial content neuronal culture/glial content of pure glial culture).

Single Synaptosome Imaging—Single synaptosome imaging was performed using reported methods *(35)*. Briefly, cortical synaptosomes (1 μg protein/well) from adult FVB mice were attached to polyethyleneimine (1:15000 w/v%) plus geltrex (1 v/v%)-coated cover glass–bottomed microplates (Whatman) by centrifugation and were incubated with 65 nM MitoTracker Green and 2.5 μM fura-4F AM in pH 7.4 buffer containing 3.5 mM KCl, 120 mM NaCl, 0.4 mM KH_2PO_4, 1.2 mM Na_2SO_4, 15 mM D-glucose, 10 mM pyruvate, and 10 mM TES for 30 min at 37°C. Buffer was then replaced with fresh buffer containing 1.3 mM $CaCl_2$, 0.4% (w/v) fatty acid–free bovine serum albumin, and 5 nM tetreamethylrhodamine methyl ester (TMRM), and wide-field images were acquired with a Nikon Eclipse Ti-PFS inverted epifluorescence microscope and a S-Fluor 40x 1.4 NA oil lens with the filters (excitation – dichroic mirror – emission in nm/bandwidth) for TMRM (543/22 – 562 – 617/73; 150 ms exposure time), MitoTracker Green (472/30 – 505 – 520/35; 150 ms) and fura-4F (340/26 (250 ms) and 387/11 (125 ms) – 409 – 510/84). Four time points were acquired at 5-min intervals, and the buffer was replaced with fresh buffer containing the desired substrate composition after the second time point. Fields of ~30,000 synaptosomes were imaged using 4×4 tiling in each time point.

Because fura-4F became essentially saturated in synaptosomes with dysregulated Ca^{2+} homeostasis, the fraction of individual synaptosomes with a higher fura-4F excitation ratio than a fixed threshold (ratio of 2, equivalent to ~6 μM) was determined. This was performed using automated image segmentation in Image Analyst MKII (Image Analyst Software, Novato, CA).

Live Imaging—Neurons were cultured for 11 days (rat neurons) or 8–9 days (mouse neurons), and then imaged live in Tyrode's medium (pH 7.4; in mM: 127 NaCl, 10 HEPES-NaOH, 2.5 KCl, 2 $MgCl_2$, and 2 $CaCl_2$, with either 30 mM glucose and/or 10 mM pyruvate, unless otherwise specified) using a Nikon CFI Plan Apo 40x/0.95 air objective on a Nikon Ti-E inverted microscope with an iXon EMCCD camera (Andor Technology), and a perfusion valve control system (VC-8, Warner Instruments), controlled by Metamorph software (Molecular Devices). All buffer changes and drug additions were made by perfusion except for MES (Figure 4c), which was directly injected into the imaging chamber to achieve immediate mixing. Field stimulations were done using an A385 current isolator and a SYS-A310 accupulser signal generator (World Precision Instruments).

VGLUT1-pHluorin fluorescence images were obtained (490/20 ex, 535/50 em, Chroma), and regions of interest were drawn over synaptic boutons using Metamorph software. Synaptic boutons were identified based on co-localization with mCherry-synaptophysin and an increase in pHluorin fluorescence after we applied ammonium chloride (50 mM). For each bouton, the background-subtracted change in fluorescence at each time point was normalized to the fluorescence in ammonium chloride (which estimates the total synaptic vesicle pool size) *(12)*, measured at the end of each run. The baseline fluorescence intensity was set to zero either 5 or 20 s before the first stimulation, and then again before the second stimulation after any change in substrate or drug addition.

For FRET experiments, sequential images were taken in the CFP (430/24 ex, 470/24 em), YFP (500/20 ex, 535/30 em), and FRET channels (430/24 ex, 535/30 em) using an ET ECFP/EYFP filter set (Chroma). Synaptic boutons were again identified based on co-localization

32

with mCherry-synaptophysin or by morphology.

The FRET/donor ratio was calculated for each bouton as described *(44)*, where FRET = $(I_{FRET} - I_{CFP}*BT_{CFP} - I_{YFP}*BT_{YFP}) / I_{CFP}$, where I_X is the background-corrected fluorescence intensity measured in a given channel. BT_{CFP} (donor bleed through) and BT_{YFP} (direct excitation of the acceptor) were calculated by expressing CFP and YFP individually and then determining the ratios of I_{FRET}/I_{CFP} and I_{FRET}/I_{YFP}, respectively.

Immunocytochemistry—Cells were fixed for 15 min in phosphate-buffered saline (PBS) containing 4% paraformaldehyde and immunostained in PBS containing 5% fetal bovine serum and 0.2% Triton X-100. Total neurons were detected using an antibody to MAP2 (Millipore, catalog# MAB3418) and astrocytes with GFAP (rabbit clone, Sigma, catalog #G9269).

References

1. Harris JJ et al. (2012) Synaptic energy use and supply. Neuron 75, 762-777
2. Shepherd GM, Harris KM (1998) Three-dimensional structure and composition of CA3-->CA1 axons in rat hippocampal slices: implications for presynaptic connectivity and compartmentalization. J Neurosci 18, 8300-8310
3. Kang JS et al. (2008) Docking of axonal mitochondria by syntaphilin controls their mobility and affects short-term facilitation. Cell 132, 137-148
4. Scheff SW et al. (2007) Synaptic alterations in CA1 in mild Alzheimer disease and mild cognitive impairment. Neurology 68, 1501-1508
5. Cheng HC et al. (2010) Clinical progression in Parkinson disease and the neurobiology of axons. Ann Neurol 67, 715-725
6. Pathak D et al. (2013) Energy failure: does it contribute to neurodegeneration? Ann Neurol 74, 506-516
7. Choi SW et al. (2011) Intrinsic bioenergetic properties and stress sensitivity of dopaminergic synaptosomes. J Neurosci 31, 4524-4534
8. Verburg J, Hollenbeck PJ (2008) Mitochondrial membrane potential in axons increases with local nerve growth factor or semaphorin signaling. J Neurosci 28, 8306-8315
9. McNay EC et al. (2000) Decreases in rat extracellular hippocampal glucose concentration associated with cognitive demand during a spatial task. Proc Natl Acad Sci U S A 97, 2881-2885
10. Rex A et al. (2009) Stimulus-dependent changes of extracellular glucose in the rat hippocampus determined by in vivo microdialysis. Physiol Behav 98, 467-473
11. Yasuda T et al. (2013) Neurodegenerative changes initiated by presynaptic dysfunction. Transl Neurodegener 2, 16
12. Nemani VM et al. (2010) Increased expression of alpha-synuclein reduces neurotransmitter release by inhibiting synaptic vesicle reclustering after endocytosis. Neuron 65, 66-79
13. Onoa B et al. (2010) Vesicular monoamine and glutamate transporters select distinct synaptic vesicle recycling pathways. J Neurosci 30, 7917-7927
14. Berthet A et al. (2014) Loss of mitochondrial fission depletes axonal mitochondria in midbrain dopamine neurons. J Neurosci 34, 14304-14317
15. Pellerin L, Magistretti PJ (2012) Sweet sixteen for ANLS. Journal of cerebral blood flow and metabolism: official journal of the International Society of Cerebral Blood Flow and Metabolism 32, 1152-1166
16. Voglmaier SM et al. (2006) Distinct endocytic pathways control the rate and extent of synaptic vesicle protein recycling. Neuron 51, 71-84
17. Mozhayeva MG et al. (2002) Development of vesicle pools during maturation of hippocampal synapses. J Neurosci 22, 654-665
18. Sudhof TC, Rizo J (2011) Synaptic vesicle exocytosis. Cold Spring Harb Perspect Biol 3,
19. Pyle JL et al. (2000) Rapid reuse of readily releasable pool vesicles at hippocampal synapses. Neuron 28, 221-231
20. Vilchez D et al. (2007) Mechanism suppressing glycogen synthesis in neurons and its demise in progressive myoclonus epilepsy. Nature neuroscience 10, 1407-1413
21. Foss SM et al. (2013) Multiple dileucine-like motifs direct VGLUT1 trafficking. J Neurosci 33, 10647-10660
22. Imamura H et al. (2009) Visualization of ATP levels inside single living cells with fluorescence resonance energy transfer-based genetically encoded indicators. Proc Natl Acad Sci U S A 106, 15651-15656
23. Imamura H, Noji H (2009) [Imaging of intracellular ATP using novel fluorescent probes]. Tanpakushitsu Kakusan Koso 54, 1937-1944

24. Tsuyama T et al. (2013) In vivo fluorescent adenosine 5'-triphosphate (ATP) imaging of Drosophila melanogaster and Caenorhabditis elegans by using a genetically encoded fluorescent ATP biosensor optimized for low temperatures. Anal Chem 85, 7889-7896

25. Lin RY et al. (1998) Human monocarboxylate transporter 2 (MCT2) is a high affinity pyruvate transporter. J Biol Chem 273, 28959-28965

26. Budzinski KL et al. (2011) Measurements of the acidification kinetics of single SynaptopHluorin vesicles. Biophys J 101, 1580-1589

27. Egashira Y et al. (2015) Monitoring of Vacuolar-Type H+ ATPase-Mediated Proton Influx into Synaptic Vesicles. J Neurosci 35, 3701-3710

28. Smythe E et al. (1989) Formation of coated vesicles from coated pits in broken A431 cells. J Cell Biol 108, 843-853

29. Heidelberger R (2001) ATP is required at an early step in compensatory endocytosis in synaptic terminals. J Neurosci 21, 6467-6474

30. Rangaraju V et al. (2014) Activity-driven local ATP synthesis is required for synaptic function. Cell 156, 825-835

31. Holz RW et al. (1989) MgATP-independent and MgATP-dependent exocytosis. Evidence that MgATP primes adrenal chromaffin cells to undergo exocytosis. J Biol Chem 264, 5412-5419

32. Kuner T et al. (2008) Photolysis of a caged peptide reveals rapid action of N-ethylmaleimide sensitive factor before neurotransmitter release. Proc Natl Acad Sci U S A 105, 347-352

33. Grafstein B, Forman DS (1980) Intracellular transport in neurons. Physiol Rev 60, 1167-1283

34. Keating DJ (2008) Mitochondrial dysfunction, oxidative stress, regulation of exocytosis and their relevance to neurodegenerative diseases. J Neurochem 104, 298-305

35. Choi SW et al. (2012) No consistent bioenergetic defects in presynaptic nerve terminals isolated from mouse models of Alzheimer's disease. J Neurosci 32, 16775-16784

36. Berg J et al. (2009) A genetically encoded fluorescent reporter of ATP:ADP ratio. Nat Methods 6, 161-166

37. Nagase M et al. (2014) On-site energy supply at synapses through monocarboxylate transporters maintains excitatory synaptic transmission. J Neurosci 34, 2605-2617

38. Patel AB et al. (2014) Direct evidence for activity-dependent glucose phosphorylation in neurons with implications for the astrocyte-to-neuron lactate shuttle. Proc Natl Acad Sci U S A 111, 5385-5390

39. Lundgaard I et al. (2015) Direct neuronal glucose uptake heralds activity-dependent increases in cerebral metabolism. Nat Commun 6, 6807

40. Nunnari J, Suomalainen A (2012) Mitochondria: in sickness and in health. Cell 148, 1145-1159

41. Hua Z et al. (2011) v-SNARE composition distinguishes synaptic vesicle pools. Neuron 71, 474-487

42. Madisen L et al. (2010) A robust and high-throughput Cre reporting and characterization system for the whole mouse brain. Nat Neurosci 13, 133-140

43. Yao J et al. (2011) 2-Deoxy-D-glucose treatment induces ketogenesis, sustains mitochondrial function, and reduces pathology in female mouse model of Alzheimer's disease. PLoS One 6, e21788

44. Xia Z, Liu Y (2001) Reliable and global measurement of fluorescence resonance energy transfer using fluorescence microscopes. Biophys J 81, 2395-2402

Chapter II: Dynamin-related protein 1 is required for normal mitochondrial bioenergetic

and synaptic function in CA1 hippocampal neurons

Abstract

Disrupting particular mitochondrial fission and fusion proteins leads to the death of specific neuronal populations; however the normal functions of mitochondrial fission in neurons are poorly understood, especially *in vivo*, which limits the understanding of mitochondrial changes in disease. Altered activity of the central mitochondrial fission protein dynamin-related protein 1 (Drp1) may contribute to the pathophysiology of several neurologic diseases. To study Drp1 in a neuronal population affected by Alzheimer's disease (AD), stroke, and seizure disorders, we post-natally deleted Drp1 from CA1 and other forebrain neurons in mice (CamKII-Cre, Drp1$^{lox/lox}$ (Drp1cKO)). While most CA1 neurons survived for more than one year, their synaptic transmission was impaired, and Drp1cKO mice had impaired memory. In Drp1cKO cell bodies, we observed marked mitochondrial swelling, but no change in the number of mitochondria in individual synaptic terminals. Using ATP FRET sensors, we found that cultured neurons lacking Drp1 (Drp1KO) could not maintain normal levels of mitochondrial-derived ATP when energy consumption was increased by neural activity. These deficits occurred specifically at the nerve terminal, but not the cell body, and were sufficient to impair synaptic vesicle cycling. Although Drp1KO increased the distance between axonal mitochondria, mitochondrial-derived ATP still decreased similarly in Drp1KO boutons with and without mitochondria. This indicates that mitochondrial-derived ATP is rapidly dispersed in Drp1KO axons, and that the deficits in axonal bioenergetics and function are not caused by regional energy gradients. Instead, loss of Drp1 compromises the intrinsic bioenergetic function of axonal mitochondria, thus revealing a mechanism by which disrupting mitochondrial dynamics can cause dysfunction of axons.

Introduction

Mitochondrial dynamics—the balance between mitochondrial fission and fusion—regulate mitochondrial quality control by segregating poorly functioning mitochondria for degradation while mixing the contents of healthy mitochondria *(1,2)*. In neurons, fission uniquely facilitates movement of mitochondria down narrow distal axons *(3,4)*. Disruptions of this movement, and of other neuron-specific functions, may explain why systemic mutations in mitochondrial fusion and fission proteins specifically cause death of neurons. However, the roles and requirements of these proteins also differ *between* neuronal types *(1)*. For example, mutations in the fusion protein optic atrophy 1 (Opa1) cause degeneration of retinal ganglion neurons *(5)*, and mutations in the fusion protein mitofusin-2 (Mfn2) or the fission protein ganglioside-induced differentiation-associated protein 1 (GDAP1) cause peripheral neuropathy (Charcot-Marie-Tooth type *(6,7)*).

There are several potential reasons why specific neurons have unique requirements for fission-fusion proteins. First, the functions of these proteins may be more critical in vulnerable neuronal populations. Recently, we showed that most midbrain DA neurons are uniquely vulnerable to loss of the central mitochondrial fission protein dynamin-related protein 1 (Drp1) *(4)*, a GTPase recruited to fission sites on the outer mitochondrial membrane *(1)*. Loss of Drp1 depletes axonal mitochondria, which is followed by axonal degeneration and neuronal death. However, a subpopulation of midbrain DA neurons survive, despite losing their axonal mitochondria, suggesting that they have lower needs for energy or other mitochondrial functions in their axons *(4)*. Do unique requirements for mitochondrial dynamics underlie differential neuronal vulnerability? Do resistant neurons compensate with other fission or fusion mechanisms? Do the functions of fission differ between neurons? Notably, Drp1 may also have mitochondria-independent functions in synaptic vesicle release *(8)*. Addressing these issues could help elucidate the physiological functions of mitochondrial dynamics in the nervous

system and reveal how shifts in the fission-fusion balance contribute to selective neuronal death in neurodegenerative diseases, including Huntington's disease, Parkinson's disease (PD) and Alzheimer's disease (AD) *(1,4)*, and in other neurologic disorders, including stroke and epilepsy *(9-11)*.

To understand mitochondrial dynamics, it would be useful to know why mitochondrial fission is needed in the nervous system in the first place, and how loss of fission affects mitochondrial functions in specific cell types. Notably, Drp1 knockout did not change respiration or ATP levels in resuspended mouse embryonic fibroblasts (MEFs) *(12,13)*, indicating that mitochondrial fission is not required for respiration in these cells. However, neuronal respiration may be more sensitive to Drp1 loss. Indeed, Drp1 loss markedly decreased the number of mitochondria in axons and the cell body in midbrain DA neurons *in vivo (4)*, and reduced staining of complex I and IV activity in cerebellar neurons *in vivo (14)*. However, it is unclear whether these changes translate into decreased ATP levels in neurons and, if so, whether this decrease compromises neuronal function. Furthermore, Drp1 loss caused cell death in cerebellar and most midbrain DA neurons *(4,14)*, which challenges our ability to dissociate the specific effects of Drp1 loss on mitochondrial function from other non-specific changes that accompany cell death.

To learn how disrupting mitochondrial fission contributes to selective neurodegeneration, we studied the function of Drp1 in CA1 hippocampal neurons and its role in mitochondrial bioenergetics. Surprisingly, despite losing Drp1, most CA1 neurons survived for more than one year *in vivo*, although their function was compromised, leading to deficits in synaptic transmission and memory. To begin to understand how loss of Drp1 causes neuronal dysfunction, we examined the role of Drp1 in mitochondrial bioenergetics. We found that Drp1 is required to maintain normal mitochondrial-derived ATP levels specifically in axons (but not the cell body), and that the loss of this function is unrelated to the distribution of mitochondria within axons.

Results

To selectively delete Drp1 from CA1 hippocampal neurons, we bred floxed Drp1 mice *(13)* with CamKIIalpha (CamKCre) mice, which express Cre recombinase from P19 in a subset of hippocampal neurons, including nearly all CA1 neurons, and in scattered cortical and other neurons throughout the forebrain *(15,16)*. Drp1cKO (Drp1lox/lox;CamKII-Cre) mice were the progeny of Drp1lox/lox and Drp1wt/lox;CamKII-Cre. Drp1WT included control mice (Drp1wt/lox and Drp1lox/lox) lacking the Cre transgene. Drp1cKO mice were born in roughly normal Mendelian proportions (control 46.6%, Drp1 heterozygotes 29.8%, Drp1cKO 23.6%, n=191), and no differences in survival were noted. Drp1cKO and control mice had similar body weights through 10 months of age (Figure 1a).

To confirm Cre expression in CA1 neurons, we crossed Drp1cKO mice with floxed tdTomato reporter mice *(17)*. In 1-month-old tdTomato-CamKCre control (tdTomato$^{lox/wt}$;CamKII-Cre) and Drp1cKO-tdTomato-CamKCre (Drp1$^{lox/lox}$;tdTomato$^{lox/wt}$;CamKII-Cre) mice, ≥98% of CA1 neurons (immunostained for NeuN) showed tdTomato fluorescence, indicating that they expressed Cre (Figure 1b). Conversely, all TdTomato+ cells expressed NeuN, indicating that Cre was only expressed in neurons (Figure 1c). We found that Cre was expressed in ≈50% of cells in the dentate gyrus, though at much lower levels than in CA1 (Figure 1d and e). There was very little expression of Cre in CA3 neurons, but it was also expressed in scattered neurons throughout the cortex (not shown). CA1 neurons in Drp1cKO mice had markedly decreased Drp1 expression at 1 year of age (Figure 1f and g).
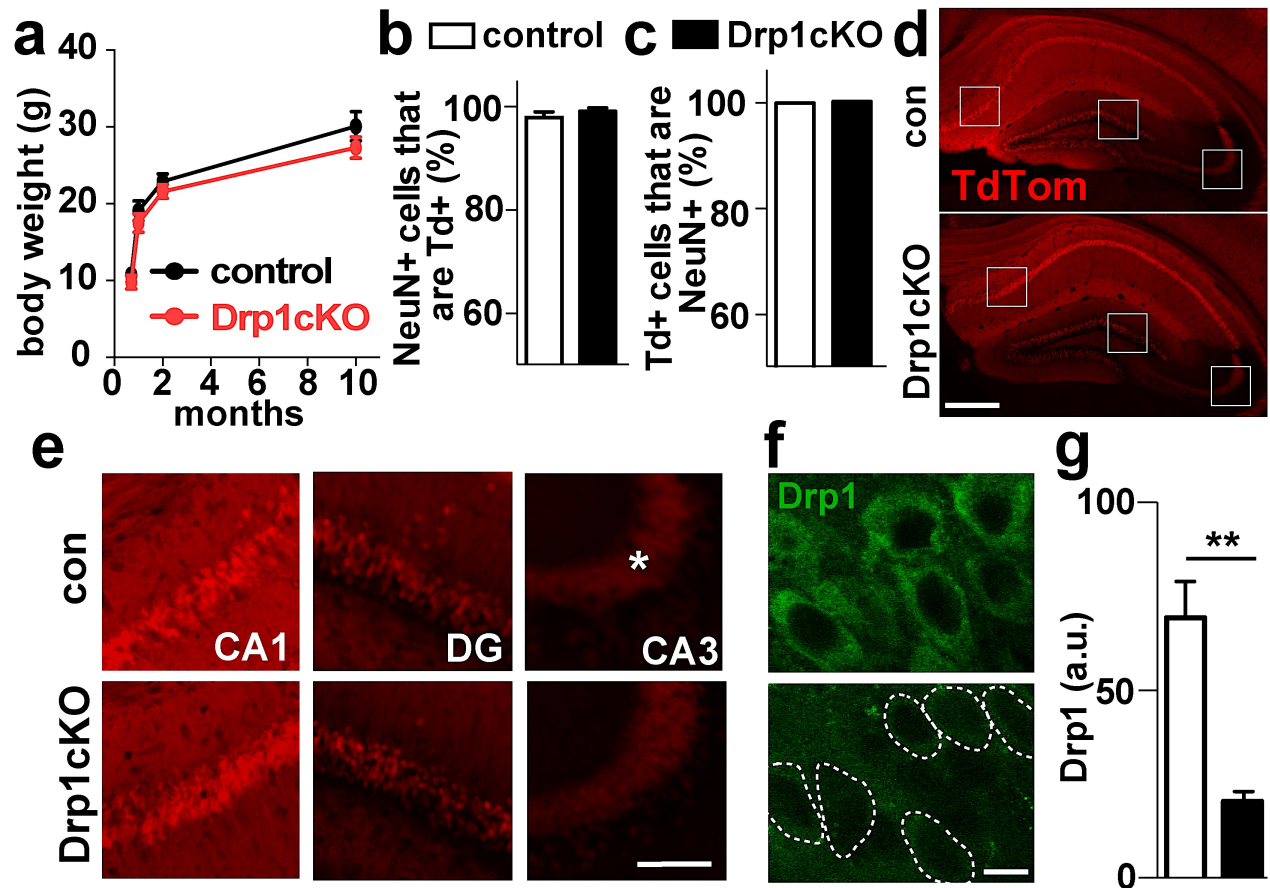
Figure 1. Cre-expression and Drp1 loss in the hippocampus. (a) Weights of Drp1cKO (Drp1$^{lox/lox}$;CamKII-Cre) and control (Drp1$^{lox/lox\ or\ lox/wt}$) mice were similar through 10 months. Data are means ± SEM; n= 6–14 mice/group. (**b**) Cre-expression in CA1 was assessed using tdTomato-CamKCre control (tdTomato$^{lox/wt}$;CamKII-Cre) and Drp1cKO-tdTomato-CamKCre (Drp1$^{lox/lox}$;tdTomato$^{lox/wt}$;CamKII-Cre) mice. Almost all CA1 neurons (marked by NeuN) expressed TdTomato, indicating that they expressed Cre. (**c**) All TdTomato-positive cells expressed NeuN, indicating that all cells expressing Cre are neurons. Data are means ± SEM; n=3 mice/genotype, 4–6 slices/mouse. (**d**) TdTomato was expressed by neurons in CA1 and the dentate gyrus (DG) (≈ 50%), with very little expression in CA3. Scale bar is 400 mm. (**e**) Enlarged insets of CA1, CA3 and DG, indicated by white boxes in (**d**). Almost no TdTomato expression was detected in CA3 neurons, but fibers synapsing on CA3 can be visualized and are marked by an asterisk. Scale bar is 100 mm. (**f**) Drp1 staining of brain sections from 1-year-old control and Drp1cKO mice. Outlines of cell bodies were defined by co-staining with MAP2 (not shown). Scale bar is 10 mm. (**g**) CA1 neurons from Drp1cKO mice had markedly lower Drp1 levels (quantified per cell body) than Drp1WT (control). Data are means ± SEM; **p<0.01 by unpaired two-tailed *t* test, n=4 mice/genotype, 4–6 slices/mouse.

Drp1 loss decreases CA1 volume, but has little effect on the survival of CA1 neurons

Deleting Drp1 promotes loss of most midbrain DA neurons within 1–2 months *(4)*, and most cerebellar Purkinje neurons within 6 months *(14)*. To determine whether Drp1cKO similarly compromises survival of CA1 neurons, we examined the effects of Drp1cKO on CA1 volume (Figure 2a, b and d). Surprisingly, at 5 months, CA1 volume did not significantly decrease, and by 1 year, CA1 volume was still ≈70% of controls (Figure 2d). There was a similar trend towards decreased volume of the entire hippocampus at 13 months (p=0.06) (Figure 2c and e), suggestive of hippocampal atrophy in Drp1cKO mice. The density of NeuN-positive cells within CA1 was not significantly changed even at 1 year (Figure 2f). Considering the decrease in CA1 volume at 1 year, loss of Drp1 may have caused synaptodendritic rarefaction*(18,19)*, in addition to some neuronal death. Nonetheless, most CA1 neurons in Drp1cKO mice survive beyond 1 year, indicating that CA1 hippocampal neurons are more resistant to Drp1 loss than cerebellar Purkinje neurons and most midbrain DA neurons *(4,14)*.
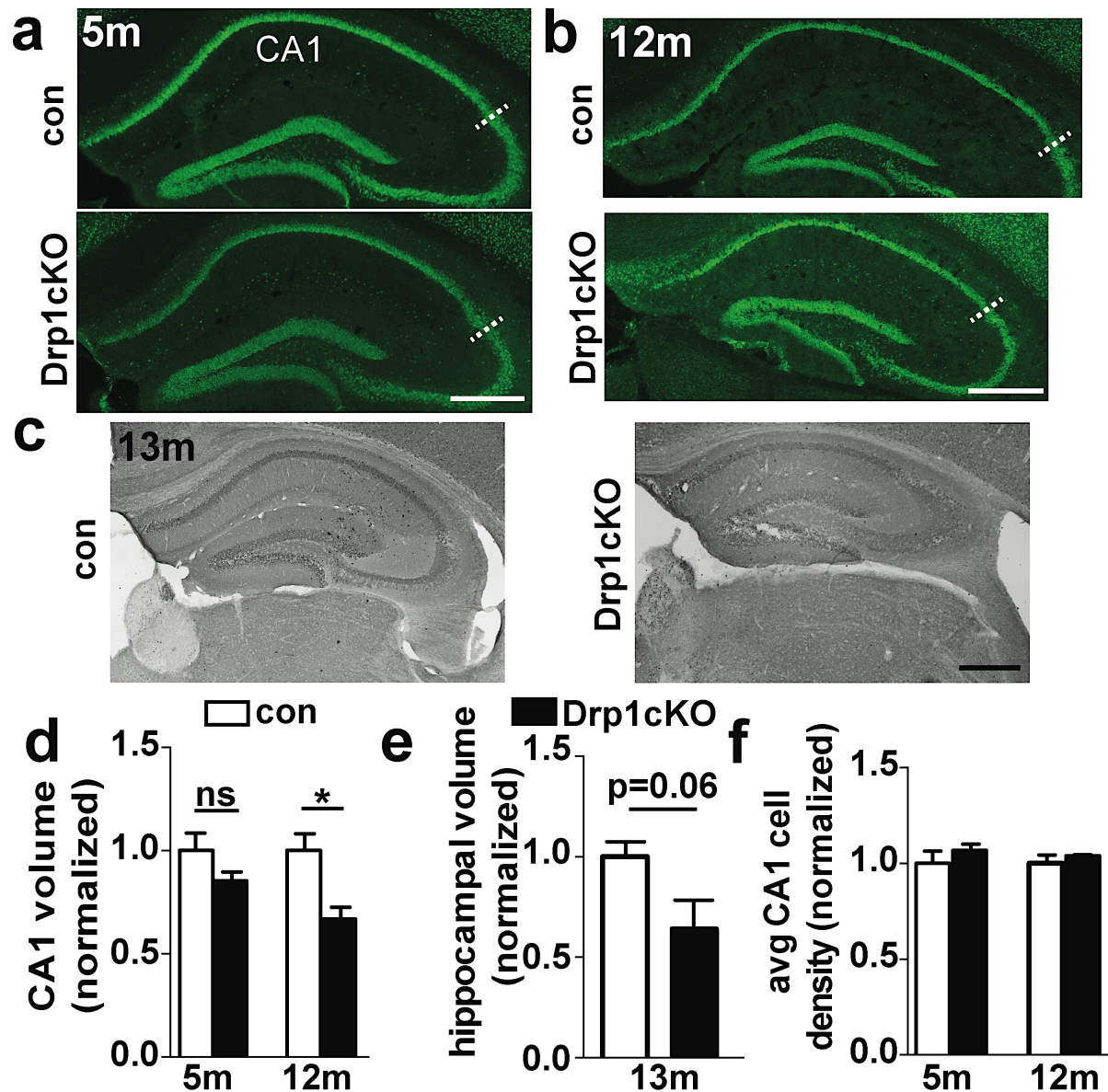
Figure 2. Drp1cKO mice develop atrophy of CA1. (**a** and **b**) NeuN staining of (**a**) 5- and (**b**) 12-month-old Drp1WT (control) and Drp1cKO brain sections, with CA1 defined by calbindin staining (not shown). The lateral margin of CA1 is demarcated by hashed white lines. Scale bars are 400 mm. (**c**) Sections from 13-month-old tdTomato-Drp1cKO (Drp1$^{lox/lox}$;tdTomato$^{lox/wt}$;CamKII-Cre) and tdTomato-CamKCre control (Drp1$^{wt/wt}$;tdTomato$^{lox/wt}$;CamKII-Cre) stained with peroxidase for dsRed to visualize tdTomato+ cells. Scale bar is 400mm. (**d**) CA1 volume of Drp1cKO mice was similar to controls at 5 months, but significantly decreased by 12 months. Data are means ± SEM, ns = not significant, *p<0.05 versus respective control group by two-way ANOVA and Sidak *post hoc* test, n=3 mice/group (with 10–18 slices of hippocampus examined per mouse). (**e**) 13-month-old tdTomato-Drp1cKO mice showed a strong trend towards decreased total hippocampal volume versus controls. Data are means ± SEM; p=0.06 by unpaired two-tailed *t* test, n=3–4 mice/group (with 12-26 slices of hippocampus examined per mouse). (**f**) Drp1cKO showed no change in average CA1 cell density at 5 or 12 months compared to controls. Data are means ± SEM; ns by two-way ANOVA, n=3–4 mice/group (4 slices examined per mouse).

Drp1 is required for normal spatial memory and synaptic function

To determine if Drp1 is required for normal hippocampal function, we examined how Drp1cKO affects spatial learning and memory in the Morris water maze. Drp1cKO mice showed normal learning at 5 and 8 months, based on an analysis of learning curves with a linear mixed effects model[20] (Figure 3a and Figure 4). However, in probe trials carried out 24 and 72 hours after the last training trial, these mice did not favor the target quadrant as well as controls (Figure 3b). Drp1cKO mice performed normally in cued platform trials, had normal swim speeds, and showed no abnormalities in open-field behavior (Figure 3a and Figure 5a and b), indicating that their water maze deficits were not caused by deficits in vision or motor function.

Next, we examined the function of CA1 neurons in acute hippocampal slices with extracellular field recordings in CA1 after stimulating the Schaffer collaterals. Drp1cKO mice had marked lower field excitatory post-synaptic potentials (EPSPs) than controls (Figure 3c). To determine if these effects result from pre- or post-synaptic changes, we examined paired-pulse ratios, which were unchanged in Drp1cKO slices (Figure 3d). These results suggest that pre-synaptic strength was normal in Drp1cKO mice, consistent with the lack of Cre expression in most CA3 neurons (Figure 1d and e). Therefore, deficits in synaptic transmission likely resulted from post-synaptic changes in CA1 pyramidal cells.
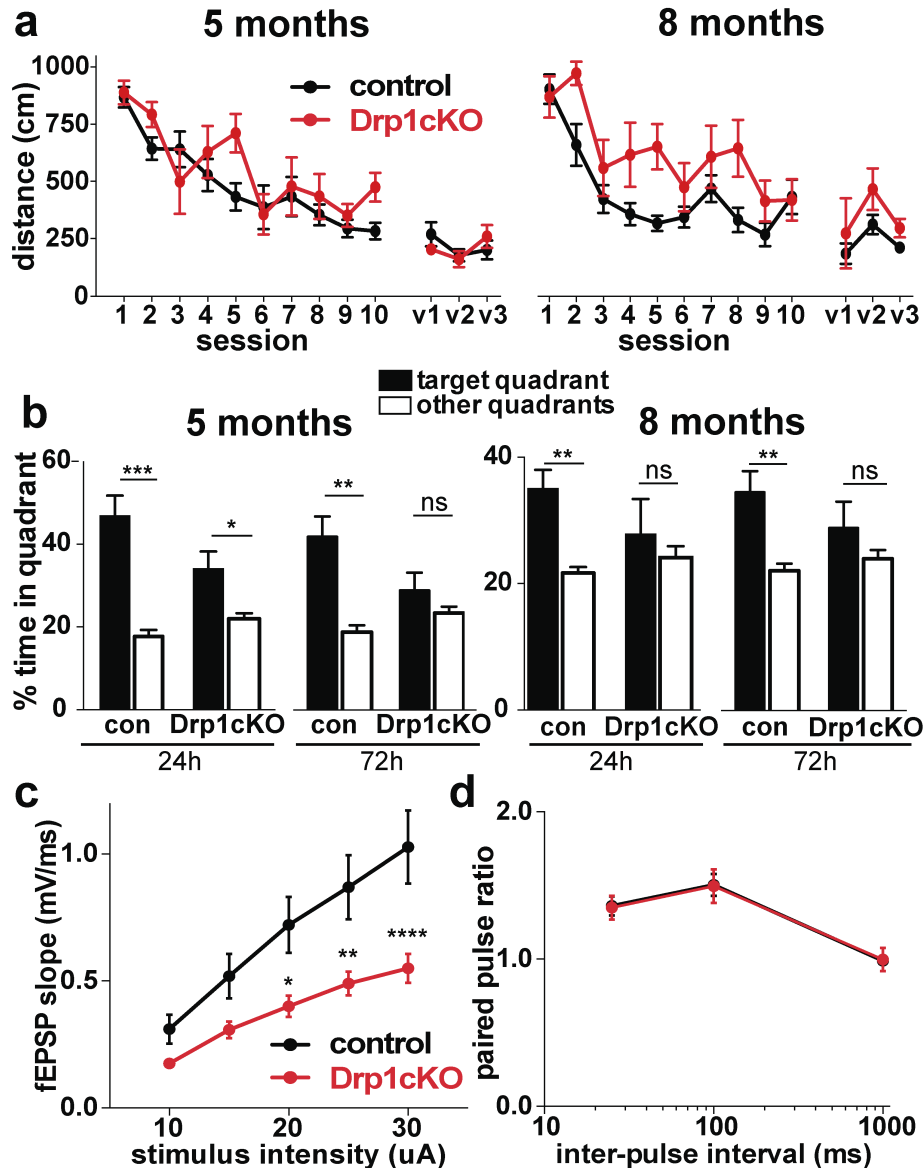
Figure 3. Drp1 loss produces deficits in memory and synaptic transmission. (**a**) Learning was evaluated by Morris water maze (MWM) hidden platform training results (sessions 1–10). Drp1cKO mice did not show significant learning deficits at 5 or 8 months (analyzed with a linear mixed effects model and Holm *post hoc* test). Visible platform training results (days v1–v3) did not differ between Drp1WT (control) and Drp1cKO. (**b**) Memory was evaluated during MWM probe trials at 24 and 72 h, based on the percent time spent in the target quadrant compared to the average of the other three quadrants. Drp1cKO mice showed memory deficits at both 5 and 8 months. Data are means ± SEM; ns = not significant, *$p<0.05$, **$p<0.01$, ***$p<0.001$ by paired one-tailed *t* test, n=7–16 mice/group. (**c** and **d**) The impact of Drp1cKO on the electrophysiologic function of CA1 neurons was assessed in acute hippocampal slices by stimulating the Schaffer collaterals, and performing extracellular field recordings in CA1. At 7–9 months, Drp1cKO mice showed impaired synaptic transmission in CA3-CA1 (input/output slopes), but no change in paired-pulse facilitation compared to Drp1WT (control). Data are means ± SEM; *$p<0.05$, **$p<0.01$, ****$p<0.0001$ by two-way ANOVA with repeated-measures and Sidak *post hoc* test, n=13–17 slices/group.
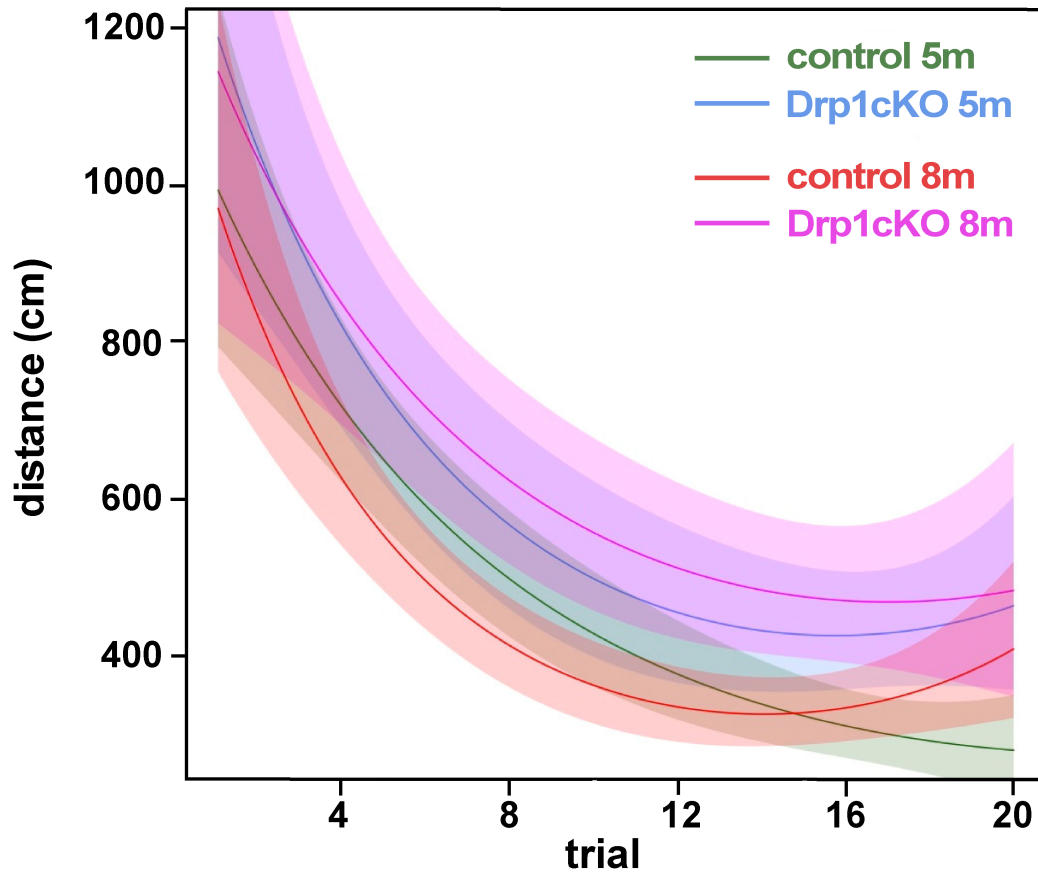
Figure 4. Linear mixed effect modeling of Drp1cKO and control learning throughout Morris water maze. Based on the linear mixed effects model, we estimated hidden distance trajectories for each genotype (i.e., Drp1WT (control) and Drp1cKO) at 5 and 8 months over trials 1–20; 95% confidence intervals are indicated by the shading around each curve.
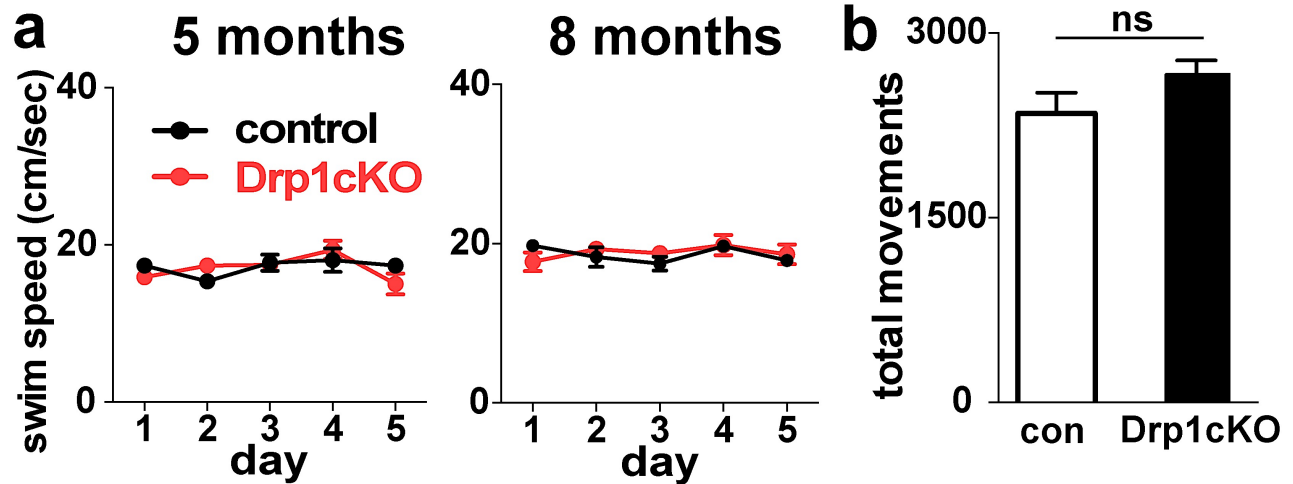
Figure 5. Drp1 loss does not affect motor activity in vivo. a) Drp1cKO and Drp1WT (control) mice showed no differences in swim speed during 5 days of hidden Morris water maze training, suggesting that differences in test results were not due to motor deficits. (**b**) Motor activity in open field showed no difference between the groups. Total movements of 4–month-old control and Drp1cKO mice were measured for 15 min in open field. Data are means ± SEM; ns=not significant by unpaired two-tailed *t* test, n=7 mice/group.

Drp1 loss changes morphology, but not mass or synaptic localization, of mitochondria in CA1 neurons

To understand how Drp1 loss compromises neuronal function, we first examined its effect on mitochondrial morphology and distribution in CA1 neurons. At the cell body, many Drp1cKO neurons developed characteristic swollen mitochondria between 1 and 3 months of age, identified by Tom20 immunofluorescence (Figure 6a and b), similar to those observed after Drp1 deletion in other neuronal types *(4,13)*_ENREF_4. This suggests that mitochondrial fission is lost between 1 and 3 months. Surprisingly, the percentage of neurons with swollen mitochondria decreased somewhat between 5 and 12 months (Figure 6b), despite having low levels of Drp1 (Figure 1f and g). However, unlike the effects of Drp1 loss in DA neurons *(4)*, mitochondrial content (mitochondrial intensity/cytoplasmic area) was unchanged in CA1 neurons, even in 1-year-old animals (Figure 6c). Mitochondrial content was also unchanged in proximal dendrites (Figure 6d, e), and the morphology of dendritic mitochondria was grossly normal despite swollen mitochondria at the cell body. Drp1cKO mitochondria were larger, but their length/width (Feret) ratio was unchanged (Figure 6f, g and h). While the cristae structure was intact in most Drp1cKO mitochondria, some larger mitochondria had disrupted cristae (Figure 6f).

Next, we examined the mitochondria in CA1 axons, particularly those that project to the entorhinal cortex (EC) *(21)*. We visualized the synapses and mitochondria (Figure 6i) by co-injecting Cre-dependent reporter viruses expressing mCherry-synaptophysin and mitoGFP *(4)* into CA1 of 6-month-old Drp1cKO (Drp1$^{lox/lox}$;CamKII-Cre) and CamKCre (CamKII-Cre) control mice. Animals were sacrificed at ≈7 months, and we confirmed that all injections hit CA1, but not areas outside of the hippocampus (not shown). Mitochondria in Drp1cKO axons were not larger than controls (Figure 6j). There was a strong trend for increased size of boutons (Figure 6k). Interestingly, unlike midbrain DA axons *(4)*, the percentage of boutons containing mitochondria

was unchanged (Figure 6I), suggesting that mitochondria in CA1 axons target the synapse independent of Drp1.
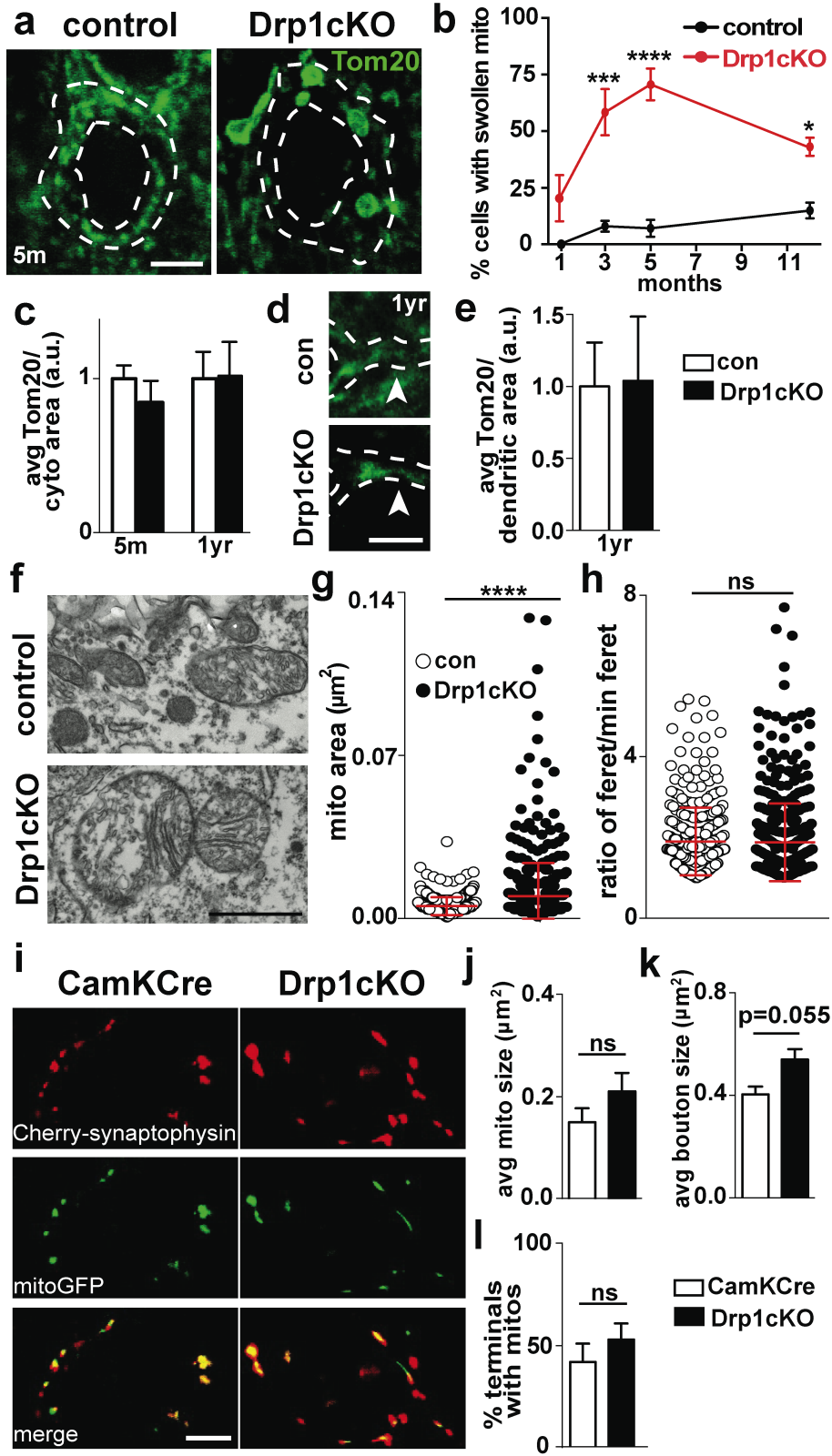
a control   Drp1cKO
                              Tom20
5m

b

c

d   1yr
con

Drp1cKO

e

f control

Drp1cKO

g

h

i CamKCre   Drp1cKO
Cherry-synaptophysin

mitoGFP

merge

j

k   p=0.055

l

50

Figure 6. Drp1 loss alters mitochondrial morphology but fails to deplete mitochondria from CA1 synapses. (**a and d**) Staining for the mitochondrial marker Tom20 in the CA1 of brain slices from 5-month-old (a) and 1-year-old (d) Drp1cKO and Drp1WT (control) mice. Outlines of cell bodies and dendrites (indicated by the stippled outlines and arrowheads) and the nucleus (inner stippled circles) were defined by MAP2 immunostaining (not shown). (**b**) CA1 cells showed an increase in the number of swollen mitochondria between 1 and 3 months, though the numbers decreased somewhat by 12 months. Data are means ± SEM; *$p<0.05$, ***$p<0.001$, ****$p<0.0001$ versus the control group by two-way ANOVA, n=3 mice/group (with 18–76 cells/mouse). (**c**) However, CA1 cells did not show any change in mean Tom20 fluorescence over the cytoplasm (cell body, excluding the nucleus) at 5 months or 1 year (**e**), nor in the dendrites at 1 year. Data are means ± SEM; not significant by two-way ANOVA (cell body) and unpaired two-tailed *t* test (dendrites), n=3 mice/group (with 3–5 slices/mouse). (**f** and **g**) Ultrastructural analysis of CA1 neurons at the cell body revealed larger mitochondria in Drp1cKO mice than Drp1WT (control). Dots on the scatter graph show the areas of individual mitochondria. (**h**) Mitochondria in Drp1cKO and controls were equally round, as measured by ratio of feret diameter over minimum feret diameter. Red bars show mean ± SD; ns = not significant, ****$p<0.0001$ versus the control group by unpaired two-tailed *t* test, n=67–223 mitochondria/group. (**i**) AAVs expressing mitochondria-targeted GFP (mitoGFP; green, to visualize mitochondria) and mCherry-synaptophysin (red, to visualize synaptic boutons) in DIO constructs *(22)* that express only in Cre-expressing neurons *(4)* were co-injected into the CA1 of Drp1cKO (Drp1$^{lox/lox}$;CamKII-Cre) and CamKCre (CamKII-Cre) control mice, and examined at 7 months. (**j**) The size of axonal mitochondria was unchanged by Drp1cKO (**k**), but bouton size showed a trend towards increased size (p=0.055). (**l**) The percentage of synaptic boutons containing mitochondria was unchanged. Data are means ± SEM; ns = not significant versus control group by unpaired two-tailed *t* test, n=3–4 mice/group(total of 86–1279 mitochondria). Scale bars are 5 mm (**a**, d and **i**) and 1 mm (**f**).

Drp1 loss compromises mitochondrial energy production in axons

In Drp1cKO mice, the synaptic deficits and disrupted mitochondrial morphology suggest that mitochondria lacking Drp1 may have impaired bioenergetic function. To examine the effects of Drp1 loss on energy levels, we tested the effect of Drp1 deletion (Drp1KO) on respiration and glycolysis in immortalized MEFs with a Seahorse Extracellular Flux Analyzer (Figure 7). By comparing Drp1KO and control lines, we found that respiration (basal and maximal, after treatment with the uncoupler FCCP) and glycolysis (basal and after treatment with the ATP synthase inhibitor oligomycin) were unaffected by Drp1 loss (Figure 7a and 7b). These findings are consistent with prior studies in which cell lines failed to reveal deficits in the mitochondrial membrane potential or respiration of Drp1KO mitochondria *(12,13)*, and indicate that Drp1 is not required for normal respiratory function in cell lines.

Neurons, however, are preferentially vulnerable to deficits in mitochondrial dynamics *(5-7,23)*. Drp1KO neurons have lower mitochondrial membrane potential at the cell body in culture *(4)*, and cerebellar neurons lacking Drp1 show reduced staining of complex I and IV activity before degeneration *in vivo (14)*. These results suggest neurons selectively require mitochondrial fission for energy production. To determine if Drp1 is required for normal mitochondrial bioenergetic function in neurons, we examined the effects of Drp1 loss on ATP levels in post-natal hippocampal cultures from floxed Drp1 mice *(13)*. We examined how Drp1 loss affects the distribution of mitochondria in axons by co-transfecting cells with either mCherry-Cre (to delete Drp1) or mCherry control, mitoGFP (to visualize mitochondria), and BFP2-synaptophysin (to distinguish axons from dendrites). Loss of Drp1 markedly increased the size of mitochondria within axons (Figure 8a,b) and the distance between mitochondria (Figure 8c). These findings are similar to those in studies that knocked down Drp1 with RNAi *(24)*. The percentage of synaptic boutons containing mitochondria was unchanged (Figure 8d), consistent with our *in vivo* results (Figure 6l).
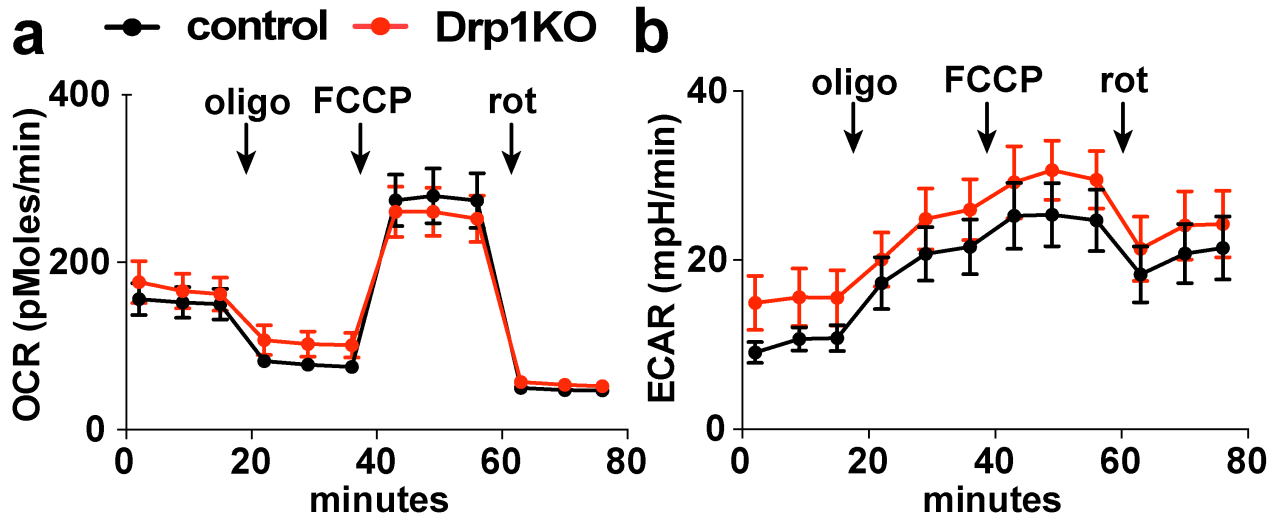
Figure 7. Drp1 loss does not alter respiration or glycolysis in mouse embryonic fibroblasts (MEFs). MEFs lacking Drp1 were cultured, and mitochondrial respiration and glycolysis were measured with a 96-well Seahorse Extracellular Flux Analyzer. (**a**) Drp1KO did not affect basal or maximal (post-FCCP) respiration rates. (**b**) Drp1KO did not significantly affect the rate of extracellular acidification, a surrogate for glycolysis. Oligomycin (oligo, 1 mM) blocks ATP synthase, FCCP (1 mM) uncouples mitochondria, and rotenone (rot, 1 mM) blocks complex I. Data show the average metabolic rates of four wild-type (WT) and knock-out (KO) MEF cell lines, normalized to cell number determined by DAPI staining. Data are means ± SEM; n=8 cell lines/group (18 wells/cell line).
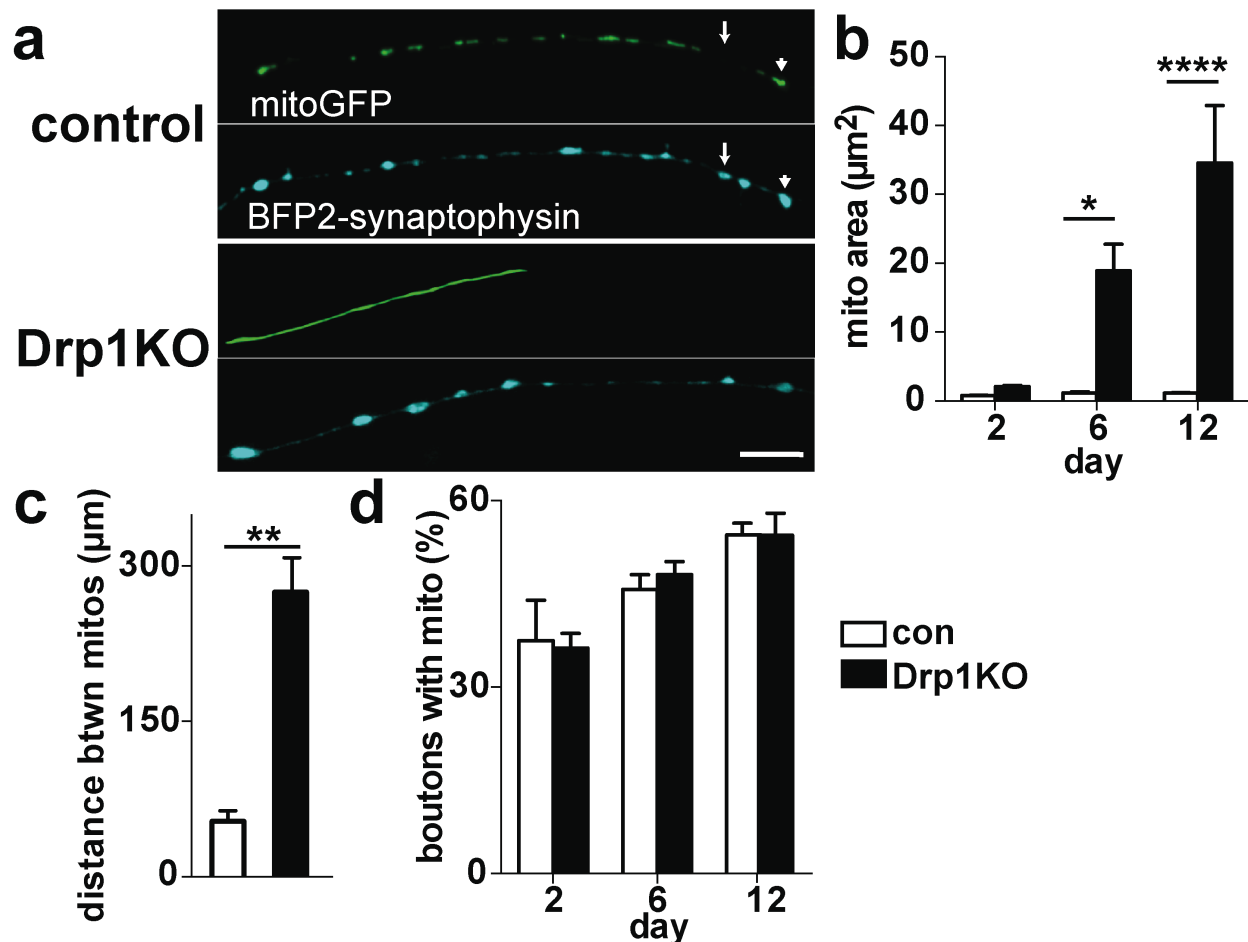
Figure 8. Drp1KO disrupts the distribution of mitochondria at the nerve terminal in cultured neurons. Primary hippocampal cultures from floxed Drp1 mice were co-transfected with either mCherry-Cre (to delete Drp1 (Drp1KO)) or mCherry (control), mitochondria-targeted GFP (to visualize mitochondria) and BFP2-synaptophysin (to distinguish axons from dendrites). (**a**) Drp1KO and control synapses with (arrowhead) and without (arrow) mitochondria. (**b**) Drp1KO axons had significantly bigger mitochondria. Data are means ± SEM; *p<0.05 and ****p<0.0001 versus respective controls by two-way ANOVA with repeated-measures and Sidak *post hoc* test, n=4-5 coverslips/group. (**c**) Drp1KO also markedly increased the distance between axonal mitochondria. **p<0.01, versus control by unpaired two-tailed *t* test, n=3 coverslips/group. (**d**) The proportion of boutons occupied by mitochondria was unchanged. ns by two-way ANOVA, n=4–5 coverslips/group. Scale bar is 10 mm.

To assess how loss of mitochondrial fission affects intrinsic bioenergetic function in neurons, we co-transfected Drp1$^{lox/lox}$ hippocampal neurons with Cre recombinase (to delete Drp1) or a vector control, the ATP-based FRET sensor (ATP1.03^{YEMK}) *(25)*, and mitoFarRed (to visualize mitochondria). We examined ATP levels when neurons were in Tyrodes buffer with standard high glucose (≈30 mM, greater than extracellular brain glucose levels which are ≈1–1.5 mM *(26,27)*) and 10 mM pyruvate (where glycolysis or respiration supports ATP production *(28)*). As expected, Drp1KO failed to change baseline ATP levels at the cell body or synapse (Figure 9a).

Next, we determined if Drp1KO mitochondria have normal bioenergetic function. We examined ATP levels in the acute absence of glucose and with glycolytic inhibitors (2.5–5 mM 2-deoxyoglucose, 1 mM iodoacetate) to force neurons to rely on mitochondrial ATP. Under these conditions, Drp1KO axons could not maintain their ATP levels after acute electrical stimulation (10 Hz for 60 s), which augments ATP requirements in axons by increasing synaptic vesicle cycling *(28)*, (Figure 9b). Therefore, Drp1KO mitochondria cannot maintain ATP levels in axons when energy requirements are increased. In contrast, Drp1KO mitochondria maintained ATP levels at the cell body (Figure 9c), suggesting axonal mitochondria have less capacity to maintain ATP levels than those at the cell body and/or that neural activity selectively increases ATP consumption in axons.

Why does Drp1KO decrease mitochondria-derived ATP in axons? Perhaps Drp1KO mitochondria have intrinsic deficits in their ability to produce ATP. Alternatively, axonal mitochondria are farther apart in Drp1KO neurons (Figure 8c), which may create regional gradients of ATP between them. To distinguish these possibilities, we examined ATP levels in synapses, with and without mitochondria (Figure 9d and e). Surprisingly, despite increased separation between mitochondria in Drp1KO axons, ATP levels were similar in boutons with and without mitochondria. These results suggest Drp1KO axonal mitochondria have intrinsic deficits in their ability to produce ATP.

To determine if decreased ATP in Drp1KO synapses is significant, we examined its impact on synaptic vesicle cycling, a key function that consumes much ATP in axons *(28)*. To observe synaptic vesicle cycling in individual boutons, we used a VGLUT1-pHluorin reporter with a pH-sensitive GFP targeted to the lumen of synaptic vesicles *(29)*. In the acidified lumen of the vesicle, pHluorin does not fluoresce; however, after fusing with the plasma membrane at the synapse and becoming exposed to the alkaline environment, pHluorin fluoresces and is re-quenched with re-internalization and re-acidification of the vesicle *(29)*. Without glycolysis, mitochondrial-derived ATP is required to support pre-synaptic ATP levels and maintain endocytosis*(28)*. However, deleting Drp1, while simultaneously inhibiting glycolysis, completely blocked endocytosis after 10 Hz*60 s stimulation (Figure 9f), which promotes the preferential release of vesicles in the recycling pool *(30)*. Therefore, mitochondria require Drp1 for normal ATP production in axons, and its loss decreases mitochondria-derived ATP sufficiently to impair synaptic vesicle cycling. These bioenergetic defects may underlie the electrophysiologic and functional deficits in Drp1cKO mice *in vivo*.
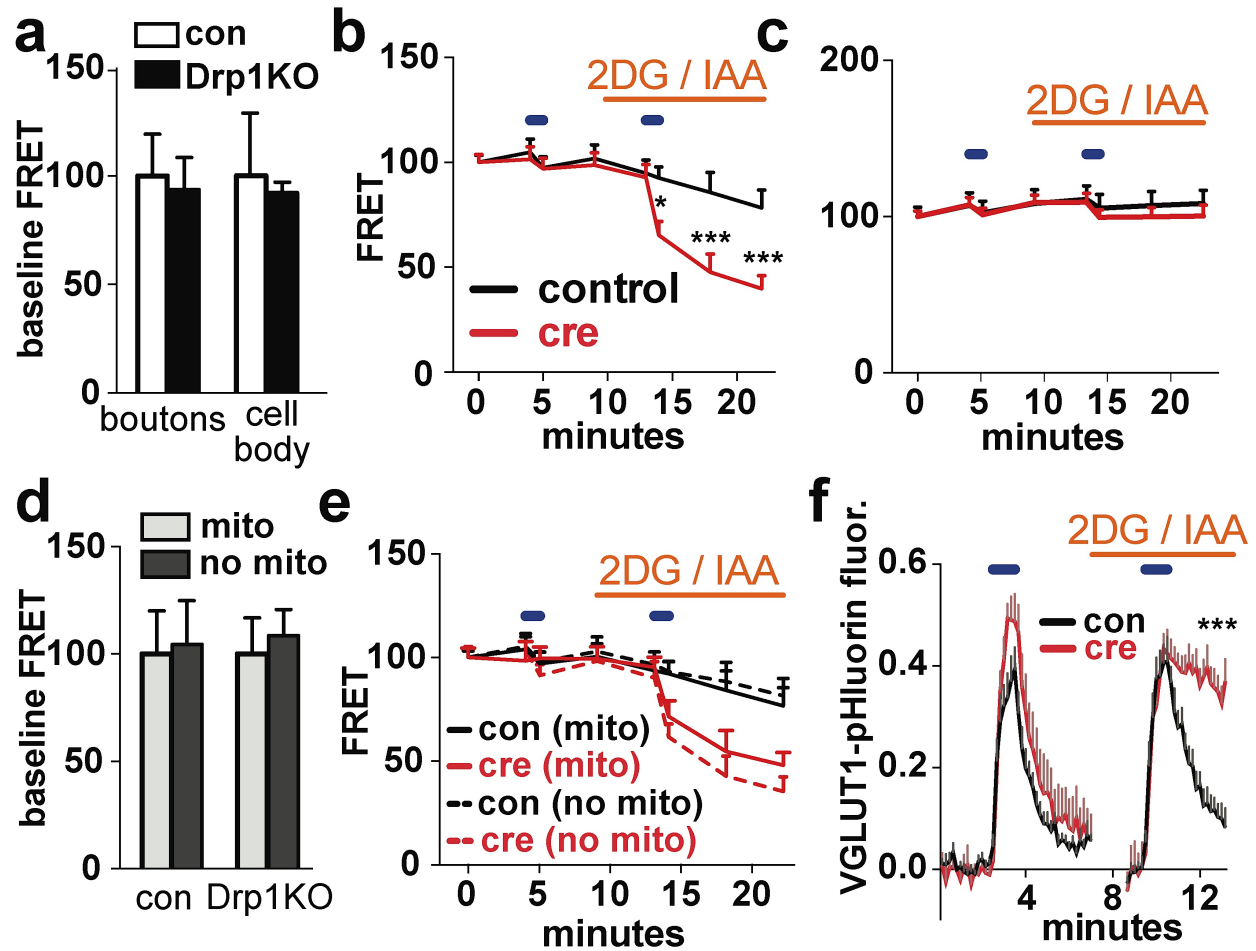
Figure 9. Drp1 is required for normal mitochondrial bioenergetics, specifically in axons. Drp1-floxed primary hippocampal cultures were co-transfected with an ATP-based FRET sensor (ATP1.03^{YEMK}) *(25)*, mitoFarRed (to visualize mitochondria) and either a control vector (con) or Cre (Drp1KO). (**a**) At baseline, Drp1KO and control neurons in pyruvate and glucose showed similar levels of ATP in boutons and at the cell body, as measured by FRET. (**b**) In the acute absence of glucose, Drp1KO neurons showed significantly decreased ATP levels at the synapse after stimulation at 10Hz*60 s (blue horizontal bars) when forced to fully rely on mitochondria for ATP (by blocking glycolysis with glycolytic inhibitors 2-deoxyglucose (2DG) and iodoacetate (IAA) (orange horizontal bar)). (**c**) ATP levels were not depleted at the cell body, even when glycolysis was inhibited. (**d** and **e**) ATP levels were not changed in synaptic boutons, with and without mitochondria, at baseline or after stimulation. Data are means ± SEM; *p<0.05, ***p<0.001 versus control by two-way ANOVA with repeated-measures and Sidak *post hoc* test, n= 10 coverslips/group, (with 80–140 boutons and 10–15 cell bodies sampled per group)). (**f**) VGLUT1-pHluorin was used to measure synaptic vesicle cycling in individual synapses. Drp1KO markedly impaired endocytosis when glycolysis was blocked. Data are means ± SEM; ***p<0.001 versus control group by unpaired two-tailed *t* test for extent of endocytosis [(amplitude endocytosis)/(amplitude exocytosis)]. n=8–10 coverslips/group, (86–111 boutons per group).

Discussion

Disrupted mitochondrial dynamics may contribute to the pathophysiology of neurologic disorders that affect several distinct neuronal populations *(1,9-11)*. However, little is known about why changes in the fission-fusion balance affect neurons more than other cells, or why some neuronal populations are more susceptible than others. Here, we showed that CA1 hippocampal neurons are more resistant to Drp1 loss than previously studied neuronal types, although they still require Drp1 for normal synaptic function. We showed that Drp1 loss in hippocampal neurons compromises the intrinsic function of axonal mitochondria, causing significant deficits in their ability to maintain normal ATP levels and synaptic vesicle cycling.

Mitochondrial fission is required for the bioenergetic function of axonal mitochondria. Why are neurons vulnerable to disruptions in mitochondrial fusion and fission proteins? *(5-7,23)* Mitochondrial fission facilitates targeting of mitochondria down long distal processes, and loss of this targeting likely contributes to neuronal vulnerability *(3,4)*. However, impaired axonal targeting cannot explain deficits in CA1 hippocampal neurons; these cells maintain mitochondria in axons, even without Drp1. Instead, we showed that Drp1 is required for intrinsic respiration of mitochondria in axons, as Drp1KO mitochondria cannot maintain normal ATP levels in their axons when under increased-energy demands.

Several reasons may explain why mitochondrial fission is required specifically for axonal bioenergetics. First, disrupted fission may compromise the intrinsic function of axonal mitochondria, possibly by changing their normal turnover *(31)*, which could cause dysfunctional mitochondria to accumulate. Indeed, the rate of mitochondrial turnover may differ greatly between mitochondria in axons and the cell body *(32)*. Second, axonal bioenergetics may be particularly sensitive to changes in mitochondrial distribution. Drp1KO markedly increased the space between axonal mitochondria in culture, which might cause regional energy gradients that would not occur at the cell body. However, we found mitochondria-derived ATP levels were

similar in Drp1KO boutons with and without mitochondria, despite the increased distance between mitochondria. Whether the distance between mitochondria may be even greater *in vivo* to potentially create these gradients is unknown. Nonetheless, these data suggest that changes in the distribution of axonal mitochondria alone cannot explain the susceptibility of axons to Drp1 loss.

Third, Drp1KO compromises the intrinsic function of mitochondria in the cell body and axons, but the energy demands are greater in axons. Indeed, synaptic transmission is the primary consumer of energy in the brain *(33)*, and in particular, synaptic vesicle cycling appears to require large amounts of energy *(28)*. The disproportionate energy needs in axons may contribute to their early loss in neurodegenerative diseases involving energy failure and in mitochondrial models of these diseases *(4,34-37)*. Additionally, the energy requirement in axons may vary considerably between neuronal types. For instance, SN DA neurons have particularly long projections, large axonal arbors, and poor myelination *(38,39)*, which might require more energy than other neuronal populations.

CA1 hippocampal neurons are relatively resistant to Drp1 loss.

Better understanding why different neuronal populations have unique requirements for specific mitochondrial fission and fusion proteins could shed light on the normal functions of mitochondrial dynamics in the brain and on how disruptions of these functions contribute to neurodegeneration *(1)*. For example, cerebellar Purkinje cells die within 6 months of losing Drp1 *(14)*, but most midbrain DA neurons die within 1 month *(4)*. However, a subset of midbrain DA neurons and their axons are far more resistant to Drp1 loss and survive with very few axonal mitochondria *(4)*. Here, we showed that CA1 hippocampal neurons are also resistant to Drp1 loss, with most surviving to at least 1 year. However, in contrast to resistant midbrain DA neurons *(4)*, Drp1 loss fails to decrease the number of mitochondria in CA1 axon terminals. Although some CA1 terminals might have actually lost mitochondria but atrophied before

examination at 7 months, mitochondria within the surviving CA1 terminals sharply contrast with our observations in Drp1KO midbrain dopaminergic terminals, where surviving axons lose almost all of their mitochondria *(4)*.

Why Drp1 loss differentially affects axonal mitochondria in these two neuron types is unknown. Hippocampal neurons might have distinct pathways for mitochondrial fission that are not present in midbrain DA neurons. However, this seems unlikely: deleting Drp1 impacts mitochondrial morphology at the cell body similarly in both cell types. Alternatively, mitochondria may be preferentially lost from midbrain DA axons because they are longer and more susceptible to differences in axonal motility. However, axonal length alone cannot explain the differences, as even the proximal axons of nigrostriatal DA neurons lacking Drp1 have fewer mitochondria *(4)*. Other steric or undefined differences in mitochondria and/or axons may contribute to differences in axonal targeting. We believe mitochondria in CA1 axons reflect the continued ability of mitochondria to reach the axon after Drp1 is lost, rather than an inability to degrade those mitochondria that reached the nerve terminal before Drp1 was lost. Indeed, we examined the synaptic mitochondria more than 4 months after appearance of the characteristic swollen mitochondria with Drp1 loss at the cell body, a time interval that far exceeds estimates of mitochondrial lifespan *(40)*. Nonetheless, we cannot exclude this possibility, as very little is known about mitochondrial lifespan in neurons and their axons, and Drp1KO could prolong their lifespan by impairing mitochondrial turnover *(41)*.

Implications for Drp1 in the pathophysiology of neurologic diseases.

We showed that CA1 hippocampal neurons—susceptible to degeneration in AD, stroke, and seizure disorders *(42-44)*—require Drp1 for respiration and synaptic function. Interestingly, Drp1 has been mechanistically linked to the pathogenesis of AD in several studies. For example, amyloid-beta may mediate toxicity by increasing Drp1 function and producing excessive fission *(45)*. In contrast, mutant tau produce toxicity by downregulating Drp1 in *Drosophila (46)*. With

the current study, these findings suggest that too much and too little fission are detrimental and that normal neuronal functions may depend on a fine balance between mitochondrial fission and fusion. Changes in mitochondrial fission may also affect the pathophysiology of stroke and seizure, in which Drp1 is a therapeutic target *(9-11)*. Furthermore, AD, seizures and stroke are associated with increased synaptic transmission and impaired metabolism *(32,47-49)*, and changes in mitochondrial fission might contribute to or synergize with these alterations.

Our Drp1cKO mouse provides an excellent model to study the effects of mitochondrial fission in these neurological disorders. This model is the first to both avoid early developmental changes and separate the normal functions of Drp1 from cell death processes, which could confound analyses. Building upon the physiological functions of Drp1 identified here, the Drp1cKO model can now be used to elucidate the role of this protein in models of neurological disorders that target the hippocampus.

Materials and Methods

Animals

Floxed Drp1 mice have been described *(13)*. CamKCre *(15)* and tdTomato mice *(17)* were obtained from Jackson Laboratory. Mice were group-housed in a colony maintained with a standard 12 h light/dark cycle and given food and water ad libitum. Experiments were performed on age-matched mice of either sex. No differences between sexes were noted in any of the experiments. Experiments were conducted according to the *Guide for the Care and Use of Laboratory Animals*, as adopted by the National Institutes of Health, and with approval of the University of California, San Francisco, Institutional Animal Care and Use Committee.

Behavioral testing

Learning and memory was assessed with the Morris water maze (MWM) test *(50)*. Briefly, mice underwent two sessions of hidden-platform training separated by a 2 h intersession rest. Each session consisted of two trials. This training was performed each day for 5 days. The platform was removed and memory probe trials were performed 24 h and 72 h after the last training day. Three sessions of visible platform training were performed the next day after training and probe trials were complete, as a control.

EthoVision video-tracking system (Noldus, Netherlands) was used to record and track mice. Open field locomotor activity was performed as described *(4)*. Briefly, mice were habituated for at least 1 h before recording activity for 15 min with an automated Flex-Field/Open Field Photobeam Activity System (San Diego Instruments, San Diego, CA). All behavioral experiments were performed with the examiner blind to genotype.

Slice preparation and electrophysiology

Transverse hippocampal slices were cut at 400 mm as described *(51)*. Briefly, mice were anesthetized by isoflurane inhalation and sacrificed by decapitation. Their brains were isolated

and immediately placed in an ice-cold solution containing 234 mM sucrose, 2.5 mM KCl, 1.25 mM NaH_2PO_4, 10 mM $MgSO_4$, 26 mM $NaCO_3$, 11 mM glucose, and 1.3 mM ascorbic acid. Brains were sliced on a Leica VS100 vibroslicer (Leica, Germany). Slices were incubated for at least 1 h in oxygenated artificial cerebrospinal fluid (aCSF) containing 126 mM NaCl, 2.5 mM KCl, 1.25 mM NaH_2PO_4, 1 mM $MgSO_4$, 26 mM $NaCO_3$, 10 mM glucose, and 2 mM $CaCl_2$ at room temperature (RT) before being transferred to a submerged recording chamber. Each slice was equilibrated for 10–20 min before recording. For extracellular field EPSP recordings, aCSF-filled glass pipette was placed in the *stratum radiatum,* and the Schaffer-collateral pathway was stimulated with a concentric bipolar electrode. Electrophysiological recordings were filtered, digitized, and acquired with WinLTP (Bristol, UK, RRID:nif-0000-31907). Analysis was performed with WinLTP and Original pro 8.0 (Origin Labs).

Stereotaxic injection of recombinant adeno-associate virus (AAV)

Intracranial injections of AAV1-EF1α-DIO-mitoGFP (8×10^{12} VG/ml) or mCherry-synaptophysin (3×10^{12} VG/ml)*(4)* were performed in ≈6-month-old CamKCre or Drp1cKO mice. Mice were anaesthetized with 2,2,2-tribromoethanol (Alfa Aesar; 500 mg/kg) and secured with a stereotaxic frame (Kopf). Viruses were mixed at a 1:1 ratio and then injected unilaterally (0.5 mL) into the CA1 (A/P, 2.1 mm from bregma; M/L, 2 mm; D/V from skull, 1.4 mm) at a rate of 0.2 mL/min with a Hamilton syringe and cannula (33 gauge). Animals were sacrificed at 7 months of age. Quantification was performed by ImageJ software and the "Analyze Particles" plug-in for synaptic and mitochondrial size, and the ImageJ colocalization plug-in for mitochondrial occupancy at the synapse (RRID:nif-0000-30467).

Histology

For histology experiments, mice were anaesthetized and perfused with phosphate buffered saline (PBS), and then 4% paraformaldehyde. Brains were then removed, postfixed in PFA

(overnight, or for 2h for Drp1 staining), and cryoprotected in 30% sucrose. Coronal brain slices (30 mm or 50 mm for Drp1 levels) were prepared using a sliding microtome (Leica SM2000R). To analyze hippocampal volume, brain slices (40 mm thickness) were frozen in superchilled isopentane and prepared with a Leica cryostat (Leica CM1900).

For immunofluorescence, sections were blocked for ≥1 h in PBS with 0.2% Triton X-100 and 10% bovine calf serum and then incubated with primary antibodies overnight at RT. The following primary antibodies were used: mouse anti-Drp1 (1:200; BD Biosciences clone 8); chicken anti-MAP2 (1:1500; Abcam Cat# ab5392 RRID:AB_2138153); mouse anti-NeuN (1:1000; Millipore Cat# MAB377 RRID:AB_2298772); rabbit anti-Tom20 (1:500; Santa Cruz, Cat# SC-11415, RRID:AB_2207533); mouse anti-MAP2 (1:1000; Millipore Cat# MAB3418 RRID:AB_94856); rabbit anti-calbindin (1:20000; Swant Cat# 300 RRID:AB_10000347); rabbit anti-dsRed (1:1000; Clontech, Cat# 632496 RRID:AB_10015246). Sections were rinsed and incubated for 2 h at RT with the corresponding secondary antibodies: Alexa Fluor 488, 594, or 647 anti-mouse, chicken, or rabbit IgG (1:250–1:500; Invitrogen). For peroxidase staining, sections were incubated with rabbit anti-dsRed, followed by biotinylated goat anti-rabbit IgG (1:300; Vector Laboratories, Burlingame, CA; BA-1000, RRID:AB_2313606), and subsequently streptavidin-conjugated horseradish peroxidase (HRP) (1:300; Vectastain ABC kit, Vector Laboratories). Immunostaining was visualized with hydrogen peroxide and 3,3'-diaminobenzidine (DAB, Sigma).

Brain sections were imaged with a laser-scanning confocal microscope (LSM510-Meta; Carl Zeiss) with a 63x (1.4 NA) PlanApo oil objective, a Nikon Ti-E inverted microscope with a 60x (1.2 NA) PlanApo water objective, or a Keyence inverted microscope BZ-9000 with a 10x (0.45 NA) CFI PlanApo λ objective. Volume was calculated with the Cavalieri principle *(52)*. Quantification of fluorescence and area were performed blind to genotype with MetaMorph software (version 7.7.3.0; Universal Imaging, RRID:SciRes_000136). Neuronal density was calculated by dividing the total fluorescence of NeuN in a fixed area in CA1 (a surrogate for the

total number of neurons in this area) by the average NeuN intensity per CA1 neuron. Quantification of cells with swollen mitochondria was scored blind to genotype, based on the presence of 3 or more swollen mitochondria in a cell (a subjective criteria chosen to distinguish Drp1cKO versus control mitochondria).

Neuronal culture and live imaging

Post-natal hippocampal neuronal cultures were prepared from P0 Drp1$^{lox/lox}$ mice as described *(4)* and transfected via electroporation (Amaxa) with one or more of the following constructs, all expressed in the pCAGGS vector downstream of the chicken actin promoter *(29)*: ATP-YEMK (kind gift of Dr. Noji, Osaka University) *(25)*, mCherry-synaptophysin *(53)*, BFP2-synaptophysin, VGLUT1-pHluorin-ires-mCherry-synaptophysin *(29,53)*_ENREF_31, Cre recombinase *(4)*, mCherry-Cre, mCherry, mitoGFP *(54)*, mitoFarRed, or mitoTagBFP. mitoFarRed and mitoTagBFP were generated by fusing TagRFP657 or TagBFP (kind gifts from Vladislav Verkhusha (Albert Einstein)), respectively, to the mitochondria-targeting sequence, cytochrome C oxidase subunit VIII *(55,56)*. Neurons were cultured for 8–11 days before live imaging or analysis.

Live imaging was performed in Tyrode's medium (pH 7.4; 127 mM NaCl, 10 mM HEPES-NaOH, 2.5 mM KCl, 2 mM MgCl$_2$, and 2 mM CaCl$_2$ with 30 mM glucose and/or 10 mM pyruvate) on a Nikon Ti-E inverted microscope with an iXon EMCCD camera (Andor Technology) and a perfusion valve control system (VC-8, Warner Instruments) controlled by MetaMorph Software. Field stimulation (10 Hz*60 s) was performed with an A385 current isolator and a SYS-A310 accupulser signal generator (World Precision Instruments). Glycolysis was inhibited with 2-DG [2.5–5 mM, Sigma-Aldrich] and iodoacetate [1mM, Sigma-Aldrich].

VGLUT1-pHluorin fluorescence images were obtained (490/20 ex, 535/50 em, Chroma) and regions of interest were drawn over synaptic boutons with MetaMorph software. Synaptic boutons were identified based on co-localization with mCherry-synaptophysin and an increase

in pHluorin fluorescence after applying ammonium chloride (50 mM). For each bouton, the background-subtracted change in fluorescence at each time point was normalized to the fluorescence in ammonium chloride (which estimates the total size of the synaptic vesicle pool) *(30)* measured at the end of each run. The baseline fluorescence intensity was set to zero at t=100 s before the first stimulation and t=170 s before the second stimulation.

For FRET experiments, sequential images were taken in the CFP (430/24 ex, 470/24 em), YFP (500/20 ex, 535/30 em), and FRET channels (430/24 ex, 535/30 em) with an ET ECFP/EYFP filter set (Chroma). Synaptic boutons were identified based on co-localization with mCherry-synaptophysin or determined by morphology for experiments with mitoFarRed. Synaptic boutons were classified as containing or lacking mitochondria based on images taken immediately before and after the imaging run. The FRET/donor ratio was calculated for each bouton as described *(57)*, where FRET = $(I_{FRET} - I_{CFP}*BT_{CFP} - I_{YFP}*BT_{YFP}) / I_{CFP}$, such that I_X is the background-corrected fluorescence intensity measured in a given channel. BT_{CFP} (donor bleed through) and BT_{YFP} (direct excitation of the acceptor) were calculated by expressing CFP and YFP individually and determining the ratios of I_{FRET}/I_{CFP} and I_{FRET}/I_{YFP}, respectively.

Respiration and glycolysis in MEFs

Respiratory and glycolytic rates in four wild-type and four knock-out MEF cell lines were measured with the Seahorse Extracellular Flux (XF) Analyzer 96-well plate reader. MEFs were seeded at 20,000 cells/well 24 h before reading. Then, they were incubated in Seahorse DMEM with 30 mM glucose 1 h before and also during metabolic readings. Respiration and glycolysis were simultaneously measured based on oxygen consumption rates and media acidification, respectively. Oligomycin (1 mM) was injected, followed by FCCP (1 mM) and then rotenone (1 mM). Metabolic rates were normalized to cell numbers based on DAPI counts.

Statistical analysis

To analyze learning by MWM testing, we fit a linear mixed effects model*(20)* of the natural log of the distance traveled on time (trial) using the R Project for Statistical Computing (RRID:nif-0000-10474) package lme4. To allow for nonlinearity in the curves, we included a quadratic effect of time. We included fixed intercepts and slopes for each of the two genotypes, each of the two age groups, possible interactions of these effects, and random intercepts for each mouse to account for the correlation among repeated observations.

The assumptions of a normal distribution (normality) and equal variance among the groups (homoscedasticity) were checked by looking at the distribution of the residuals (difference between observed and fitted values) and the fitted values from the model. A natural logarithmic transformation of the response variable was deemed necessary since the assumptions of normality and homoscedasticity were violated. The estimates from the model were back transformed to the original scale *(58)*.

We used the fitted model to obtain estimates of the mean distance on the fourth and eighth trials for each group. We used the function sim() from the arm package to obtain 5000 simulations of the estimates and compute a 95% confidence interval (CI) around each estimate as the 2.5^{th} and 97.5^{th} quantiles of these draws. We calculated p-values for differences between groups by inverting the simulated CIs around the differences *(59)*. These p-values were corrected for multiple comparisons using the method of Holm.

References

1. Itoh K et al. (2013) Mitochondrial dynamics in neurodegeneration. Trends Cell Biol 23, 64-71
2. Twig G et al. (2008) Fission and selective fusion govern mitochondrial segregation and elimination by autophagy. EMBO J 27, 433-446
3. Verstreken P et al. (2005) Synaptic mitochondria are critical for mobilization of reserve pool vesicles at Drosophila neuromuscular junctions. Neuron 47, 365-378
4. Berthet A et al. (2014) Loss of mitochondrial fission depletes axonal mitochondria in midbrain dopamine neurons. J Neurosci 34, 14304-14317
5. Alexander C et al. (2000) OPA1, encoding a dynamin-related GTPase, is mutated in autosomal dominant optic atrophy linked to chromosome 3q28. Nat Genet 26, 211-215
6. Züchner S et al. (2004) Mutations in the mitochondrial GTPase mitofusin 2 cause Charcot-Marie-Tooth neuropathy type 2A. Nature genetics 36, 449-451
7. Niemann A et al. (2005) Ganglioside-induced differentiation associated protein 1 is a regulator of the mitochondrial network: new implications for Charcot-Marie-Tooth disease. J Cell Biol 170, 1067-1078
8. Li H et al. (2013) A Bcl-xL–Drp1 complex regulates synaptic vesicle membrane dynamics during endocytosis. Nature Cell Biology 15, 773-785
9. Grohm J et al. (2012) Inhibition of Drp1 provides neuroprotection in vitro and in vivo. Cell Death Differ 19, 1446-1458
10. Qiu X et al. (2013) Role of mitochondrial fission in neuronal injury in pilocarpine-induced epileptic rats. Neuroscience 245, 157-165
11. Zuo W et al. (2014) Mitochondria autophagy is induced after hypoxic/ischemic stress in a Drp1 dependent manner: The role of inhibition of Drp1 in ischemic brain damage. Neuropharmacology 86C, 103-115
12. Ishihara N et al. (2009) Mitochondrial fission factor Drp1 is essential for embryonic development and synapse formation in mice. Nat Cell Biol 11, 958-966
13. Wakabayashi J et al. (2009) The dynamin-related GTPase Drp1 is required for embryonic and brain development in mice. J Cell Biol 186, 805-816
14. Kageyama Y et al. (2012) Mitochondrial division ensures the survival of postmitotic neurons by suppressing oxidative damage. J Cell Biol 197, 535-551
15. Tsien JZ et al. (1996) Subregion- and cell type-restricted gene knockout in mouse brain. Cell 87, 1317-1326
16. Horn KE et al. (2013) DCC expression by neurons regulates synaptic plasticity in the adult brain. Cell reports 3, 173-185
17. Madisen L et al. (2010) A robust and high-throughput Cre reporting and characterization system for the whole mouse brain. Nat Neurosci 13, 133-140
18. Marty S, Peschanski M (1995) Effects of target deprivation on the morphology and survival of adult dorsal column nuclei neurons. J Comp Neurol 356, 523-536
19. Li Z et al. (2004) The importance of dendritic mitochondria in the morphogenesis and plasticity of spines and synapses. Cell 119, 873-887
20. Laird NM, Ware JH (1982) Random-effects models for longitudinal data. Biometrics 38, 963-974
21. Iijima T et al. (1996) Entorhinal-hippocampal interactions revealed by real-time imaging. Science 272, 1176-1179
22. Sohal VS et al. (2009) Parvalbumin neurons and gamma rhythms enhance cortical circuit performance. Nature 459, 698-702
23. Waterham HR et al. (2007) A lethal defect of mitochondrial and peroxisomal fission. N Engl J Med 356, 1736-1741
24. Wang X et al. (2009) Impaired balance of mitochondrial fission and fusion in Alzheimer's disease. J Neurosci 29, 9090-9103

25. Imamura H et al. (2009) Visualization of ATP levels inside single living cells with fluorescence resonance energy transfer-based genetically encoded indicators. Proceedings of the National Academy of Sciences of the United States of America 106, 15651-15656

26. McNay EC et al. (2000) Decreases in rat extracellular hippocampal glucose concentration associated with cognitive demand during a spatial task. Proc Natl Acad Sci U S A 97, 2881-2885

27. Rex A et al. (2009) Stimulus-dependent changes of extracellular glucose in the rat hippocampus determined by in vivo microdialysis. Physiol Behav 98, 467-473

28. Rangaraju V et al. (2014) Activity-driven local ATP synthesis is required for synaptic function. Cell 156, 825-835

29. Voglmaier SM et al. (2006) Distinct endocytic pathways control the rate and extent of synaptic vesicle protein recycling. Neuron 51, 71-84

30. Nemani VM et al. (2010) Increased expression of alpha-synuclein reduces neurotransmitter release by inhibiting synaptic vesicle reclustering after endocytosis. Neuron 65, 66-79

31. Tanaka A et al. (2010) Proteasome and p97 mediate mitophagy and degradation of mitofusins induced by Parkin. The Journal of Cell Biology 191, 1367-1380

32. Pathak D et al. (2013) Energy failure-does it contribute to neurodegeneration? Ann Neurol,

33. Harris JJ et al. (2012) Synaptic energy use and supply. Neuron 75, 762-777

34. Scheff SW et al. (2007) Synaptic alterations in CA1 in mild Alzheimer disease and mild cognitive impairment. Neurology 68, 1501-1508

35. Li H et al. (2001) Huntingtin aggregate-associated axonal degeneration is an early pathological event in Huntington's disease mice. J Neurosci 21, 8473-8481

36. Cheng HC et al. (2010) Clinical progression in Parkinson disease and the neurobiology of axons. Ann Neurol 67, 715-725

37. Betarbet R et al. (2000) Chronic systemic pesticide exposure reproduces features of Parkinson's disease. Nature neuroscience 3, 1301-1306

38. Braak H, Del Tredici K (2004) Poor and protracted myelination as a contributory factor to neurodegenerative disorders. Neurobiol Aging 25, 19-23

39. Matsuda W et al. (2009) Single nigrostriatal dopaminergic neurons form widely spread and highly dense axonal arborizations in the neostriatum. J Neurosci 29, 444-453

40. Vincow ES et al. (2013) The PINK1-Parkin pathway promotes both mitophagy and selective respiratory chain turnover in vivo. Proc Natl Acad Sci U S A 110, 6400-6405

41. Tanaka A et al. (2010) Proteasome and p97 mediate mitophagy and degradation of mitofusins induced by Parkin. J Cell Biol 191, 1367-1380

42. Abe K et al. (1995) Ischemic delayed neuronal death. A mitochondrial hypothesis. Stroke 26, 1478-1489

43. Mattson MP, Magnus T (2006) Ageing and neuronal vulnerability. Nat Rev Neurosci 7, 278-294

44. Padurariu M et al. (2012) Hippocampal neuronal loss in the CA1 and CA3 areas of Alzheimer's disease patients. Psychiatria Danubina 24, 152-158

45. Cho D-H et al. (2009) S-nitrosylation of Drp1 mediates beta-amyloid-related mitochondrial fission and neuronal injury. Science (New York, NY) 324, 102-105

46. Duboff B et al. (2012) Tau Promotes Neurodegeneration via DRP1 Mislocalization In Vivo. Neuron 75, 618-632

47. Khurana DS et al. (2013) Mitochondrial dysfunction in epilepsy. Seminars in pediatric neurology 20, 176-187

48. Vossel KA et al. (2013) Seizures and epileptiform activity in the early stages of Alzheimer disease. JAMA Neurol 70, 1158-1166

49. Sims NR, Muyderman H (2010) Mitochondria, oxidative metabolism and cell death in stroke. Biochim Biophys Acta 1802, 80-91

50. Harris JA et al. (2010) Many Neuronal and Behavioral Impairments in Transgenic Mouse Models of Alzheimer's Disease Are Independent of Caspase Cleavage of the Amyloid Precursor Protein. The Journal of Neuroscience 30, 372-381

51. Dubal DB et al. (2014) Life extension factor klotho enhances cognition. Cell Rep 7, 1065-1076

52. Simic G et al. (1997) Volume and number of neurons of the human hippocampal formation in normal aging and Alzheimer's disease. The Journal of comparative neurology 379, 482-494

53. Hua Z et al. (2011) v-SNARE composition distinguishes synaptic vesicle pools. Neuron 71, 474-487

54. Nakamura K et al. (2011) Direct membrane association drives mitochondrial fission by the Parkinson disease-associated protein alpha-synuclein. J Biol Chem 286, 20710-20726

55. Morozova KS et al. (2010) Far-red fluorescent protein excitable with red lasers for flow cytometry and superresolution STED nanoscopy. Biophys J 99, L13-15

56. Subach OM et al. (2008) Conversion of red fluorescent protein into a bright blue probe. Chem Biol 15, 1116-1124

57. Xia Z, Liu Y (2001) Reliable and global measurement of fluorescence resonance energy transfer using fluorescence microscopes. Biophys J 81, 2395-2402

58. Yang J (June 2012) Interpreting Coefficients in Regression with Log-Transformed Variables. Cornell Statistical Consulting Unit. http://www.cscu.cornell.edu/news/statnews/stnews83.pdf.

59. Altman DG BJ (2011) How to obtain the P value from a confidence interval. BMJ 343:d2304,

Chapter III: Mitochondrial fission maintains neuronal ER-mitochondrial contacts and calcium homeostasis in models of Alzheimer's disease

Abstract

Mitochondrial fission occurs in multiple neuronal populations and may contribute to the pathophysiology of neurological diseases, including Alzheimer's disease (AD). However, the normal functions of fission and the critical fission protein, dynamin-related protein 1 (Drp1), in neurons are poorly understood. In particular, Drp1 mediates mitochondrial fission at points of contact between the ER and mitochondria (mitochondrial-associated membranes, MAMs)); however, whether fission affects the number or function of MAMs is unknown. Furthermore, both Drp1 and MAMs are upregulated in AD models, and both were suggested to independently mediate toxicity. Therefore, we hypothesized that MAM function requires fission and that loss of fission may rescue MAM-induced pathogenic changes in a model of AD. To test this, in cultured neurons lacking Drp1 (Drp1KO), we found that Drp1 loss disrupted the number and size of MAMs, revealing a novel function of Drp1 in regulating MAMs in neurons. Surprisingly, expression of AD-associated mutant human amyloid precursor protein (hAPP) synergized with Drp1 to further disrupt calcium homeostasis. Moreover, in vivo, simultaneous Drp1 loss and hAPP expression dramatically and synergistically impaired learning and memory. This work elucidates new functions of mitochondrial fission in neurons and identifies MAMs as a potential site where mitochondrial fission converges to influence the pathophysiology of AD.

Introduction

Mitochondria are dynamic organelles that undergo fusion and fission, and disruptions in the fusion-fission balance may lead to neurodegeneration *(1)*. Indeed, mutations or increased levels of disease-related proteins (for example, amyloid precursor protein (APP) *(2)* and amyloid beta (Aβ) *(3)* in Alzheimer's disease (AD) models) augment mitochondrial fragmentation, indicative of increased relative rates of fission versus fusion. Whether this increased fragmentation actually causes degeneration is unclear; however, inhibiting mitochondrial fission by disrupting the central mitochondrial fission protein Drp1 (dynamin-related protein 1) can protect against the toxicity of several disease-related proteins *(4-6)*.

Inhibiting fision too severely can also be toxic. For instance, Drp1 mutations in patients cause many neurological disorders, ranging from encephalopathy and neonatal lethality to refractory epilepsy *(7-10)*. Additionally, insufficient mitochondrial fission caused by inhibition of Drp1 by mutant tau (a frontotemporal dementia with parkinsonism-17 linked mutation), or disruption of the Parkinson's disease (PD) proteins PINK1 and Parkin, cause excessive mitochondrial tubulation and neurodegeneration in models of AD *(11,12)* and PD *(13-15)*. Despite these implications, we still do not fully understand why neurons need mitochondrial fission and why too little fission leads to neuronal dysfunction and death.

Previous work gives some insight into the importance of fission in neurons. Neurons require Drp1 to target mitochondria down distal axons *(16,17)*. Additionally, Drp1KO may impair mitochondria and neurons by disrupting mitophagy. Fission is widely hypothesized to support mitochondrial function by facilitating the turnover of dysfunctional mitochondria *(18)*. Without fission, mitochondria may be too large for autophagosomes to engulf them, causing dysfunctional mitochondria to accumulate *(19,20)*.

However, mitochondrial fission may also support mitochondrial function more directly. Previous studies show that neurons lacking Drp1 cannot maintain normal levels of mitochondrial-derived ATP at the nerve terminal *(19)*, where high energy levels are required to

support synaptic vesicle cycling *(21,22)*. Drp1 may also be directly involved in other neuronal functions. Indeed, mitochondrial fission by Drp1, which occurs at the points of contact between mitochondria and the ER [known as ER mitochondria-associated membranes (MAMs)], regulates the shape of mitochondria. These data suggest that the extent of mitochondrial fission and/or the shape of the mitochondria may influence the number and/or function of these contacts, even if Drp1 is not present precisely when MAMs form *(23)*. However, an upstream role for Drp1 in MAM formation and function remains to be proven. MAMs critically regulate calcium and lipid transfer between the ER and mitochondria *(24)*, and disrupting these contacts could lead to mitochondrial dysfunction and predispose to disease, especially AD, which has been linked to increases in ER-mitochondria co-localization and function *(25-27)*.

In light of the possible links between Drp1, MAMs and AD, we hypothesized that Drp1-mediated fission is required to maintain MAMs and their functions, and that Drp1-loss protects against upregulated MAMs in AD models. To test this, we examined MAMs in primary neuronal cultures lacking Drp1 (Drp1KO). The loss of Drp1 significantly decreased the number and size of MAMs and also disrupted calcium signaling in the cytosol and ER. In contrast to our hypothesis, expression of mutant human APP (hAPP) decreased the number of MAMs and synergized with Drp1KO to further impair calcium dynamics. We also found that simultaneously decreasing Drp1 and expressing hAPP severely impaired learning and memory in vivo, further suggesting that Drp1-loss synergizes with hAPP to functionally impair neurons instead of rescuing hAPP-induced deficits.

Results

Drp1KO and hAPP disrupt ER-mitochondria contacts

MAMs mark the sites of fission prior to Drp1 recruitment *(23)*; however, Drp1 may still impact

the number, structure, or function of MAMs, even if they can form without Drp1. Given that Drp1

critically regulates mitochondrial morphology *(17,19,20)*, we hypothesized that MAMS would

require Drp1.

We modeled Drp1 loss in primary hippocampal neurons *(19)* by transfecting floxed Drp1

hippocampal neurons with Cre recombinase to remove Drp1 (Drp1KO), or a vector control. As

previously published, Cre expression altered mitochondrial morphology and distribution in vitro

(data not shown) *(19)*. We created three-dimensional (3D) reconstructions of confocal Z-stacks

showing neuronal cell bodies from control and Drp1KO cells expressing eYFP-ER (yellow) and

mito-FarRed (red), and we identified contact regions as areas with persistent co-localization of

the two probes for >3 min (Figure 1a). We found that Drp1KO cells showed significantly fewer

persistent MAMs with a smaller total area, which was also evident in quantification of the most

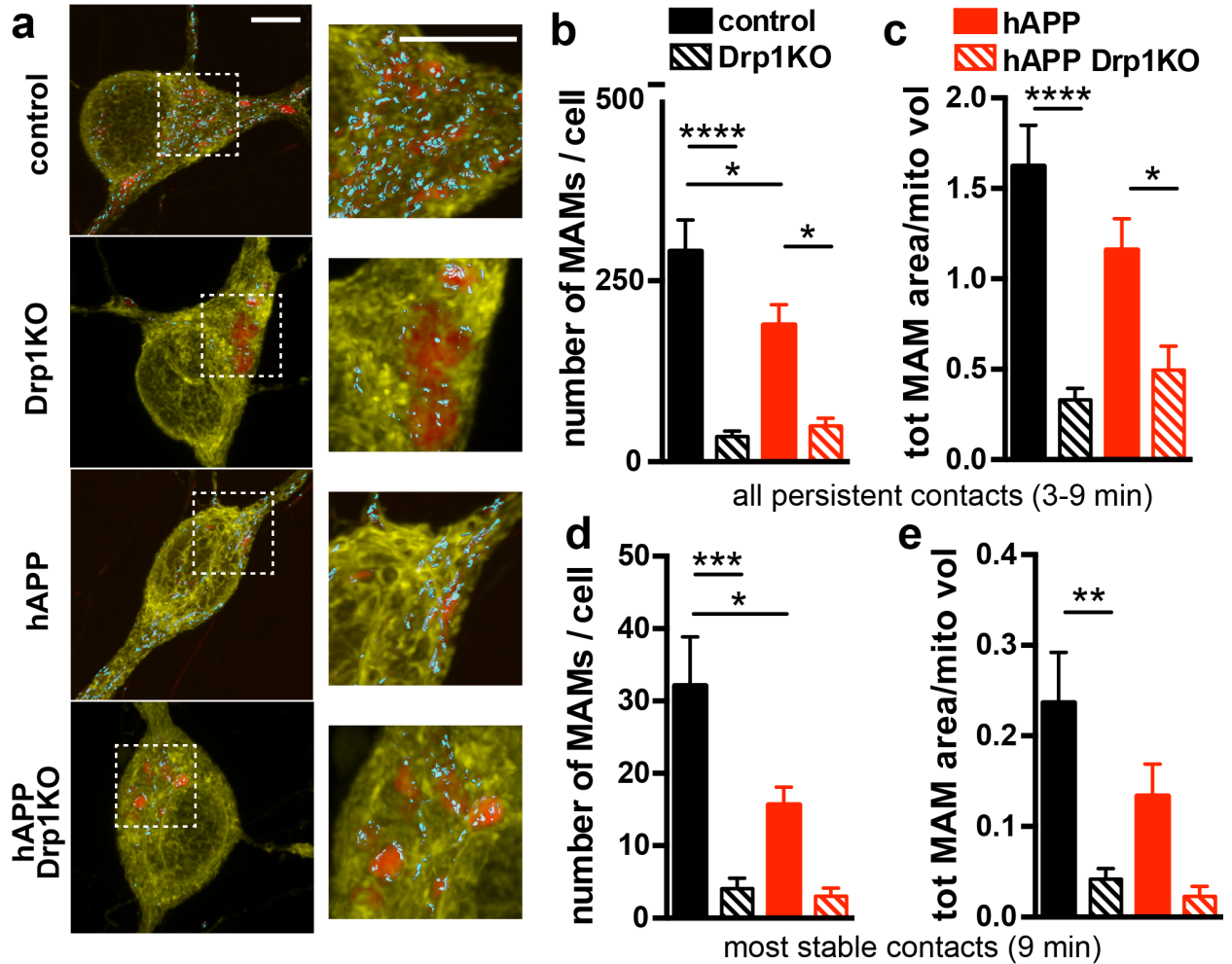stable contacts (which lasted 9 min, Figures 1b-e).

Figure 1: Drp1 loss decreases MAMs in cultured neurons.
Primary hippocampal cultures from floxed Drp1 mice were co-transfected with Cre (to delete Drp1; Drp1KO), mutant hAPP, and/or control vector (control), as well as reporters to visualize the ER (yellow, eYFP-ER) and mitochondria (red, mitoFarRed). (a) Three-dimensional reconstructions of confocal Z-stacks (rendered via max projection) showing neuronal cell bodies with contact regions identified by areas with ER-mitochondria co-localization (cyan; with surface rendering). (b) Drp1KO cells show significantly fewer persistent MAMs (defined as contacts lasting 3–5, 6–8, and 9 min), with or without hAPP expression. hAPP expression alone led to decreased MAM numbers/cell. (c) Drp1KO decreased the total area of ER-mitochondria contacts (normalized to total mitochondrial volume) with or without hAPP. (d and e) In the most stable contacts (lasting 9 min), Drp1KO and hAPP individually reduced MAM number, and Drp1KO reduced total MAM area. n=8–11 coverslips/group (with 11–12 cells/group). Data show mean ± SEM; *p<0.05, **p<0.01, ****p<0.001, ****p<0.0001 by one-way ANOVA with multiple comparisons and Holm-Sidak *post hoc* test. Scale bars are 5 μm.

Although the regulation of MAMs is poorly understood, prior studies show that Aβ and mutant APP increase the number, function, and/or content of MAMs *(26)*. Considering that Aβ may also mediate toxicity by increasing Drp1 function *(28)*, we hypothesized that APP and Drp1 might converge at the level of MAMs, and that deleting Drp1 might prevent the effects of Aβ on increasing MAMs *(29)*. Thus, we overexpressed mutant human APP ((hAPP, Swedish and Indiana mutations) *(30,31)*) in hippocampal neurons by transfection.

We identified neurons expressing hAPP by co-expressing hAPP with a fluorescent reporter, mitoTagBFP. All neurons expressing the reporter also expressed hAPP, which we confirmed with the 8E5 antibody (Elan, Figure 2a). Consistent with previous reports *(32)*, hAPP decreased PSD-95 density significantly (Figures 2b–e), indicating that sufficient levels of hAPP were expressed to produce biologic effects. Interestingly, Drp1 loss alone affected PSD-95 punctae intensity significantly.

After validating the pathogenic effect of hAPP in our model, we examined whether Drp1KO could block hAPP's effect on MAMs. Although Aβ increases the number of MAMs in fixed neurons *(26)*, we found that mutant hAPP significantly decreased the number of MAMs in live neurons. Therefore, in contrast to our hypothesis, Drp1 did not rescue hAPP's effect. Indeed, considering that both Drp1 loss and hAPP decrease MAMs similarly and Drp1KO is able to enhance hAPP's effect, we formulated a new hypothesis that Drp1 loss and hAPP instead converge to disrupt MAM and neuronal function.
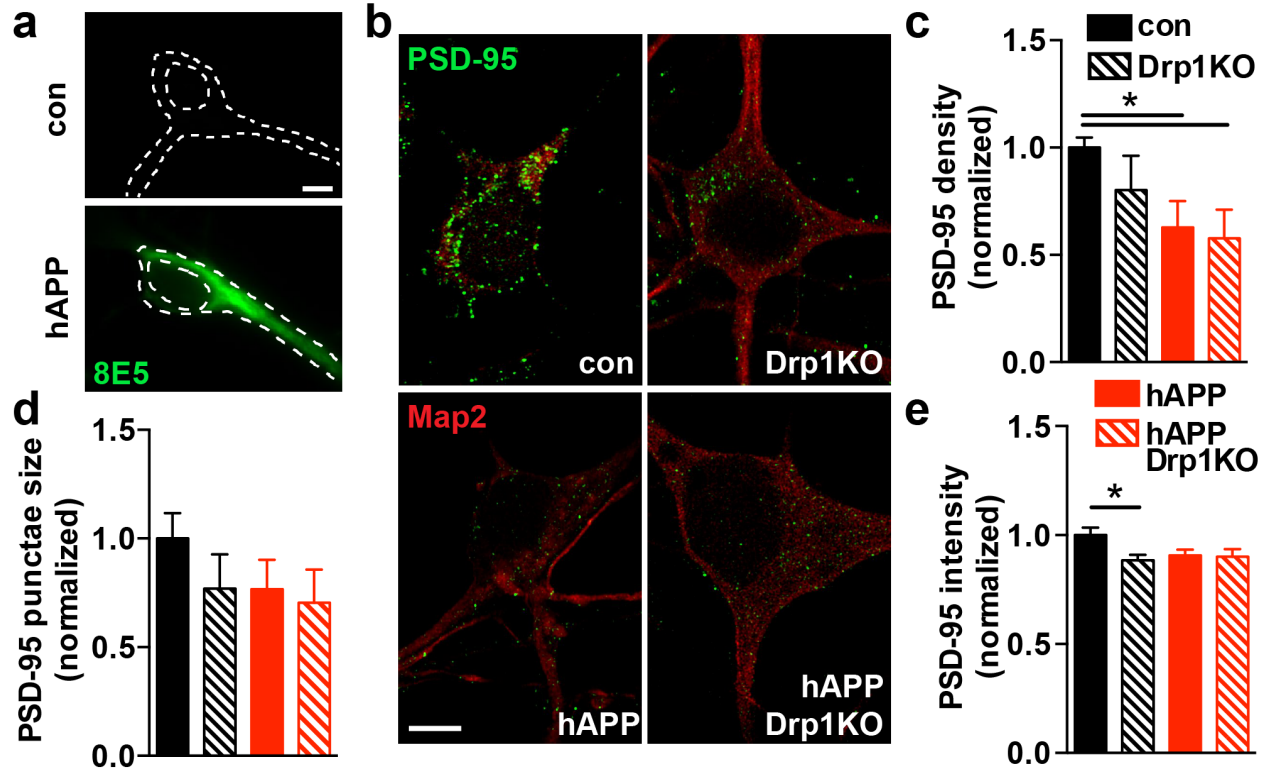
Figure 2: hAPP disrupts PSD-95 post-synaptic densities. Floxed Drp1 hippocampal neurons were co-transfected with Cre (Drp1KO), mutant hAPP, and/or a control vector (con), as well as the mitochondrial marker mitoTagBFP (as a transfection marker). (a) Neurons transfected with hAPP express the protein, as assessed by the 8E5 antibody that is specific to human APP. (b) PSD-95 staining of fixed cultures, with cell body and proximal dendrites marked by Map2. (c–e) hAPP expression and Drp1KO each decreased PSD-95 punctae density, size, and intensity (in particular - hAPP significantly decreased density and Drp1KO significantly decreased intensity). Data are means ± S.E.M.; *p<0.05 by one-way ANOVA and Holm-Sidak *post hoc* test. n=6–8 coverslips/group (with 18–24 cells per group). Scale bars are 5 μm.

Drp1KO and mutant hAPP converge to disrupt calcium dynamics

Cytosolic calcium (cytCa^{2+}) phosphorylates Drp1 to regulate its function *(33,34)*; however, little is known about whether Drp1 normally affects calcium metabolism, especially in neurons. Considering that ER-mitochondria contacts modulate calcium dynamics and transfer from the ER to the mitochondria *(24)*, as well as our finding that Drp1KO decreases the total number and area of these contacts (Figure 1), we next hypothesized that Drp1KO neurons may have impaired calcium homeostasis.

We first examined cytCa^{2+} levels, which are regulated in part by the ER and mitochondria *(35-38)*. We co-transfected Drp1$^{lox/lox}$ primary hippocampal neurons with GCaMP6f (a fluorescent-based calcium sensor with high temporal resolution) and either Cre recombinase (to remove Drp1) or a vector control. We then induced calcium influx and simulated calcium dynamics during neural activity with electrical field stimulation (30 hz * 3 s and 10 hz * 60s to target resting and ready synaptic vesicle pools, respectively *(22)*). hAPP alone increased cytCa^{2+}, showing a significant genotype-effect (Figure 3a and b). Much more prominent, however, was the combination of hAPP and Drp1KO, which dramatically decreased cytCa^{2+}, suggesting that Drp1 is required for calcium dynamics and Drp1KO and hAPP converge to dysregulate cytCa^{2+}. These effects were independent of probe expression level or basal calcium and similar in a subset of neurons with comparable baseline levels of GCaMP6f (Figures 4a and b), indicating that changes in amplitude were not the result of differences in transfection level.

APP is cleaved into multiple products, including Aβ that is secreted from the cell. Prior studies revealed that Aβ impacts both ER-mitochondria contacts and cytosolic calcium *(26,39)*. To understand whether Aβ mediates hAPP's effect, we measured cytosolic calcium dynamics using Drp1$^{lox/lox}$ primary hippocampal neurons transfected with a vector control or Cre recombinase and incubated for 48 hours with either scrambled or recombinant Aβ 1–42. Aβ alone failed to replicate the synergistic hAPP-Drp1KO effects on cytCa^{2+}, despite increasing

cytCa^{2+}, as shown previously (Figures 3c and d) *(39)*. Instead, the hAPP effect may be

mediated through hAPP itself or another cleavage product. We also controlled for the effects of

transfection with the mApple marker. We found that within a subset of mApple expression levels

that did not correlate with amplitude, our results were consistent with Figure 3 (Figures 4c and
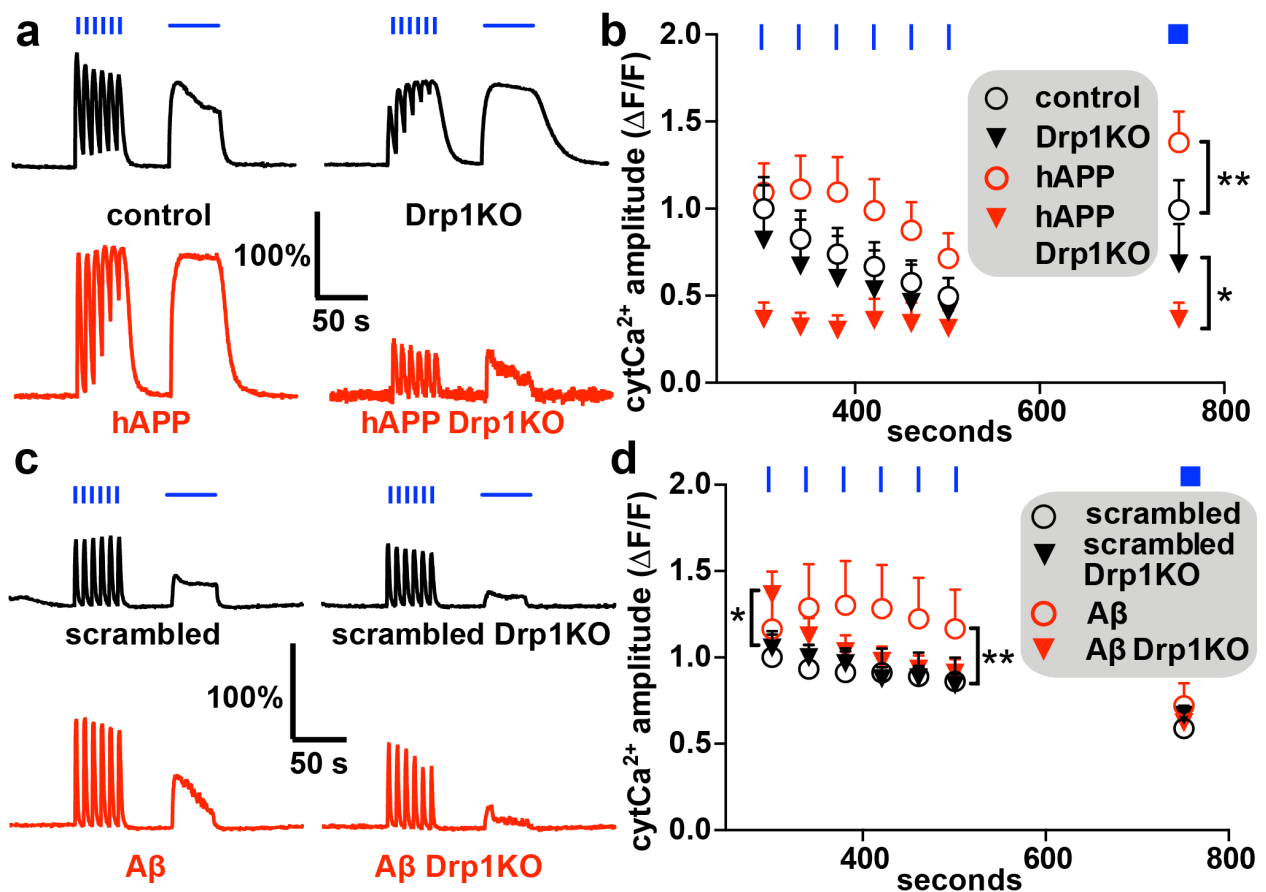
d).

Figure 3: Drp1KO and hAPP converge to decrease evoked cytosolic calcium at the cell body in neurons. Drp1KO and control neurons were co-transfected with the cytosolic calcium (cytCa^{2+}) sensor GCaMP6f *(40)* and either mutant hAPP or vector control (control) and subjected to electrical stimulation at 30 Hz * 3 s (blue vertical bars) and 10 Hz * 60 s (horizontal blue bar). (a) Drp1KO alone did not affect evoked cytCa^{2+}, while hAPP increased it, and hAPP Drp1KO markedly decreased it. n=7–8 coverslips/group (with 17–60 cells/group) (c and d) In lieu of hAPP expression, cultures were treated with 2 μM scrambled or recombinant Aβ 1–42 for 48 h. Aβ slightly increased cytCa^{2+} after 30 Hz * 3 s, but not 10 Hz * 60 s stimulation, and the combination of Drp1KO and Aβ also increased cytCa^{2+} compared to Drp1KO alone. n=13–16 coverslips/group (with 25–126 cells/group). Data are representative traces normalized to baseline and control (a and c) and means ± S.E.M. (b and d); (c) *p<0.05 Drp1KO versus hAPP Drp1KO, **p<0.01 control versus hAPP, (d) *p<0.05 scrambled Drp1KO versus Aβ Drp1KO, **p<0.01 scrambled versus Aβ indicating significance of genotype as a source of variation by two-way ANOVA with multiple comparisons and Holm-Sidak *post hoc* test.
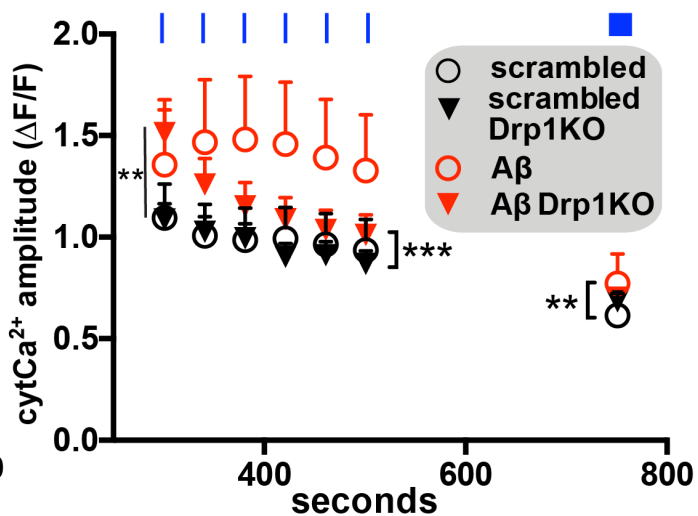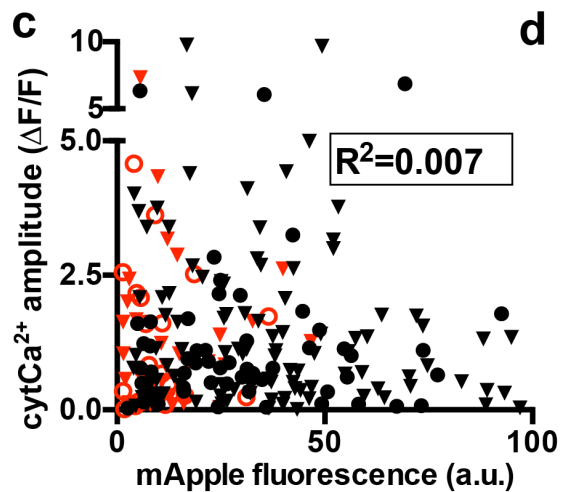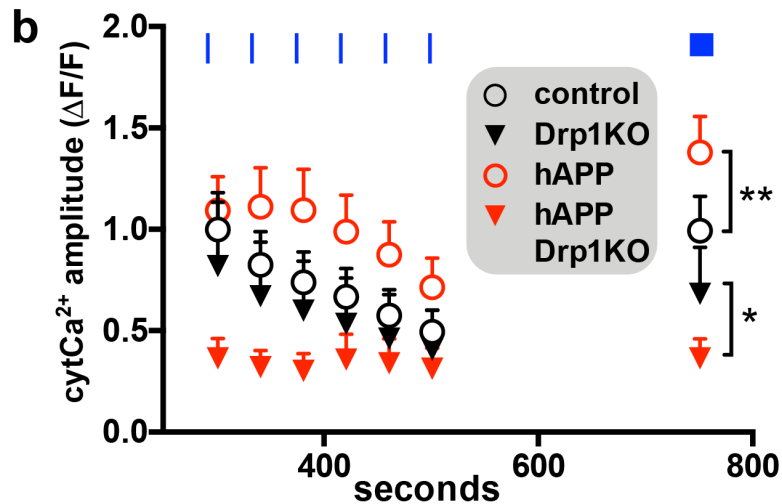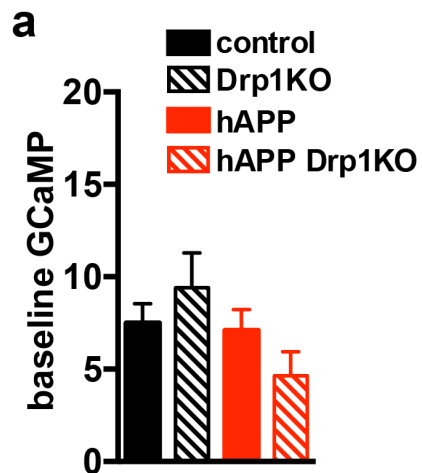
Figure 4: Cytosolic calcium differences are not due to varied transfection levels. Drp1-floxed primary neurons were co-transfected with the cytosolic calcium sensor GCaMP6f **(40)** and a control vector (control), Cre (Drp1KO), and/or mutant hAPP. (a) A subset of each group with similar baseline GCaMP6f values. Data are means ± S.E.M; differences between baselines were not significant by one-way ANOVA with Holm-Sidak *post hoc* test, n=7–8 coverslips/group (with 17–34 cells/group). (b) Within similar baseline values, Drp1KO had no effect on cytCa^{2+} responses, while hAPP increased it. However, Drp1KO combined with hAPP expression markedly decreases evoked cytCa^{2+}. Data are means ± S.E.M.; *p<0.05 Drp1KO versus hAPP Drp1KO, **p<0.01 control versus hAPP indicating significance of genotype as a source of variation by two-way ANOVA with multiple comparisons and Holm-Sidak *post hoc* test. n=7–8 coverslips/group (with 17–34 cells/group). Drp1-floxed primary hippocampal cultures were co-transfected with the cytosolic calcium sensor GCaMP6f, ires-mApple, and a control vector (control) or Cre (Drp1KO). Neurons were treated for 48 h before imaging with 2 µM scrambled or recombinant Aβ 1–42. (c) A subset of each group with similar mApple values did not show a correlation between mApple versus amplitude of calcium response to the first 30 Hz * 3 s stimulation on a per cell basis. Data are individual cells; Pearson correlation coefficient=0.007 with p=0.2043, n=23–106 cells/group. (d) Drp1KO had no effect on the calcium amplitude, while Aβ increased the cytosolic calcium response versus the scrambled control. Data are (c) per cell and (d) means ± S.E.M.; **p<0.01 scrambled Drp1KO versus Aβ Drp1KO (straight line) by two-way ANOVA and Holm-Sidak *post hoc* test; **p<0.01 scrambled Drp1KO versus Aβ Drp1KO, ***p<0.001 scrambled versus Aβ (notched lines) indicating significance of genotype as a source of variation by two-way ANOVA with multiple comparisons and Holm-Sidak *post hoc* test, n=12–16 coverslips/group (with 23–106 cells/group).

We next assessed how Drp1KO-induced changes in MAMs impact calcium homeostasis in the ER and mitochondria, and if these changes underlie the effects of Drp1KO and hAPP on cytCa^{2+}. First, we assessed if Drp1KO compromises calcium release from the ER when stimulated with caffeine (10 mM [41]) to target ryanodine (RYR) receptors, which are enriched near ER-mitochondria contacts [42]. Interestingly, Drp1 loss slightly decreased the amplitude of the cytCa2+ response to caffeine, which was further decreased by hAPP expression (Figures 5a and b). Moreover, hAPP expression, with or without Drp1, caused a longer response and/or slower clearance after stimulation with caffeine (Figures 5a and c).

A decrease in cytosolic calcium after ER release could occur due to multiple possible mechanisms. We explored two possible mechanisms – whether ER calcium is compromised or calcium transfer from the ER to the mitochondria is disrupted, blunting the release into the cytosol. To differentiate between these possibilities, we directly measured calcium release from the ER with a genetically-encoded calcium sensor targeted to the ER, R-CEPIA1er [43], which we co-transfected with vector control, Cre, and/or hAPP. Neither Drp1KO nor hAPP affected ER calcium release (erCa^{2+}) after caffeine stimulation (Figure 5d). These results suggest that Drp1KO and hAPP do not directly disrupt calcium dynamics via ER release, but, instead, may impact ER-mitochondrial calcium transfer. Thus, we directly measured calcium changes in the mitochondria using a genetically encoded calcium sensor targeted to the mitochondria, Cepia2mt [43]. We measured mitoCa^{2+} after electrical field stimulation (30 hz * 3 sec) and ER calcium release stimulated by caffeine (10 mM), and found that neither Drp1KO nor hAPP altered calcium levels in the mitochondria. This result was surprising given that MAM numbers and size were decreased, and may indicate that each remaining MAM has compensatory, upregulated function. Additionally, it suggests that another mechanism may be responsible for the impaired ER-cytosol calcium transfer, such changes in calcium release from inositol triphosphate receptors (ER receptors also enriched in MAMs [24]) or alterations in mitochondrial calcium influx and efflux. Future studies will explore these possible mechanisms.
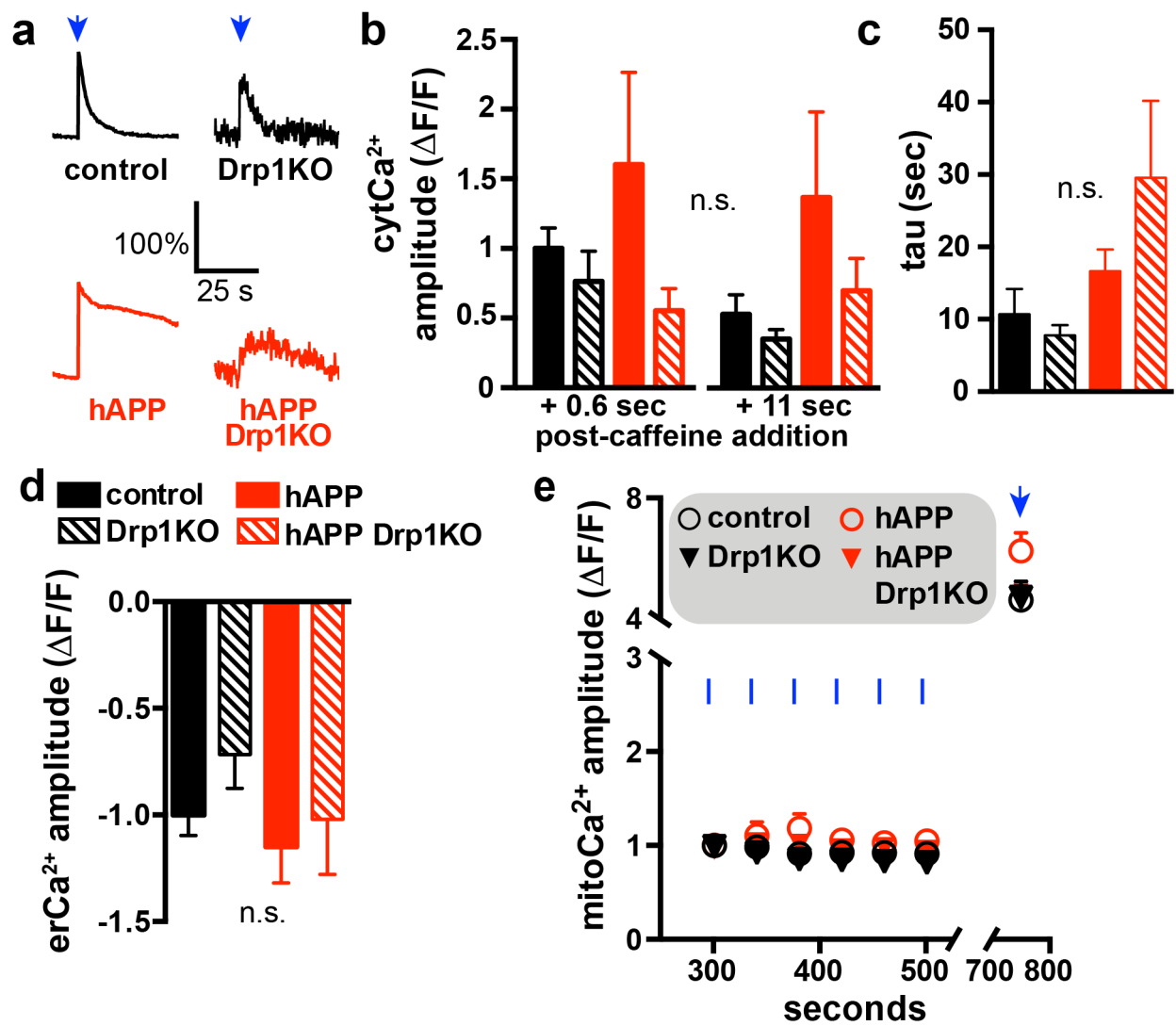
Figure 5: Drp1KO and hAPP disrupt ER calcium responses in the cytosol at the cell body and do not alter calcium responses in the mitochondria. Drp1KO neurons with or without mutant hAPP were co-transfected with the cytosolic calcium sensor GCaMP6f *(40)*, mitochondrial-targeted calcium sensor Cepia2mt, or ER-targeted calcium sensor R-CEPIA1er *(43)*. (a) ER calcium release was stimulated with 10 mM caffeine (blue arrows), and calcium levels were measured in the cytosol. (b) Drp1KO decreased calcium release, hAPP increased it, and hAPP Drp1KO decreased it (+0.6 sec after caffeine addition), albeit with a prolonged (+11 sec) response. (c) The extended response was reflected in the buffering rate–time constant, tau. n=16–21 coverslips/group (with 30–83 cells/group). Data are representative traces normalized to baseline and control (100%) and means ± S.E.M; (b and c) comparisons are not significant (n.s.) by one-way ANOVA with multiple comparisons and Holm-Sidak *post hoc* test, though control versus hAPP Drp1KO were significantly different by an unpaired *t*-test (p<0.05) in (b) and near significant (p=0.0865) in (c). (d) ER calcium was measured using R-CEPIA1er while stimulating release (measured as a decrease in calcium) with caffeine (25 mM). Neither hAPP nor Drp1KO significantly affected the magnitude of ER calcium release. n=8–10 coverslips/group (with 11–17 cells/group). Data are means ± S.E.M; (d) comparisons are not significant (n.s.) by one-way ANOVA with multiple comparisons and Holm-Sidak *post hoc* test. (e) Neither Drp1KO nor hAPP altered calcium transfer to the mitochondria upon electrical stimulation (blue bars) or ER calcium release stimulated with caffeine (blue arrow). Data are means ± S.E.M; caffeine responses were not significantly different by one-way ANOVA with multiple comparisons and Holm-Sidak *post hoc* test. n=10-14 coverslips/group (with 13-23 cells/group).

Calcium changes are energy-independent

ATP-dependent pumps maintain calcium levels in the ER and mitochondria *(44,45)*, and previous work has shown that Drp1 and hAPP impair respiration *(19,46,47)*. Therefore, insufficient energy (rather than direct effects of ER-mitochondria contacts) may disrupt calcium homeostasis. Alternatively, calcium changes could lie upstream of energy production. Optimal cytCa2+ and mitoCa^{2+} are required for efficient oxidative phosphorylation *(36)*, and therefore the calcium changes may cause the respiration deficits. To distinguish between these possibilities, we co-expressed Drp1$^{lox/lox}$ hippocampal neurons with a FRET-based ATP sensor (ATP1.03^{YEMK} *(48)*) and either Cre (to delete Drp1), hAPP, or vector control. To specifically measure mitochondrial-derived ATP, we examined FRET levels in the acute absence of glucose and in the presence of glycolytic inhibitors 2-deoxyglucose (2DG) and iodoacetate (IAA) *(19,22)*. As expected, ATP levels at the cell body were slightly, but significantly, decreased, while Drp1KO axons could not maintain ATP levels *(19)* (Figure 6a and b, Figures 7a and b). However, hAPP expression alone did not cause mitochondrial ATP deficits at the cell body or synapse, nor did it further decrease ATP levels in Drp1KO neurons, even with electrical stimulation to increase energy demands (Figures 6a and b, Figures 7a and b). Moreover, the decrease in mitochondrial-derived ATP at the synapse in Drp1KO neurons was blocked by glucose (as evident during the first stimulation), even though the calcium deficits occur in buffer with glucose. Therefore, decreased ATP does not disrupt calcium homeostasis or ER mitochondrial contacts.

Given the energy requirement needed to maintain calcium gradients, disruptions in calcium dynamics could also impact ATP consumption. We monitored the decline rate in ATP levels after blocking all energy production using oligomycin (to inhibit respiration), 2DG, and IAA (to block glycolysis). However, neither Drp1KO nor hAPP affected ATP consumption, showing no difference immediately after drug addition, when effects would be most acute (Figures 6c and d). These experiments suggest that changes in calcium dynamics do not affect baseline cellular ATP consumption. Notably, this paradigm provides the best available estimate of basal

ATP consumption at a single-cell level, although it may not detect the impact of processes that

are sensitive to even small decreases in ATP levels.
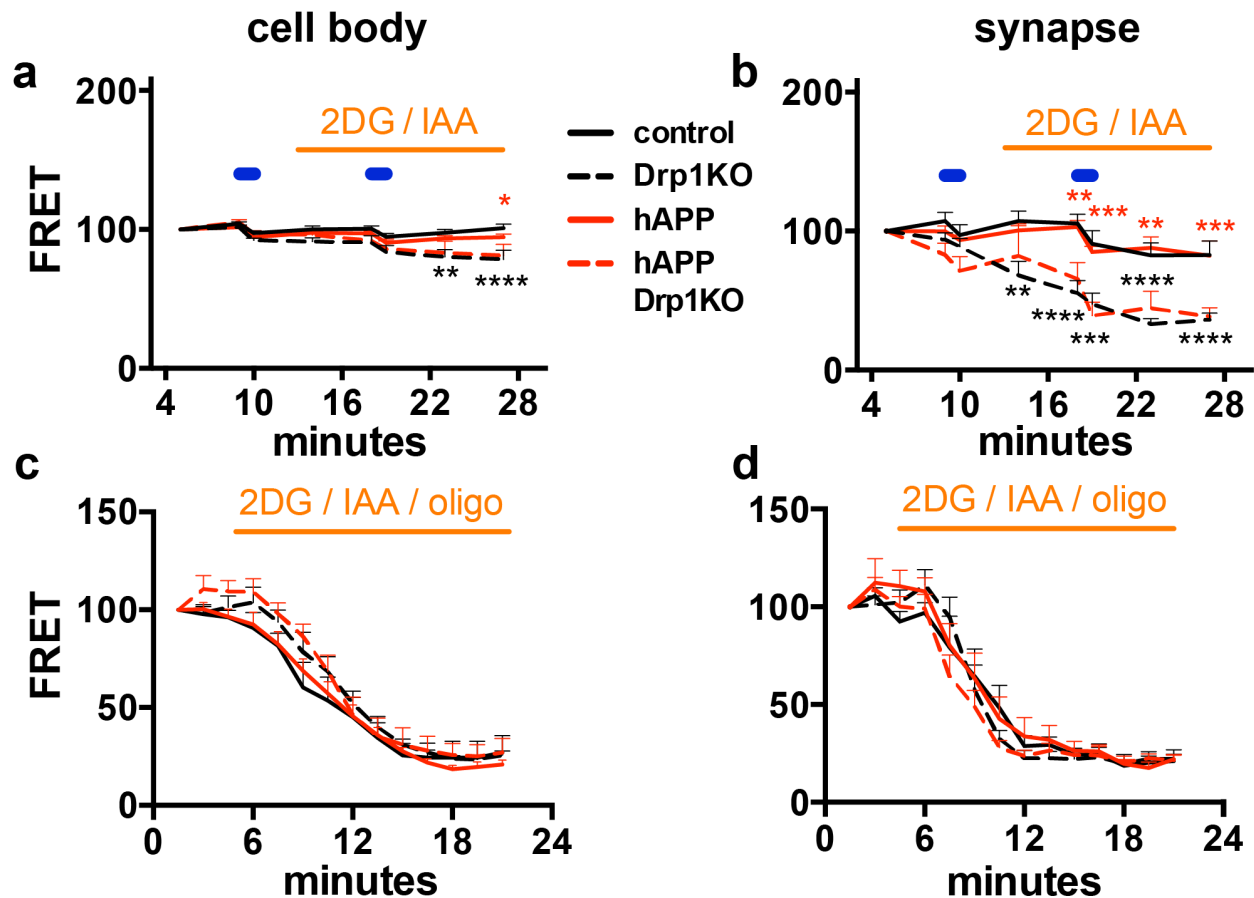
Figure 6: hAPP Drp1KO does not affect mitochondrial-derived ATP production or basal ATP consumption. Drp1KO and control neurons, with or without mutant hAPP, were co-transfected with an ATP-based FRET sensor (ATP1.03^{YEMK}) *(49)*. (a) Drp1KO neurons showed mild significantly decreased ATP levels at the cell body after stimulation at 10 Hz * 60 s (blue horizontal bars) when forced to fully rely on mitochondria for ATP (in the acute absence of glucose combined with glycolytic inhibitors 2-deoxyglucose (2DG) and iodoacetate (IAA); orange horizontal bar). (b) ATP levels were markedly depleted at the synapse when glycolysis was inhibited. hAPP did not affect ATP levels. n=6–12 coverslips/group (with 67–105 boutons and 15–22 cells per group). (c and d) To estimate basal ATP consumption, we simultaneously blocked glycolytic production with 2DG and IAA and respiration with oligomycin (oligo). Rates of consumption did not differ between groups at the cell body (c) or the synapse (d), as indicated by the initial slope of decline in ATP level. n=6–8 coverslips/group (with 56–68 boutons and 6–10 cells per group). Data are means ± S.E.M.; *p<0.05, **p<0.01, ***p<0.001, ****p<0.0001 control versus Drp1KO (black) and hAPP versus hAPP Drp1KO (red) by two-way ANOVA with repeated measures and Holm-Sidak *post hoc* test.
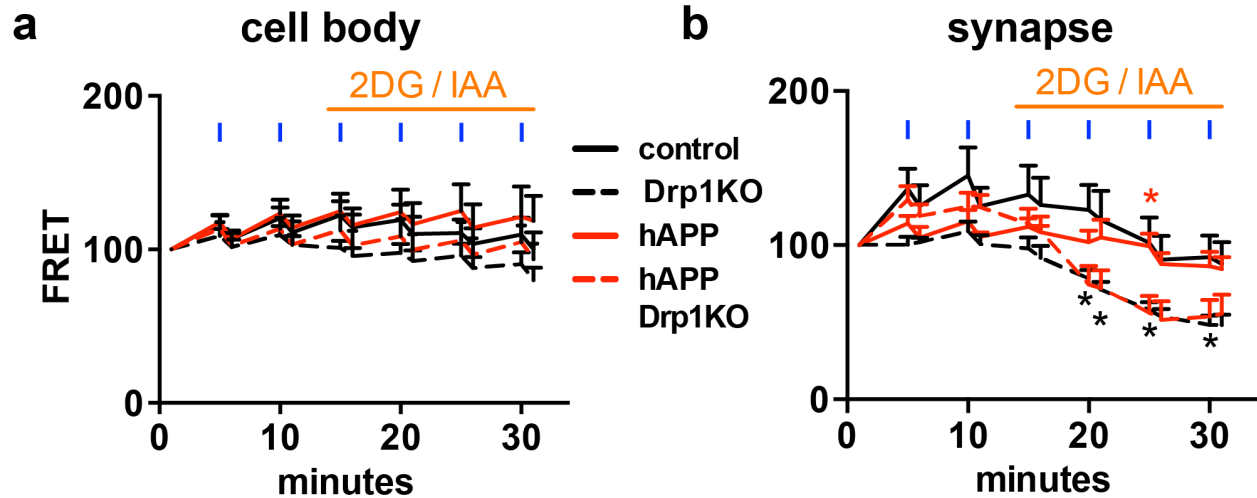
Figure 7: hAPP and Drp1KO do not converge to cause mitochondrial ATP deficits at the cell body or synapse, even during enhanced energy demands. Drp1-floxed hippocampal neurons were co-transfected with an ATP-based FRET sensor (ATP1.03^{YEMK}) *(49)* and a control vector (control), Cre (Drp1KO), and/or mutant hAPP. (a and b) To measure mitochondrial ATP production, glycolysis was blocked with 2-deoxyglucose (2DG) and iodoacetate (IAA) in the acute absence of glucose (orange bar). Neurons were stimulated at 30 Hz * 3 s (blue horizontal bars). (a) No mitochondrial ATP production differences were observed at the cell body. (b) Neurons lacking Drp1 were unable to maintain ATP levels at the synapse; no effect of hAPP was observed. Data are means ± S.E.M.; *$p < 0.05$ control versus Drp1KO (black) and hAPP versus hAPP Drp1KO (red) by two-way ANOVA with repeated measures and Holm-Sidak *post hoc* test. n=7–11 coverslips/group (with 72–106 boutons and 9–14 cells per group).

Drp1 loss and hAPP independently impact histopathological changes in vivo

A pathologic increase in ER-mitochondria contacts has been proposed as a convergent

mechanism of degeneration in AD models *(25,27,29,50)*, and interventions that decrease ER-

mitochondria contacts might be protective. Thus, Drp1KO, which decreases ER mitochondria

contacts, might be protective in AD models. On the other hand, our findings that hAPP

unexpectedly decreased (rather than increased) the number of ER-mitochondria contacts in our

model system, and that cytosolic calcium responses are synergistically decreased by the

combination of hAPP and Drp1KO, raises the alternative possibility that these changes are

actually toxic and that Drp1KO might exacerbate hAPP toxicity.

To distinguish between these possibilities in vivo, we used a Drp1 conditional knock-out

model (Drp1cKO) in which Drp1 is deleted post-natally from a subset of hippocampal neurons,

including essentially all CA1 neurons and in scattered cortical and other neurons throughout the

forebrain (cre is expressed from ≈P19 under the control of the CamKIIalpha promoter in

CamKCre mice) *(19)*. CamKCre mice were crossed with an AD mouse model hAPP-J20 *(51)*,

hereafter referred to as hAPP, which expresses mutant hAPP (Swedish, Indiana) in all neurons

under the PDGF-beta promoter. To generate mice expressing hAPP on a Drp1cKO background

(hAPP;Drp1$^{lox/lox}$;CamKII-Cre), we bred CamKCre;Drp1 $^{wt/lox}$ and hAPP;Drp1$^{lox/lox}$ mice. The

resulting progeny (total n=246 mice) were born in roughly Mendelian proportions, including

controls that lacked Cre (Drp1$^{wt/lox}$ and Drp1$^{lox/lox}$, 26.4%), Drp1 heterozygotes (Drp1$^{lox/wt}$;CamKII-

Cre,13.0%), Drp1cKO (Drp1$^{lox/lox}$;CamKII-Cre, 16.7%), hAPP that lacked Cre (hAPP;Drp1$^{wt/lox}$

and hAPP;Drp1$^{lox/lox}$, 20.3%), hAPP Drp1 heterozygotes (hAPP;Drp1$^{wt/lox}$;CamKII-Cre, 13.8%),

and hAPP Drp1cKO (hAPP;Drp1$^{lox/lox}$;CamKII-Cre, 9.75%). As expected, hAPP mice had

decreased survival (Figure 8a) *(52)*, which was not enhanced by Drp1cKO. All genotypes had

similar body weights through 7 months of age (Figure 8b).
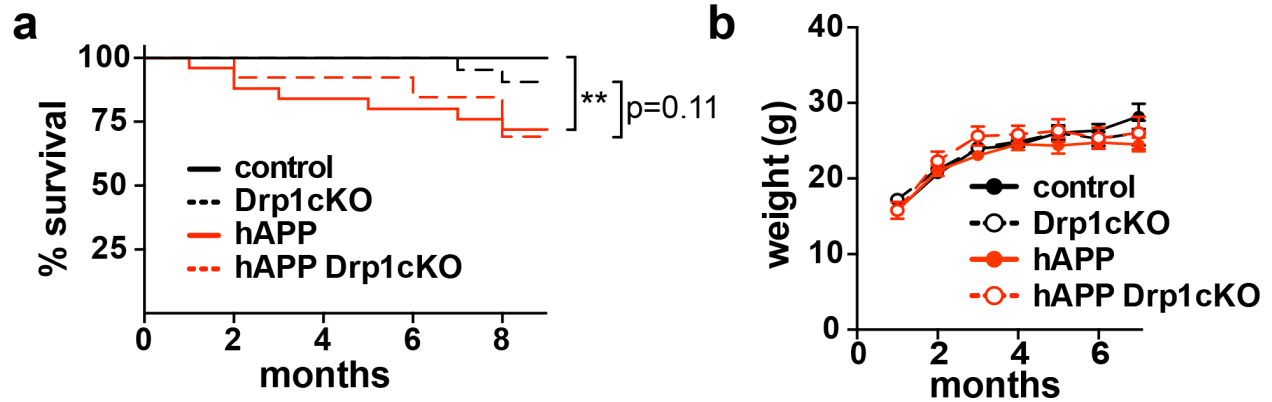
Figure 8: hAPP Drp1cKO survival and weights. (a) Control mice (Drp1$^{wt/lox}$ and Drp1$^{lox/lox}$) versus hAPP (J20-hAPP;Drp1$^{wt/lox}$ and J20-hAPP;Drp1$^{lox/lox}$) and Drp1cKO (Drp1$^{lox/lox}$;CamKII-Cre) versus hAPP Drp1cKO (J20-hAPP;Drp1$^{lox/lox}$;CamKII-Cre) showed significant and near-significant survival differences. Data are means ± S.E.M.; p=0.11, **p<0.01 by Log-rank Mantel-Cox test, n=13–30 mice/group. (b) No weight differences were observed between genotypes up to 7 months. Data are means ± S.E.M.; n=5–42 mice/group/age.

Pathologically, concurrent loss of Drp1 and hAPP did not affect the extent of age-dependent Aβ-plaque deposition (Figures 9a and b). Likewise, hAPP expression alone did not affect hippocampal and CA1 volume and did not enhance the loss of hippocampal volume seen in Drp1cKO mice at 6 or 12 months of age (Figures 9c and d, Figure 10a). It also did not affect CA1 cell density at these time points (Figure 10b). Therefore, hAPP did not affect the mild, age-dependent neuronal loss seen in Drp1cKO mice *(19)*.
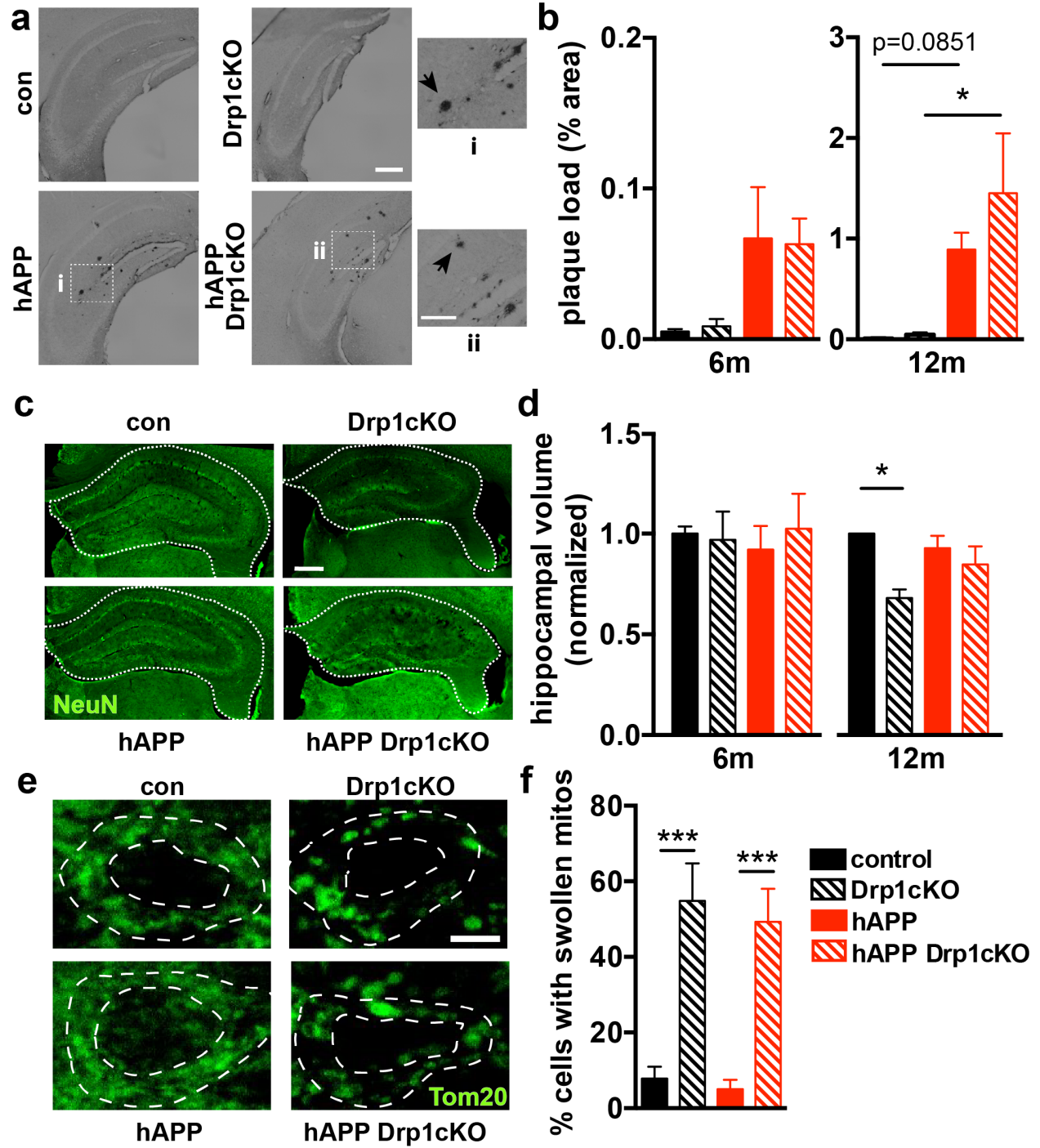
Figure 9: Drp1 loss and hAPP do not converge to affect cell loss, mitochondrial morphology, or Aβ deposition. (a) Aβ deposition was stained with 82E1 antibody in 12-month-old mice. Examples of plaques indicated by arrowheads. Scale bar is 400 µm. (b) hAPP expression led to Aβ deposition at 6 and 12 months, although comparisons did not reach significance until 12 months. n=4–5 mice/group (with 3 slices of hippocampus examined per mouse). (c) Neuronal cell bodies labeled by NeuN staining of 12-month-old mice. Hippocampi indicated by dotted outlines. Scale bar is 400 µm. (d) Hippocampal volume was similar between groups at 6 months. Drp1 loss decreased the hippocampal volume at 12 months. n=3–4 mice/group (with 5–8 slices of hippocampus examined per mouse). (e) Mitochondria in CA1 neurons in hippocampal slices from 6 and 7-month-old Drp1WT (control), Drp1cKO, J20-hAPP (hAPP), and J20-hAPP Drp1cKO (hAPP Drp1cKO) mice, identified by Tom20 immunofluorescence. Outlines of cell bodies and dendrites (outer stippled outlines) and nuclei (inner stippled circles) were defined by Map2 staining (not shown). Scale bar is 5 µm. (f) Drp1KO increased the proportion of cells with swollen mitochondria, while hAPP had no effect. n=4 mice/group (with 3 slices of hippocampus examined per mouse). Data are means ± S.E.M.; p=0.0851, *p<0.05, ***p<0.001 by one-way ANOVA and Holm-Sidak *post hoc* test.
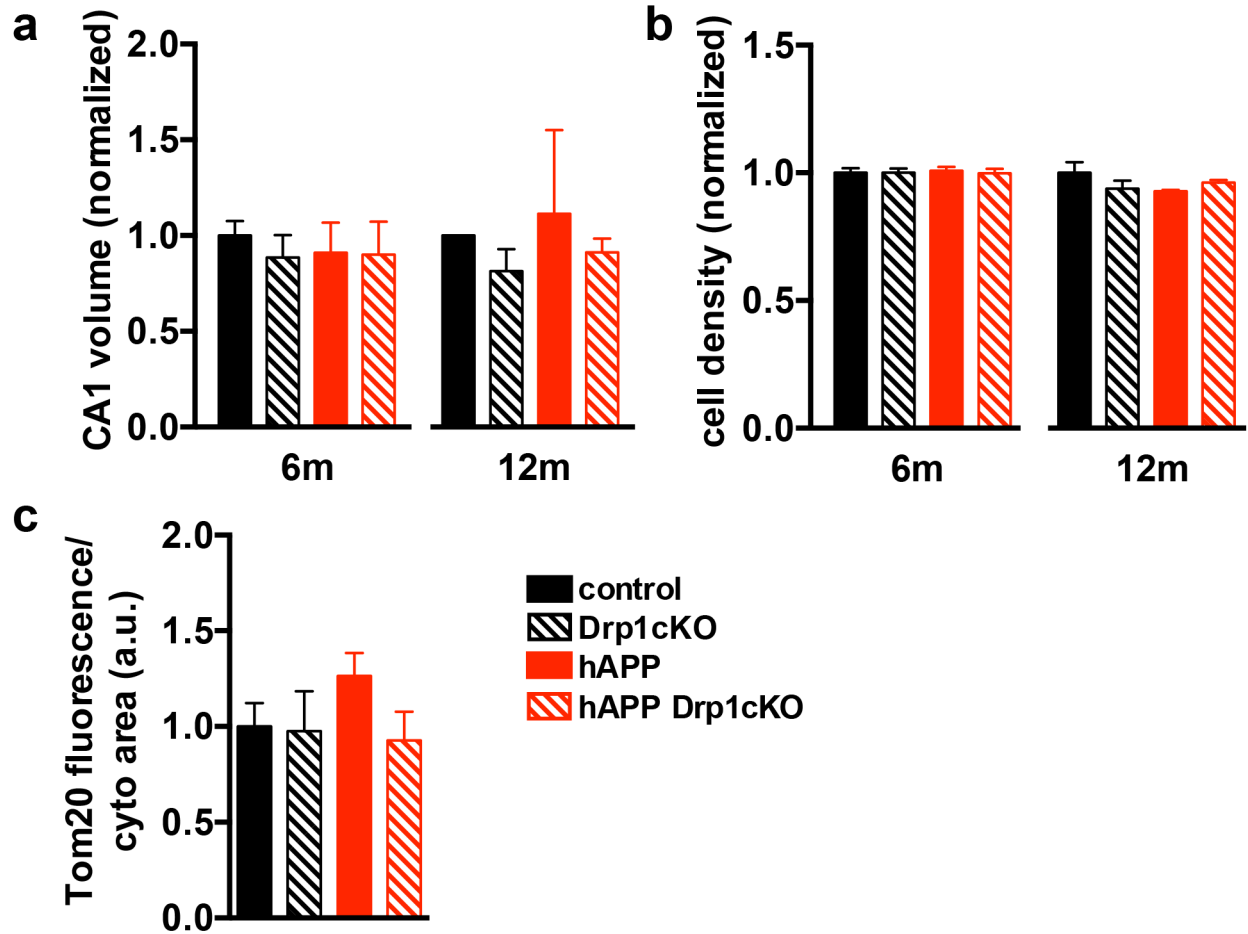
Figure 10: Drp1cKO and hAPP do not impact mitochondrial mass, CA1 volume or cell density. (a) Quantification of NeuN staining of CA1 volume. All groups have similar CA1 volume at 6 and 12 months. Data are means ± S.E.M.; comparisons are not significant by one-way ANOVA and Holm-Sidak *post hoc* test, n=3-4 mice/group (with 3–8 slices of hippocampus examined per mouse). (b) Drp1cKO and hAPP Drp1cKO mice did not show any decrease in CA1 cell density at 6 or 12 months of age. Data are means ± S.E.M.; comparisons are not significant by one-way ANOVA and Holm-Sidak *post hoc* test n=4–5 mice/group (with 8 cells examined per mouse). (c) CA1 cells did not show differences in mean Tom20 fluorescence in the cytoplasm (cell body excluding the nucleus) at 6 months in slices from Drp1WT (control), Drp1cKO, J20-hAPP (hAPP), and J20-hAPP Drp1cKO (hAPP Drp1cKO) mice. Data are means ± S.E.M.; hAPP versus control or hAPP Drp1cKO is not significant by one-way ANOVA and Holm-Sidak *post hoc* test, n=4 mice/group (with 3 slices of hippocampus examined per mouse).

Memory changes occur independently of cell death

We next tested whether there was a functional convergence of hAPP and Drp1KO in vivo, and found that Drp1KO markedly worsened the adverse effects of hAPP on learning and spatial memory. With Morris water maze (MWM) testing, we found that hAPP Drp1cKO mice could not learn the platform location, even over the course of 14 training sessions, indicating a strong functional synergism of Drp1 loss and hAPP in vivo (Figure 11a). In contrast, Drp1cKO mice showed subtle but significant learning deficits, while hAPP mice showed a strong trend for learning deficits, based on rank-order analysis of latency. The spatial deficits of Drp1cKO and hAPP mice were confirmed in probe memory trials 24 and 72 hours after the last training trial; both groups reached the former location of the target platform slower than controls and did not cross its former location as frequently (Figures 11e and f). All genotypes exhibited learning in visible trials, indicating that visible deficits were not wholly responsible for the learning deficits, particularly the severe deficits in hAPP-Drp1cKO (Figure 11b). Controls most quickly improved their learning in visible trials because these trials were held first (before hidden training), and therefore learning the initial task influenced the visible outcome. All genotypes had similar swim speeds (Figure 11c). In open field testing, Drp1cKO, hAPP and hAPP-Drp1cKO mice showed hyperactivity compared to controls (Figure 11d). These results indicate that deficits were not due to motor impairments and that Drp1 loss markedly worsens (rather than prevents) the adverse effects of hAPP on neuronal function. Notably, these synergistic effects of Drp1cKO occurred without changes in mitochondrial morphology or mass, which was similar between Drp1cKO and hAPP Drp1cKO in vivo (Figures 9e and f, Figure 10c).
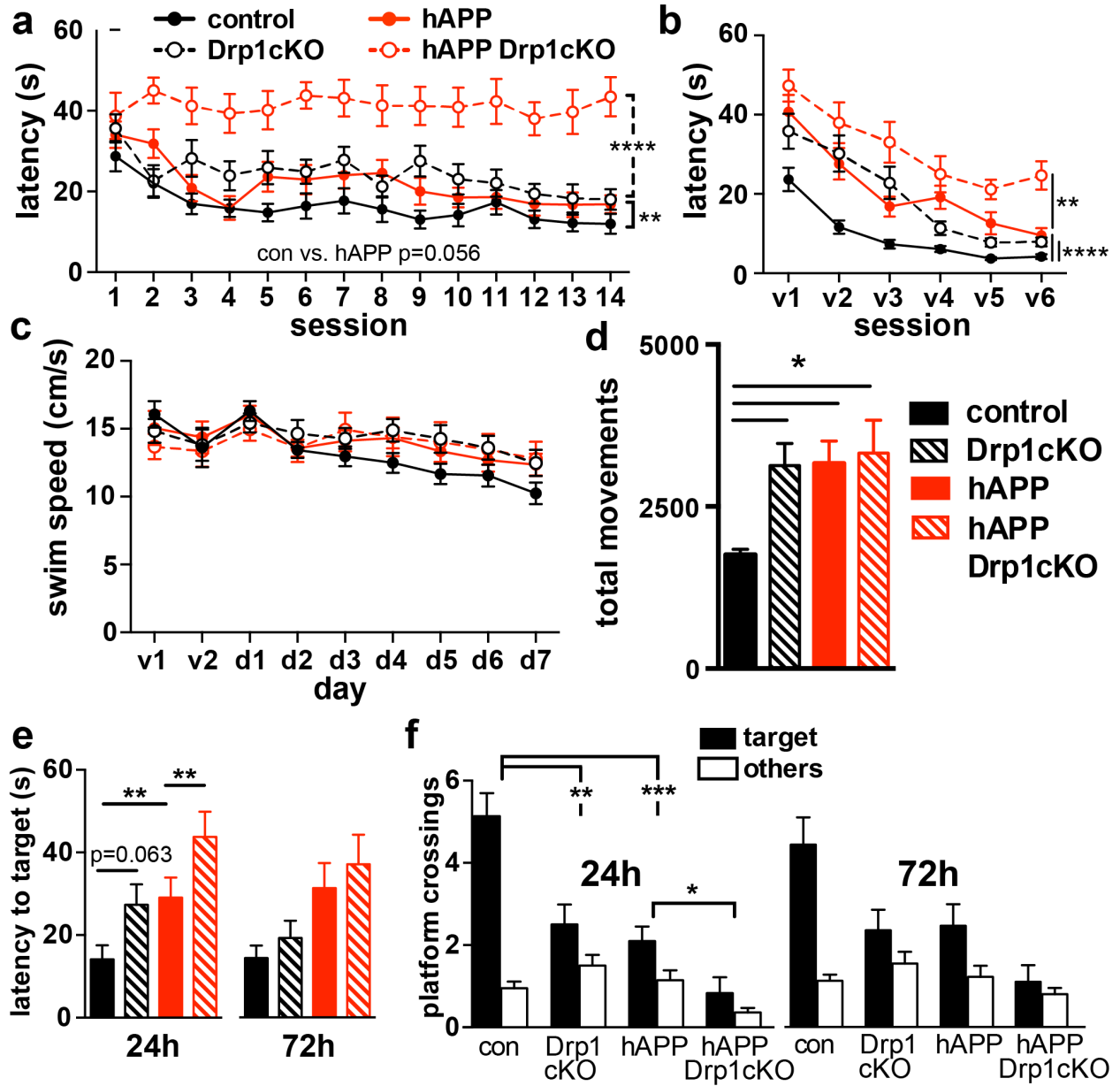
Figure 11: Drp1 loss and hAPP synergistically worsen learning and memory deficits.
(a) Learning and memory were evaluated by Morris water maze (MWM) over 7 days (sessions 1–14) of hidden-platform training in 6–7-month-old mice. Drp1cKO and hAPP showed significant and near significant learning deficits compared to Drp1WT (control). J20-hAPP Drp1cKO (hAPP Drp1cKO) mice showed significant learning deficits compared with J20-hAPP (hAPP) mice. (b) Visible platform training results differed between groups, but also showed learning within groups, indicating visual function. Data are means ± S.E.M.; **p<0.01, ****p<0.0001 by average rank latency with mixed effect modeling, n=12–22 mice/group. (c) No swim speed differences were evident throughout 2 days of visible and 7 days of hidden Morris water maze training, suggesting that differences in test results were not due to motor deficits. Data are means ± S.E.M.; not significant by two-way ANOVA with repeated measures, n=12–22 mice/group. (d) Total movements of 6–7-month-old Drp1cKO, hAPP, and hAPP Drp1cKO mice showed increased motor activity in open field. Mice were tracked for 15 min in open field. Data are means ± S.E.M.; **p<0.05 by one-way ANOVA and Holm-Sidak *post hoc* test, n=9–12 mice/group. (e and f) Memory was evaluated using MWM probe trials at 24 and 72 h after hidden-platform training, measured by (e) latency to former platform location (target) and (f) number of platform crossings of the former platform (target) versus an equivalent platform location in the other quadrants (other). Drp1cKO, hAPP, and hAPP Drp1cKO mice showed significant memory deficits. n=12-22 mice/group. Data are means ± S.E.M.; p=0.063, *p<0.05, **p<0.01, ***p<0.001 by Cox proportional hazards regression models (latency) and Quasi-Poisson generalized linear models (platform crossings).

Discussion

Here we identified a new and robust function for mitochondrial fission in regulating ER-mitochondria contacts and calcium metabolism, expanding our understanding of the roles of Drp1 in neurons. Additionally, we demonstrated that Drp1 combined with hAPP in an AD model to destabilize MAMs and further impair neuronal calcium dynamics, manifesting in vivo as severely impaired learning and memory. These results provide new insights into the mechanisms of Drp1 in AD models and its potential as a therapeutic target.

Drp1-mediated fission regulates neuronal MAMs and calcium dynamics

Elegant work has shown that ER-mitochondrial contacts mark the sites of Drp1-mediated fission before Drp1 recruitment *(23)*. However, we do not know if mitochondrial fission at these sites also plays a role in forming or maintaining these contacts. Here, we demonstrate that Drp1 stabilizes MAMs in neurons, perhaps due to its role in regulating mitochondrial morphology and the marked morphologic changes that occur with its loss in vitro and in vivo *(17,19)*. This requirement for Drp1 bolsters previous evidence that Drp1 serves an intrinsic function in mitochondria *(19)* and that its impact on mitochondrial function is not merely secondary to its role in mitochondrial turnover *(53)*.

Drp1's critical role in regulating the stability and size of MAMs suggests that changes in Drp1 will also influence the functions of MAMS in calcium dynamics and lipid homeostasis. In support of this hypothesis, we found that mitochondrial calcium levels increase less after ER calcium releases through ryanodine receptors (RYRs), consistent with a deficit in ER-calcium transfer. RYRs cause the calcium-mediated calcium response from the ER, regulate neuronal cytosolic calcium dynamics *(54,55)*, and contribute to calcium dysregulation in AD models *(56)*. Of note, RYRs localize to MAMs in other cell types *(42)*, but this was not previously shown in neurons. The striking mitochondrial calcium response to a RYR agonist, caffeine, particularly in comparison to the mitochondrial response to electrical stimulation, suggests that RYRs also

localize to MAMs in neurons and regulate ER-mitochondrial calcium transfer. Interestingly, we also observed a decrease in cytosolic calcium levels following RYR stimulation in Drp1KO neurons, without a decrease in ER calcium release or a change of calcium levels in the mitochondria. Further investigation is needed to determine if this effect is due to the number or function of RYR receptors. Alternately, calcium dynamics in mitochondria may be disrupted, altering efflux and/or influx mechanisms (effects that may not be seen in calcium levels if homeostasis is quickly reached). Future studies will investigate these possibilities.

Interestingly, the changes in calcium dynamics appear to occur independently of Drp1KO's effects on energy levels. Instead, calcium changes may lie upstream of the intrinsic bioenergetic deficit caused by Drp1 loss *(19)*. Indeed, optimal respiration requires sufficient mitochondrial and cytosolic calcium levels *(36)* and could be impaired by the decrease in cytosolic calcium upon Drp1 loss. While Drp1KO more prominently decreases mitochondrial-derived ATP levels at the synapse than the cell body *(19)*, ATP levels were also decreased slightly at the cell body (Figure 6a). The more severe bioenergetic deficit at the axon may reflect proportionally greater energy requirements at the synapse versus cell body, rather than differences in calcium dynamics, although, both are possible. Additional studies are needed to determine if the effects on MAMs and calcium metabolism also apply other cell types.

The role of MAMs and calcium dynamics in models of AD

Dysregulation of MAMs has been implicated in multiple models of AD, suggesting that mutant presenilins, ApoE4, Aβ, and fibroblasts from AD patients increase the numbers of MAMs *(25-27)*. While we do not yet understand the precise effect of APP on MAMs, the levels of MAM-associated proteins increase in APP-based mouse models of AD *(26)*. Thus, our finding that hAPP decreases the number of MAMs is surprising. Because previous work suggests that APP-processing machinery is enriched at MAMs *(57)* a distinct APP proteolytic product may cause

the decrease in MAMs. Future studies are needed to determine whether membrane-bound APP

products are enriched in MAMs.

Our work also provides new insights into the dysregulation of calcium homeostasis in AD

models. Previous work showed that Aβ increases cytosolic calcium responses, such as to

excitatory amino acids, and that, physiologically, APP is required for neuronal calcium dynamics

(39,58,59). Consistent with this data, we found that hAPP and Aβ modestly increase the

cytosolic calcium response. Interestingly, only hAPP synergized with Drp1 loss, suggesting a

distinct role for hAPP (or other APP proteolytic products) in calcium dynamics and potentially

MAM stability. Furthermore, previous studies have suggested that increased calcium responses

are pathogenic *(59)*. However, Drp1 loss decreases the calcium response and further impairs

learning and memory. These results suggest that an increased calcium response may actually

be compensatory and protective in AD models, instead of pathogenic. Alternatively, the calcium

disruption caused by Drp1KO-hAPP synergy may tip the balance too far in the other direction.

Implications for Drp1 in the pathogenesis of AD

Changes in mitochondrial fission may contribute to the pathophysiology of AD and other

neurodegenerative disorders *(1-4,60-62)*. Drp1 levels are frequently increased in AD models

and post-mortem tissue from AD patients while levels of fusion proteins are decreased *(63,64)*,

suggesting a shift towards fission in the fission-fusion balance. However, if excessive

mitochondrial fission does occur and contribute to neurodegeneration in AD, then blocking Drp1

might have decreased the toxicity of hAPP. We found that blocking mitochondrial fission

markedly worsened (rather than prevented) hAPP toxicity, suggesting that increased

mitochondrial fragmentation is a protective response and does not drive toxicity. Indeed,

because Drp1 downregulation mediates tau-related toxicity *(65)*, Drp1 upregulation in AD may

be compensatory. By distinguishing between these possibilities, we will better understand

disease pathophysiology to develop potential therapeutic approaches targeting mitochondrial

dynamics. Notably, sufficient disruption of fission-fusion in either direction may cause toxicity, as seems to occur with both peripheral neurophathy (fusion protein Mfn2, fission protein GDAP1 *(66,67)*) and optic atrophy (Mfn2 and Drp1 *(10,68)*). Therefore, we may not be able to precisely balance fission-fusion when therapeutically targeting Drp1 or other similar proteins.

While knocking out Drp1 was not protective functionally, its loss did not exacerbate the early death of some hAPP mice, which likely results from network hyperexcitability *(52)*. Thus, Drp1 loss may not influence overall aberrant network activity.

Overall, this work demonstrates new functions of Drp1 in regulating the function of ER-mitochondrial contacts and calcium dynamics, highlighting the versatility and necessity of fission in neurons. We also discovered new effects of hAPP on MAMs and calcium dynamics, distinguishing it from Aβ, and a surprising lack of hAPP impact on mitochondrial-derived ATP levels. Finally, we demonstrate a new point of convergence between Drp1 and hAPP, which synergizes to decrease cytosolic calcium responses. This synergy may underlie impaired learning and memory in vivo. Thus, this work establishes novel roles for Drp1 in neurons, which may contribute to Drp1's impact on the pathogenesis of multiple neurological diseases.

Materials and Methods

Animals

Floxed Drp1 *(69)* and J20 *(51)* mice have been described. CamKCre *(70)* mice were obtained from The Jackson Laboratory. Mice were group-housed in a colony maintained with a standard 12 h light/dark cycle and given food and water ad libitum. Experiments were performed on age-matched mice of either sex. No differences between sexes were noted in any of the experiments. Experiments were conducted according to the *Guide for the Care and Use of Laboratory Animals*, as adopted by the National Institutes of Health, and with approval of the University of California, San Francisco Institutional Animal Care and Use Committee.

Behavioral testing

Learning and memory was assessed with the Morris water maze (MWM) test *(71)*. Briefly, 12 sessions of visible platform training were performed before hidden platform training as a control. Mice then underwent two sessions of hidden platform training separated by a 2 h intersession rest. Each session consisted of two trials. This training was performed each day for 7 days. Then, the platform was removed and memory probe trials were performed 24 h and 72 h after the last training day, and 24 h after the fifth day of training (data not shown).

EthoVision video-tracking system (Noldus, Netherlands) was used to record and track mice. Open field locomotor activity was performed as described *(17)*. Briefly, mice were habituated for at least 1 h before recording activity for 15 min with an automated Flex-Field/Open Field Photobeam Activity System (San Diego Instruments). All behavioral experiments were performed with the examiner blind to genotype.

Histology and Immunocytochemistry

For histology experiments, mice were anaesthetized and perfused with phosphate buffered saline (PBS), and then 4% paraformaldehyde (PFA). Brains were then removed, post-fixed in

PFA overnight, and cryoprotected in 30% sucrose. Coronal brain slices (30 µm) were prepared using a sliding microtome (Leica SM2000R).

For immunocytochemistry experiments, neuronal cultures were prepared as described below on coverslips and fixed in 4% PFA for 20 minutes at room temperature (RT).

For immunofluorescence, sections and coverslips were blocked for ≥1 h in PBS with 0.2% or 0.5% (for PSD-95 and 82E1) Triton X-100 and 5–10% bovine calf serum and then incubated with primary antibodies overnight at RT. The following primary antibodies were used: chicken anti-MAP2 (1:1000; Abcam Cat# ab5392, RRID:AB_2138153); mouse anti-NeuN (1:1000; Millipore Cat# MAB377, RRID:AB_2298772); rabbit anti-Tom20 (1:500; Santa Cruz, Cat# SC-11415, RRID:AB_2207533); mouse anti-MAP2 (1:1000; Millipore Cat# MAB3418, RRID:AB_94856); rabbit anti-calbindin (1:20000; Swant Cat# 300, RRID:AB_10000347); rabbit anti-tRFP (used against TagBFP; 1:1000; Evrogen Cat# AB233, RRID:AB_2571743); mouse anti-PSD-95 (1:100; BD Biosciences Cat# 610496, RRID:AB_397862; 1:100; ABR Cat# MA1-25629, RRID:AB_795156); mouse anti-8E5 (for human APP; 1:5000 *(52)*). Sections and coverslips were rinsed and incubated for 2 h at RT with the corresponding secondary antibodies: Alexa Fluor or DyLight 350, 488, 594, or 647 anti-mouse, chicken, or rabbit IgG (1:100–1:500; Invitrogen). For peroxidase staining, sections were quenched with 3% H_2O_2 and 10% methanol in PBS, and blocked in 10% bovine calf serum and 0.2% gelatin in PBS with 0.5% Triton X-100. They were incubated with mouse anti-82E1 (1:1000; IBL - America (Immuno-Biological Laboratories) Cat# 10326, RRID:AB_10705565), followed by biotinylated goat anti-mouse IgG (1:300; Vector Laboratories, Burlingame, CA; BA-1000, RRID:AB_2313606), and subsequently streptavidin-conjugated horseradish peroxidase (HRP) (1:300; Vectastain ABC kit, Vector Laboratories). Immunostaining was visualized with hydrogen peroxide and 3,3'-diaminobenzidine (DAB, Sigma).

Brain sections and coverslips were imaged with a laser-scanning confocal microscope (Zeiss LSM510-Meta, Zeiss LSM780-NLO FLIM, or Leica TCS SP8X) with a 63x (1.4 NA)

PlanApo oil objective or (1.2 NA) C-Apochromat water objective, a Nikon Ti-E inverted microscope with a 60x (1.2 NA) PlanApo water objective, or a Keyence inverted microscope BZ-9000 with a 10x (0.45 NA) CFI PlanApo λ objective. Volume was calculated with the Cavalieri principle *(72)*. Quantification of fluorescence and area were performed blind to genotype with MetaMorph software (version 7.7.3.0; Universal Imaging, RRID:SciRes_000136). Neuronal density was calculated by dividing the total fluorescence of NeuN in 100 μm^2 by the average NeuN intensity per CA1 neuron. Quantification of cells with swollen mitochondria was scored blind to genotype, based on the presence of three or more swollen mitochondria in a cell (a subjective criteria chosen to distinguish Drp1cKO versus control mitochondria). Amyloid plaque load was calculated based on % area of the hippocampus covered by plaques. PSD-95 images were deconvolved using Huygens Deconvolution software. Density was calculated in proximal dendrites of transfected cells using ImageJ software and the "Analyze Particles" plug-in (RRID:nif-0000-30467). Colocalization of MAM images was analyzed using Imaris software and the Surface-Surface colocalization extension.

Recombinant amyloid-beta

Recombinant Aβ oligomers or scrambled 1–42 control were prepared as previously described (Miyamoto et al. 2016). Briefly, hydroxyfluroisopropanol (HFIP)-treated recombinant Aβ peptides (β-amyloid(1–42), ultra pure, HFIP, rPeptide, A1163, lot number 06021342H) or HFIP-treated scrambled peptides (β-amyloid(1–42), Scrambled, lyophilized, rPeptide, A1004) were dissolved in 22 μL of DMSO and then diluted in 978 μL of cold PBS. Both peptide solutions were allowed to oligomerize for 24 h at 4°C. Peptide concentration was determined by bicinchoninic acid (BCA) assay (Thermo Scientific, 23225). This method was previously shown to produce low-order oligomeric Aβ species, as characterized by atomic force microscopy *(73)*.

Neuronal culture and live imaging

Post-natal hippocampal neuronal cultures were prepared from P0 Drp1[lox/lox] mice as described *(17)* and transfected via electroporation (Amaxa) with one or more of the following constructs expressed in the pCAGGS vector downstream of the chicken actin promoter *(74)*: ATP-YEMK (kind gift of Dr. Noji, Osaka University) *(49)*, mCherry-synaptophysin *(75)*, BFP2-synaptophysin, Cre recombinase *(17)*, hAPP mutant (Swedish, Indiana) *(76,30)*, ires-mApple, mitoGFP *(61)*, GCaMP6f *(40)*, R-CEPIA1er *(43)*, Cepia2mt *(43)*, ER-eYFP (Clontech), mitoFarRed, or mitoTagBFP. mitoFarRed and mitoTagBFP were generated by fusing TagRFP657 or TagBFP [kind gifts from Vladislav Verkhusha (Albert Einstein College of Medicine)], respectively, to the mitochondria-targeting sequence, cytochrome C oxidase subunit VIII *(77,78)*. Neurons were cultured for 8–11 days before live imaging or analysis.

Live imaging was performed in Tyrode's medium (pH 7.4; 127 mM NaCl, 10 mM HEPES-NaOH, 2.5 mM KCl, and 2 mM $MgCl_2$, with or without 2 mM $CaCl_2$, 30 mM glucose and/or 10 mM pyruvate) on a Nikon Ti-E inverted microscope with an iXon EMCCD camera (Andor Technology) and a perfusion valve control system (VC-8, Warner Instruments) controlled by MetaMorph Software. Live imaging for MAM studies were performed on a Zeiss LSM880 confocal microscope with Airyscan detector. Field stimulations (10 Hz * 60 s and 30 Hz * 3 s) were performed with an A385 current isolator and a SYS-A310 accupulser signal generator (World Precision Instruments). Glycolysis was inhibited with 2-deoxyglucose (5 mM, Sigma-Aldrich) and iodoacetate (1 mM, Sigma-Aldrich). Respiration was inhibited with oligomycin (3 µM).

For GCaMP6f and Cepia2mt calcium experiments, images were obtained (490/20 ex, 535/50 em, Chroma) every 200 msec, while for R-CEPIA1er experiments, images were obtained (572/35 ex, 632/60 em, Chroma) every 500 msec. A region of interest was drawn over the cell body, excluding the nucleus, and the background-subtracted fluorescence was calculated for each timepoint, normalized to the baseline level of background-subtracted fluorescence and control. Cytosolic, ER and mitochondrial calcium imaging were performed in

the presence of no drugs, caffeine (10 or 25 mM; Sigma-Aldrich), carbachol (0.5 mM; Sigma-Aldrich), KCl (50 mM; Sigma-Aldrich), recombinant Aβ 1–42 oligomers (2 μM; rPeptide), or Aβ 1–42 scrambled (2 μM; rPeptide).

For FRET experiments, sequential images were taken in the CFP (430/24 ex, 470/24 em), YFP (500/20 ex, 535/30 em), and FRET channels (430/24 ex, 535/30 em) with an ET ECFP/EYFP filter set (Chroma). Synaptic boutons were identified based on morphology. The FRET/donor ratio was calculated for each bouton and cell body as described **(79)**, where FRET = $(I_{FRET} − I_{CFP}*BT_{CFP} − I_{YFP}*BT_{YFP}) / I_{CFP}$, such that I_X is the background-corrected fluorescence intensity measured in a given channel. BT_{CFP} (donor bleed through) and BT_{YFP} (direct excitation of the acceptor) were calculated by expressing CFP and YFP individually and determining the ratios of I_{FRET}/I_{CFP} and I_{FRET}/I_{YFP}, respectively.

Statistical Analysis of Morris water maze

Morris water maze data has several characteristics that make longitudinal analysis complex: the data typically contain censoring (the mice are removed from the water after a fixed amount of time if they fail to complete the task), the learning effect is often non-linear (the healthy mice often learn the maze as well as they can before the last trial and thus stop systematically improving), there is typically a learning effect of both days of trials and number of trials given that day, which leads to a "saw-tooth" learning effect, and, we should expect to see a mean-variance relation.

Rather than attempt to build a very complex statistical model to account for these data features, we took advantage of the experimental design to create a summary measure analysis **(80)**, which greatly reduced the dimensionality of the problem and allowed for simple, robust, powerful and easily interpreted results. At each trial, we first found the rank of each mouse (i.e., which mouse finished first, second, etc.) in that particular trial. Mice that failed to locate the platform were considered "tied for last". For each mouse, we then calculated the average rank

across all the trials. From this calculation, we used these simple composite scores in a standard analysis.

We had two different outcomes: average ranks of latency per mouse during hidden and visible trials. We fit two linear mixed effects models *(81)* corresponding to the outcomes described above and the factor genotype using the R package lme4 (RRID:nif-0000-10474) *(82)*. We included random effects for the effect of cohort on genotype. We tested the overall effect of genotype on average rank latency hidden and average rank latency visible using the Wald Chi-square test.

We used the fitted model to obtain estimates of the mean difference in ranks. Using the function sim() from the arm package *(83)*, we obtained 50,000 draws of the group effects, and we estimated a 95% confidence interval (CI) around each estimate as the 2.5^{th} and 97.5^{th} quantiles of these draws. We calculated p-values for differences between groups using the simulated differences, corrected for multiple comparisons using the method of Holm *(84)*.

For the memory probe trials, we analyzed two different outcomes: latency to first target platform crossing and number of platform crossings. We fit a Cox proportional hazards regression model of latency on genotype using the R package survival *(85)*. We examined the proportional hazards assumption by visual inspection of the curves of the natural logarithm of the cumulative hazard function versus latency for each of the four genotypes. Since the four curves were approximately parallel, we assumed that the proportional hazards assumption was met for this dataset. We also performed the Kaplan Meier nonparametric test as a way to visually inspect the survival function for each genotype. We included random effects for the effect of cohort on genotype.

We fit a Quasi-Poisson generalized linear model of number of platform crossings on genotype. The Quasi-Poisson generalized linear model accounts for overdispersion, allowing for more robust estimation. We fit two Quasi-Poisson models, one with an interaction term between

genotype and cohort, to insure that the treatment effect was relatively constant across cohorts, and the primary model was fit with only genotype alone, (assuming the effect of genotype was consistent across cohorts). We used a Deviance test to compare these two models, and we did not find a significant difference between them (p-value=0.166), implying that the effects were consistent across cohorts. Therefore, we chose the more parsimonious model, which is the model with only the effect of genotype.

From the Cox proportional hazards regression model, we obtained estimates of the relative risk of reaching the platform (RR), the 95% confidence interval of the relative risk, and the corresponding p-values. From the Quasi-Poisson model, we obtained estimates of the mean difference in number of platform crossing, the 95% confidence interval of the difference, and the corresponding p-values. The p-values corresponding to these outcomes were corrected for multiple comparisons using the method of Holm *(84)*.

References

1. Itoh K et al. (2013) Mitochondrial dynamics in neurodegeneration. Trends in Cell Biology 23, 64-71
2. Wang X et al. (2008) Amyloid-beta overproduction causes abnormal mitochondrial dynamics via differential modulation of mitochondrial fission/fusion proteins. Proc Natl Acad Sci U S A 105, 19318-19323
3. Cho DH et al. (2009) S-nitrosylation of Drp1 mediates beta-amyloid-related mitochondrial fission and neuronal injury. Science 324, 102-105
4. Wang W et al. (2015) Parkinson's disease-associated mutant VPS35 causes mitochondrial dysfunction by recycling DLP1 complexes. Nat Med,
5. Rappold PM et al. (2014) Drp1 inhibition attenuates neurotoxicity and dopamine release deficits in vivo. Nat Commun 5, 5244
6. Song W et al. (2011) Mutant huntingtin binds the mitochondrial fission GTPase dynamin-related protein-1 and increases its enzymatic activity. Nat Med 17, 377-382
7. Fahrner JA et al. (2016) A novel de novo dominant negative mutation in DNM1L impairs mitochondrial fission and presents as childhood epileptic encephalopathy. Am J Med Genet A,
8. Vanstone JR et al. (2016) DNM1L-related mitochondrial fission defect presenting as refractory epilepsy. Eur J Hum Genet 24, 1084-1088
9. Yoon G et al. (2016) Lethal Disorder of Mitochondrial Fission Caused by Mutations in DNM1L. J Pediatr 171, 313-316 e312
10. Waterham HR et al. (2007) A lethal defect of mitochondrial and peroxisomal fission. N Engl J Med 356, 1736-1741
11. Duboff B et al. (2012) Tau Promotes Neurodegeneration via DRP1 Mislocalization In Vivo. Neuron 75, 618-632
12. Wang X et al. (2008) Dynamin-like protein 1 reduction underlies mitochondrial morphology and distribution abnormalities in fibroblasts from sporadic Alzheimer's disease patients. Am J Pathol 173, 470-482
13. Poole AC et al. (2008) The PINK1/Parkin pathway regulates mitochondrial morphology. Proc Natl Acad Sci U S A 105, 1638-1643
14. Yang Y et al. (2008) Pink1 regulates mitochondrial dynamics through interaction with the fission/fusion machinery. Proc Natl Acad Sci U S A 105, 7070-7075
15. Liu W et al. (2011) Pink1 regulates the oxidative phosphorylation machinery via mitochondrial fission. Proc Natl Acad Sci U S A 108, 12920-12924
16. Verstreken P et al. (2005) Synaptic mitochondria are critical for mobilization of reserve pool vesicles at Drosophila neuromuscular junctions. Neuron 47, 365-378
17. Berthet A et al. (2014) Loss of mitochondrial fission depletes axonal mitochondria in midbrain dopamine neurons. J Neurosci 34, 14304-14317
18. Twig G et al. (2008) Fission and selective fusion govern mitochondrial segregation and elimination by autophagy. EMBO J 27, 433-446
19. Shields LY et al. (2015) Dynamin-related protein 1 is required for normal mitochondrial bioenergetic and synaptic function in CA1 hippocampal neurons. Cell Death Dis 6, e1725
20. Wakabayashi J et al. (2009) The dynamin-related GTPase Drp1 is required for embryonic and brain development in mice. The Journal of Cell Biology 186, 805-816
21. Rangaraju V et al. (2014) Activity-driven local ATP synthesis is required for synaptic function. Cell 156, 825-835
22. Pathak D et al. (2015) The role of mitochondrially derived ATP in synaptic vesicle recycling. J Biol Chem 290, 22325-22336
23. Friedman JR et al. (2011) ER tubules mark sites of mitochondrial division. Science 334, 358-362

24. Raturi A, Simmen T (2013) Where the endoplasmic reticulum and the mitochondrion tie the knot: the mitochondria-associated membrane (MAM). Biochim Biophys Acta 1833, 213-224

25. Area-Gomez E et al. (2012) Upregulated function of mitochondria-associated ER membranes in Alzheimer disease. EMBO J 31, 4106-4123

26. Hedskog L et al. (2013) Modulation of the endoplasmic reticulum-mitochondria interface in Alzheimer's disease and related models. Proc Natl Acad Sci U S A 110, 7916-7921

27. Tambini MD et al. (2016) ApoE4 upregulates the activity of mitochondria-associated ER membranes. EMBO Rep 17, 27-36

28. Cho D-H et al. (2009) S-nitrosylation of Drp1 mediates beta-amyloid-related mitochondrial fission and neuronal injury. Science (New York, NY) 324, 102-105

29. Schon EA, Area-Gomez E (2013) Mitochondria-associated ER membranes in Alzheimer disease. Mol Cell Neurosci 55, 26-36

30. Murrell J et al. (1991) A mutation in the amyloid precursor protein associated with hereditary Alzheimer's disease. Science 254, 97-99

31. Mullan M et al. (1992) A pathogenic mutation for probable Alzheimer's disease in the APP gene at the N-terminus of beta-amyloid. Nat Genet 1, 345-347

32. Almeida CG et al. (2005) Beta-amyloid accumulation in APP mutant neurons reduces PSD-95 and GluR1 in synapses. Neurobiol Dis 20, 187-198

33. Cereghetti GM et al. (2008) Dephosphorylation by calcineurin regulates translocation of Drp1 to mitochondria. Proc Natl Acad Sci U S A 105, 15803-15808

34. Han XJ et al. (2008) CaM kinase I alpha-induced phosphorylation of Drp1 regulates mitochondrial morphology. J Cell Biol 182, 573-585

35. Jaiswal MK et al. (2009) Impairment of mitochondrial calcium handling in a mtSOD1 cell culture model of motoneuron disease. BMC Neurosci 10, 64

36. Rizzuto R et al. (2012) Mitochondria as sensors and regulators of calcium signalling. Nat Rev Mol Cell Biol 13, 566-578

37. Kaufman RJ, Malhotra JD (2014) Calcium trafficking integrates endoplasmic reticulum function with mitochondrial bioenergetics. Biochim Biophys Acta 1843, 2233-2239

38. Zarain-Herzberg A et al. (2014) Regulation of SERCA pumps expression in diabetes. Cell Calcium 56, 302-310

39. Mattson MP et al. (1992) beta-Amyloid peptides destabilize calcium homeostasis and render human cortical neurons vulnerable to excitotoxicity. J Neurosci 12, 376-389

40. Chen TW et al. (2013) Ultrasensitive fluorescent proteins for imaging neuronal activity. Nature 499, 295-300

41. Nagarkatti N et al. (2008) Levetiracetam inhibits both ryanodine and IP3 receptor activated calcium induced calcium release in hippocampal neurons in culture. Neurosci Lett 436, 289-293

42. Garcia-Perez C et al. (2008) Physical coupling supports the local Ca2+ transfer between sarcoplasmic reticulum subdomains and the mitochondria in heart muscle. J Biol Chem 283, 32771-32780

43. Suzuki J et al. (2014) Imaging intraorganellar Ca2+ at subcellular resolution using CEPIA. Nat Commun 5, 4153

44. Palty R et al. (2010) NCLX is an essential component of mitochondrial Na+/Ca2+ exchange. Proc Natl Acad Sci U S A 107, 436-441

45. MacLennan DH et al. (1997) The mechanism of Ca2+ transport by sarco(endo)plasmic reticulum Ca2+-ATPases. J Biol Chem 272, 28815-28818

46. Wang L et al. (2016) Synaptosomal Mitochondrial Dysfunction in 5xFAD Mouse Model of Alzheimer's Disease. PLoS One 11, e0150441

47. Du H et al. (2010) Early deficits in synaptic mitochondria in an Alzheimer's disease mouse model. Proc Natl Acad Sci U S A 107, 18670-18675

48. Imamura H et al. (2009) Visualization of ATP levels inside single living cells with fluorescence resonance energy transfer-based genetically encoded indicators. Proc Natl Acad Sci U S A 106, 15651-15656

49. Imamura H et al. (2009) Visualization of ATP levels inside single living cells with fluorescence resonance energy transfer-based genetically encoded indicators. Proceedings of the National Academy of Sciences of the United States of America 106, 15651-15656

50. Area-Gomez E, Schon EA (2016) Mitochondria-associated ER membranes and Alzheimer disease. Curr Opin Genet Dev 38, 90-96

51. Mucke L et al. (2000) High-level neuronal expression of abeta 1-42 in wild-type human amyloid protein precursor transgenic mice: synaptotoxicity without plaque formation. The Journal of Neuroscience: The Official Journal of the Society for Neuroscience 20, 4050-4058

52. Roberson ED et al. (2007) Reducing endogenous tau ameliorates amyloid beta-induced deficits in an Alzheimer's disease mouse model. Science 316, 750-754

53. Twig G et al. (2008) Mitochondrial fusion, fission and autophagy as a quality control axis: the bioenergetic view. Biochim Biophys Acta 1777, 1092-1097

54. Friel DD, Tsien RW (1992) A caffeine- and ryanodine-sensitive Ca2+ store in bullfrog sympathetic neurones modulates effects of Ca2+ entry on [Ca2+]i. J Physiol 450, 217-246

55. Fagni L et al. (2000) Complex interactions between mGluRs, intracellular Ca2+ stores and ion channels in neurons. Trends Neurosci 23, 80-88

56. Stutzmann GE et al. (2006) Enhanced ryanodine receptor recruitment contributes to Ca2+ disruptions in young, adult, and aged Alzheimer's disease mice. J Neurosci 26, 5180-5189

57. Area-Gomez E et al. (2009) Presenilins are enriched in endoplasmic reticulum membranes associated with mitochondria. Am J Pathol 175, 1810-1816

58. Yang L et al. (2009) Amyloid precursor protein regulates Cav1.2 L-type calcium channel levels and function to influence GABAergic short-term plasticity. J Neurosci 29, 15660-15668

59. LaFerla FM (2002) Calcium dyshomeostasis and intracellular signalling in Alzheimer's disease. Nat Rev Neurosci 3, 862-872

60. Kamp F et al. (2010) Inhibition of mitochondrial fusion by alpha-synuclein is rescued by PINK1, Parkin and DJ-1. EMBO J 29, 3571-3589

61. Nakamura K et al. (2011) Direct membrane association drives mitochondrial fission by the Parkinson disease-associated protein alpha-synuclein. J Biol Chem 286, 20710-20726

62. Wang X et al. (2012) LRRK2 regulates mitochondrial dynamics and function through direct interaction with DLP1. Hum Mol Genet 21, 1931-1944

63. Kandimalla R, Reddy PH (2016) Multiple faces of dynamin-related protein 1 and its role in Alzheimer's disease pathogenesis. Biochim Biophys Acta 1862, 814-828

64. Manczak M et al. (2011) Impaired mitochondrial dynamics and abnormal interaction of amyloid beta with mitochondrial protein Drp1 in neurons from patients with Alzheimer's disease: implications for neuronal damage. Human molecular genetics 20, 2495-2509

65. DuBoff B et al. (2012) Tau Promotes Neurodegeneration via DRP1 Mislocalization In Vivo. Neuron 75, 618-632

66. Züchner S et al. (2004) Mutations in the mitochondrial GTPase mitofusin 2 cause Charcot-Marie-Tooth neuropathy type 2A. Nature genetics 36, 449-451

67. Palau F et al. (2009) The role of mitochondrial network dynamics in the pathogenesis of Charcot-Marie-Tooth disease. Adv Exp Med Biol 652, 129-137

68. Zuchner S et al. (2006) Axonal neuropathy with optic atrophy is caused by mutations in mitofusin 2. Ann Neurol 59, 276-281

69. Wakabayashi J et al. (2009) The dynamin-related GTPase Drp1 is required for embryonic and brain development in mice. J Cell Biol 186, 805-816

70. Tsien JZ et al. (1996) Subregion- and cell type-restricted gene knockout in mouse brain. Cell 87, 1317-1326

71. Harris JA et al. (2010) Many Neuronal and Behavioral Impairments in Transgenic Mouse Models of Alzheimer's Disease Are Independent of Caspase Cleavage of the Amyloid Precursor Protein. The Journal of Neuroscience 30, 372-381

72. Simic G et al. (1997) Volume and number of neurons of the human hippocampal formation in normal aging and Alzheimer's disease. The Journal of comparative neurology 379, 482-494

73. Vossel KA et al. (2015) Tau reduction prevents Abeta-induced axonal transport deficits by blocking activation of GSK3beta. J Cell Biol 209, 419-433

74. Voglmaier SM et al. (2006) Distinct endocytic pathways control the rate and extent of synaptic vesicle protein recycling. Neuron 51, 71-84

75. Hua Z et al. (2011) v-SNARE composition distinguishes synaptic vesicle pools. Neuron 71, 474-487

76. Mullen RJ et al. (1992) NeuN, a neuronal specific nuclear protein in vertebrates. Development 116, 201-211

77. Morozova KS et al. (2010) Far-red fluorescent protein excitable with red lasers for flow cytometry and superresolution STED nanoscopy. Biophys J 99, L13-15

78. Subach OM et al. (2008) Conversion of red fluorescent protein into a bright blue probe. Chem Biol 15, 1116-1124

79. Xia Z, Liu Y (2001) Reliable and global measurement of fluorescence resonance energy transfer using fluorescence microscopes. Biophys J 81, 2395-2402

80. Fitzmaurice G, Laird, N. and Ware, J. (2004) Applied Longitudinal Analysis New Jersey

81. Laird NM, Ware JH (1982) Random-effects models for longitudinal data. Biometrics 38, 963-974

82. Bates D MM, Bolker B and Walker S (2014) lme4: Linear mixed-effects models using Eigen and S4_. R package version 1.1-7. http://CRAN.R-project.org/package=lme4.

83. Andrew Gelman Y-SS (2014) arm: Data Analysis Using Regression and Multilevel/Hierarchical Models. http://CRAN.R-project.org/package=arm.

84. Holm S (1979) A simple sequentially rejective multiple test procedure. Scandinavian Journal of Statistics, 65-70

85. Therneau T (2014) A Package for Survival Analysis in S. http://CRAN.R-project.org/package=survival.

Conclusions and Future Directions

This thesis work advances the field's understanding of the energetic requirements at the synapse, characterizing the energy needed to power synaptic vesicle release and identifying endocytosis as a high energy requiring step. Additionally, we identify new neuronal functions of mitochondrial fission – both physiologically and pathologically – demonstrating that fission is necessary to support mitochondrial energy at the synapse, maintain ER mitochondrial-associated membranes and support calcium metabolism in neurons. In each of these areas, these studies bring up further questions that warrant future investigation.

Energy in the brain

The results from Chapter I establish a more thorough understanding of how neurons use substrates and which processes require the most energy. Notably, neurons are capable of using either glycolysis or respiration to support synaptic vesicle cycling, and shift their reliance based on substrate availability. This work bolsters the findings of a study performed concurrently from Rangaraju et al., who also identified neuron's substrate flexibility *(1)*. Additionally, the work in Chapter I further explores the energy requirements of synaptic vesicle cycling, identifying endocytosis as the step requiring the most energy. This work was also confirmed in Rangaraju et al., who defined synaptic vesicle cycling as one of the major sinks in activity-driven synaptic energy.

These studies would benefit from an in vivo application of the developed technologies. In particular, employing the ATP-based FRET sensor in vivo (in slices or ideally in live mice using viral injections) would confirm the validity of the in vitro culture findings and allow for correlations with animal behavior, such as exploration or learning and memory. In vivo studies would also take into account complexities we can only begin to model in culture – conspicuously neuron-glia metabolic interactions and the impact of network activity.

Beyond our biological comprehension, understanding how the brain uses energy may be particularly important in the context of neurodegenerative diseases. In Pathak et al. (from experiments not included in this thesis), studies showed that energetic failure could be measured in a genetic model of Leigh's disease, modeled using a complex I subunit knockout *(2)*. These proof-of-concept experiments indicate that energy failure may underlie neurodegenerative pathogenesis and can be measured using our assays. The tools developed in Chapter I could be more widely applied to various neurodegenerative models to characterize the energetic state during pathogenesis.

In our hands, we applied these tools to a model of Alzheimer's disease (AD). In spite of a wealth of literature describing mitochondrial energetic changes in AD models *(3)*, we were surprised to find that neurons expressing mutant hAPP maintain normal levels of mitochondrial-derived ATP despite previously described impairments in their morphology, and in their function - as we discuss in Chapter III. Although this work does not rule out a mitochondrial contribution to AD pathogenesis, these studies clearly show that AD-causing mutations can produce neurodegeneration independent of any effects on energy levels, raising questions about if mitochondrial energy failure truly underlies neurodegeneration in AD. Mitochondria could still contribute to AD through one of their many other, non-energetic roles in neurons. Furthermore, a more complex metabolic mechanism may contribute to AD pathogenesis, involving not only respiratory deficits but also changes in glucose metabolism. Indeed, glucose uptake and glycolytic changes have been identified in AD patients *(4,5)*, although it is unclear whether these changes are pathogenic, compensatory or incidental. The tools developed in Chapter I could be used to further dissect the energetic contributions of glycolysis vs. respiration in models of AD, clarifying the role energy changes play in the disease.

<u>New functions for mitochondrial fission</u>

Both Chapter II and Chapter III identify novel functions of dynamin-related protein 1 (Drp1) and mitochondrial fission in neurons. In Chapter II, my studies expand upon previous work to examine the requirement of Drp1 in specific neuronal populations *(6,7)*. Initial studies identified a developmental requirement for Drp1 in neurons *(8,9)*. Subsequent studies then focused on the postnatal role of Drp1, examining the population-specific requirements of the protein. In Purkinje neurons, Drp1 is required to suppress oxidative damage *(7)*; in midbrain dopaminergic neurons, Drp1 is required to maintain mitochondrial mass and axonal targeting of mitochondria *(6)*. Additionally, Drp1 loss causes rapid neuronal degeneration in this population. Drp1 may also have an energetic role in both Purkinje and dopaminergic neurons, although this has not been examined (particularly, in dopaminergic neurons, due to the technical difficulty of culturing this specific population).

As discussed in Chapter II, we add our findings to this body of literature. In hippocampal neurons, we observe two main findings. First, Drp1 is not required for the survival of most CA1 hippocampal neurons, in comparison to dopaminergic neurons, where Drp1 is required for survival. Second, Drp1 is indeed required for hippocampal neuronal function. Drp1 is necessary to maintain the intrinsic energetic function of mitochondria in the axon. Without Drp1, there is a failure in mitochondrial-ATP levels at the axon, as opposed to a problem with mitochondrial distribution. Of note, we observe that this deficit is much more marked at the synapse, as opposed to the cell body, likely due to the higher energy requirements at the synapse.

These differing population requirements for Drp1 may simply reflect differing population requirements for mitochondrial functions. Indeed, the identified functions of Drp1 markedly overlap with mitochondrial functions (including energetics and oxidative damage). In Chapter III, we identify two novel functions of Drp1 – regulating MAM number and size, and impacting neuronal calcium dynamics. Changes in MAMs likely underlie the calcium changes we observe, considering that we see a change in both ER and mitochondrial calcium dynamics. We further

speculate that Drp1 may have an effect on lipid homeostasis, which would be an interesting avenue of future experiments. Identifying lipid composition in Drp1KO neurons, from both the ER and mitochondria, could help further our understanding of Drp1's roles. However, technically, these experiments would be difficult to perform on a single-cell basis as we have done with our assays.

Mitochondrial fission in Alzheimer's disease

In Chapter III, I explored the link between Drp1 and Alzheimer's disease (AD). I found, in the context of the AD-associated amyloid precursor protein (APP), there was an enhanced requirement for Drp1, particularly for MAM function and calcium regulation. We believe that Drp1' s role in MAMs explains the convergence of Drp1KO and APP, rather than because of Drp1's role in mitochondrial morphology or distribution. This convergence on MAMs may reflect a convergence on a specific function of MAMs, such as lipid homeostasis, although we do not directly explore that possibility in this thesis. Furthermore, while our studies indicate that human APP (hAPP) and Drp1-loss do not combine to worsen mitochondrial-derived ATP levels, we do not fully rule out the possibility that energy may play a role in the intersection of fission and AD. It is possible that non-mitochondrial energetic changes in AD (particularly changes in glucose metabolism) could synergize with Drp1KO mitochondrial changes. Each of these areas of speculation would be an interesting avenue for future studies.

In contrast to our findings, other studies in AD models found that MAMs instead increased *(10-12)*. However, none of these previous studies directly investigated the impact of hAPP (mutant or overexpression) on MAM number and function. Therefore, the discrepancy between our results and these previous studies may stem from distinct effects of APP vs. Aβ and APP vs. mutant presinilins on MAM function. This could be due to either full length APP or a different proteolytic product of APP. To address this question, future studies could examine whether modulating APP processing alters the effect of APP on MAM number.

Previously, Drp1 has been implicated in AD models, causing toxicity through both up- and downregulation of the protein *(13,14)*. In the context of Drp1 upregulation, it has been suggested as a therapeutic target for inhibition, though this remains to be tested. Other studies do show that Drp1 inhibition is protective in other models of neurotoxicity and degeneration (specifically Parkinson's disease and acute brain injury models) *(15,16)*. However, our studies suggest that Drp1 inhibition in AD patients would have the opposite effect, worsening learning and memory as we saw in an AD mouse model. Further work could confirm our studies using small molecules to inhibit Drp1 *(17)*, mimicking the proposed therapeutic avenue in patients.

Our studies do not rule out the possibility that lower levels of Drp1 inhibition may ameliorate AD progression, for example by preventing excessive calcium transfer by mildly disrupting MAMs. However, they do suggest that the fission-fusion balance is a finely tuned scale and, therefore, precise tuning for therapeutic inhibition may be difficult to achieve. Further, Drp1 inhibition may disrupt core cellular functions such as mitochondrial-ATP production, oxidative state, ER-mitochondrial functions and calcium homeostasis.

Overall, the studies in this thesis bring up new questions regarding the role of energetics and fission in neurodegenerative diseases and AD progression. Future work will help clarify the contribution of energetic changes in live neurons and in vivo in AD, as well as explore more roles of mitochondrial fission.
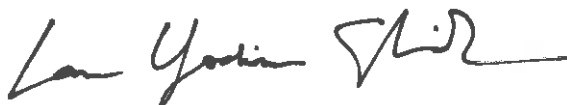
References

1. Rangaraju V et al. (2014) Activity-driven local ATP synthesis is required for synaptic function. Cell 156, 825-835

2. Pathak D et al. (2015) The role of mitochondrially derived ATP in synaptic vesicle recycling. J Biol Chem 290, 22325-22336

3. Swerdlow RH et al. (2014) The Alzheimer's disease mitochondrial cascade hypothesis: progress and perspectives. Biochim Biophys Acta 1842, 1219-1231

4. Bateman RJ et al. (2012) Clinical and Biomarker Changes in Dominantly Inherited Alzheimer's Disease. New England Journal of Medicine 367, 795-804

5. Vlassenko AG et al. (2010) Spatial correlation between brain aerobic glycolysis and amyloid-β (Aβ) deposition. Proceedings of the National Academy of Sciences of the United States of America 107, 17763-17767

6. Berthet A et al. (2014) Loss of mitochondrial fission depletes axonal mitochondria in midbrain dopamine neurons. J Neurosci 34, 14304-14317

7. Kageyama Y et al. (2012) Mitochondrial division ensures the survival of postmitotic neurons by suppressing oxidative damage. The Journal of cell biology 197, 535-551

8. Ishihara N et al. (2009) Mitochondrial fission factor Drp1 is essential for embryonic development and synapse formation in mice. Nature Cell Biology 11, 958-966

9. Wakabayashi J et al. (2009) The dynamin-related GTPase Drp1 is required for embryonic and brain development in mice. The Journal of Cell Biology 186, 805-816

10. Area-Gomez E et al. (2012) Upregulated function of mitochondria-associated ER membranes in Alzheimer disease. EMBO J 31, 4106-4123

11. Schon EA, Area-Gomez E (2013) Mitochondria-associated ER membranes in Alzheimer disease. Mol Cell Neurosci 55, 26-36

12. Tambini MD et al. (2016) ApoE4 upregulates the activity of mitochondria-associated ER membranes. EMBO Rep 17, 27-36

13. Cho D-H et al. (2009) S-nitrosylation of Drp1 mediates beta-amyloid-related mitochondrial fission and neuronal injury. Science (New York, NY) 324, 102-105

14. Duboff B et al. (2012) Tau Promotes Neurodegeneration via DRP1 Mislocalization In Vivo. Neuron 75, 618-632

15. Grohm J et al. (2012) Inhibition of Drp1 provides neuroprotection in vitro and in vivo. Cell Death Differ 19, 1446-1458

16. Rappold PM et al. (2014) Drp1 inhibition attenuates neurotoxicity and dopamine release deficits in vivo. Nat Commun 5, 5244

17. Qi X et al. (2013) A novel Drp1 inhibitor diminishes aberrant mitochondrial fission and neurotoxicity. J Cell Sci 126, 789-802

Publishing Agreement

It is the policy of the University to encourage the distribution of all theses, dissertations, and manuscripts. Copies of all UCSF theses, dissertations, and manuscripts will be routed to the library via the Graduate Division. The library will make all theses, dissertations, and manuscripts accessible to the public and will preserve these to the best of their abilities, in perpetuity.

Please sign the following statement:

I hereby grant permission to the Graduate Division of the University of California, San Francisco to release copies of my thesis, dissertation, or manuscript to the Campus Library to provide access and preservation, in whole or in part, in perpetuity.

Author Signature	Date